Technical Report Documentation Page

1. Report No. ABC-UTC-2016-C2-UNR01-Final	2. Government Accession No.	3. Recipient's Catalog No.	
4. Title and Subtitle **Development of Non-Proprietary UHPC Mix: Application to Deck Panel Joints**		5. Report Date September 2021	
		6. Performing Organization Code	
7. Author(s) Mohamed Abokifa, Mohamed A. Moustafa (https://orcid.org/0000-0002-1006-7685)		8. Performing Organization Report No.	
9. Performing Organization Name and Address Department of Civil and Environmental Engineering University of Nevada, Reno 1664 N. Virginia St., MS 0258 Reno, NV 89557		10. Work Unit No. (TRAIS)	
		11. Contract or Grant No. 69A3551747121	
12. Sponsoring Organization Name and Address Accelerated Bridge Construction University Transportation Center Florida International University 10555 W. Flagler Street, EC 3680 Miami, FL 33174	US Department of Transportation Office of the Assistant Secretary for Research and Technology And Federal Highway Administration 1200 New Jersey Avenue, SE Washington, DC 201590	13. Type of Report and Period Covered Final Report 01/2019-08/2021	
		14. Sponsoring Agency Code	
15. Supplementary Notes Visit www.abc-utc.fiu.edu for other ABC reports.			
16. Abstract Full-depth precast bridge decks are widely used to expedite the bridge construction and enhance durability. While these deck systems are challenging as their durability and performance are usually dictated by the efficiency of their field joints and closure joint materials. Hence, the commercial UHPC products have gained popularity for use in such joints because of their superior mechanical properties. However, the proprietary and relatively expensive nature of the robust UHPC mixes may pose some limitations on their future implementation. For these reasons, many research agencies along with state departments of transportations (DOTs) have sought to make the UHPC more accessible and more affordable by developing cheaper non-proprietary UHPC (NP-UHPC) mixes using local supplied materials. One of these efforts is the recent work by the ABC University Transportation Center (ABC-UTC) to develop NP-UHPC mixes for use in ABC field joints. This study documents the ABC-UTC NP-UHPC mix design and proportions, and has two main objectives. First, provide full mechanical characterization of such mix to allow for future replication and use of this material for different bridge applications as well as modeling purposes. Second, proof-test the developed NP-UHPC mixes in transverse and longitudinal field joints of the precast bridge decks. The mechanical characterization tests included flowability, compression, flexure, and direct tensile tests of the NP-UHPC mixes. Furthermore, this study included experimental testing of three full-scale precast bridge deck subassemblies with transverse NP-UHPC field joints and a single specimen with longitudinal field joint. The test parameters included NP-UHPC mixes with different steel fibers amount, different joint splice details, and joint widths. The results of this study were compared with results of similar proprietary UHPC (P-UHPC) reference specimens. The study showed that the proposed NP-UHPC mixes and field joint details can be efficiently used in the deck field joints with comparable behavior to the P-UHPC joints.			
17. Key Words Precast bridge deck panels, full-depth deck joints, full-scale testing, non-proprietary ultra-high performance concrete, mix characterization, deck-bulb-tee girders.		18. Distribution Statement No restrictions.	
19. Security Classification (of this report) Unclassified.	20. Security Classification (of this page) Unclassified.	21. No. of Pages 78	22. Price

(this page is intentionally left blank)

Development of Non-Proprietary UHPC Mix: Application to Deck Panel Joints

Final Report
September 2021

Authors
Mohamed Abokifa and Mohamed A. Moustafa

Principal Investigator: Mohamed Moustafa

Department of Civil and Environmental Engineering
University of Nevada, Reno, NV

Sponsored by
Accelerated Bridge Construction University Transportation Center

A report from

University of Nevada, Reno
Department of Civil and Environmental Engineering, MS 258
1664 N. Virginia St.
Reno, NV 89557

www.unr.edu/cee

Disclaimer

The contents of this report reflect the views of the authors, who are responsible for the facts and the accuracy of the information presented herein. This document is disseminated in the interest of information exchange. The report is funded, partially or entirely, by a grant from the U.S. Department of Transportation's University Transportation Program. However, the U.S. Government assumes no liability for the contents or use thereof.

Abstract

Full-depth precast bridge decks are widely used to expedite the bridge construction and enhance durability. While these deck systems are challenging as their durability and performance are usually dictated by the efficiency of their field joints and closure joint materials. Hence, the commercial UHPC products have gained popularity for use in such joints because of their superior mechanical properties. However, the proprietary and relatively expensive nature of the robust UHPC mixes may pose some limitations on their future implementation. For these reasons, many research agencies along with state departments of transportations (DOTs) have sought to make the UHPC more accessible and more affordable by developing cheaper non-proprietary UHPC (NP-UHPC) mixes using local supplied materials. One of these efforts is the recent work by the ABC University Transportation Center (ABC-UTC) to develop NP-UHPC mixes for use in ABC field joints. This study documents the ABC-UTC NP-UHPC mix design and proportions, and has two main objectives. First, provide full mechanical characterization of such mix to allow for future replication and use of this material for different bridge applications as well as modeling purposes. Second, proof-test the developed NP-UHPC mixes in transverse and longitudinal field joints of the precast bridge decks. The mechanical characterization tests included flowability, compression, flexure, and direct tensile tests of the NP-UHPC mixes. Furthermore, this study included experimental testing of three full-scale precast bridge deck subassemblies with transverse NP-UHPC field joints and a single specimen with longitudinal field joint. The test parameters included NP-UHPC mixes with different steel fibers amount, different joint splice details, and joint widths. The results of this study were compared with results of similar proprietary UHPC (P-UHPC) reference specimens. The study showed that the proposed NP-UHPC mixes and field joint details can be efficiently used in the deck field joints with comparable behavior to the P-UHPC joints.

Acknowledgments

This project was supported by the Accelerated Bridge Construction University Transportation Center (ABC-UTC at www.abc-utc.fiu.edu) at Florida International University (FIU), as lead institution, and Iowa State University (ISU) and the University of Nevada-Reno (UNR) as partner institutions. The authors would like to acknowledge the ABC-UTC support.

The authors would like to thank Martin Marietta for the donation of the aggregates, Leghigh Hanson for the donation of the cement slag, and Ductal® and Dramix® for the donation of the steel fibers. The authors also thank the laboratory staff at the Earthquake Engineering Laboratory at the University of Nevada, Reno for their assistance with the testing and experimental program.

Table of Contents

List of Figures

List of Tables

1. Introduction

1.1 Background

Cast-in-place (CIP) construction techniques have been widely used for many years in construction of the bridge decks around the nation. The reason for the wide implementation of these CIP systems was because they are relatively cheaper than other systems and easier to construct. However, these systems showed lack of performance, degradation in strength and less durability after spending many years in service. As a result, nearly 56,000 US bridges are considered structurally deficient based on the records of the American Road and Transportation Builders Association (ARTBA) (ARTBA bridge report, 2020). Since that bridge decks deteriorate faster than the other bridge components, more than $8 billion are spent annually on repairing or replacing these deteriorated decks (ARTBA bridge report, 2020). Approximately 85% of the US daily commuters travel on state-owned bridges, which makes it more difficult to use the traditional construction techniques or cast-in-place (CIP) methods in the replacement or rehabilitation of the deteriorated decks.

This has paved the way to a wider implementation of the prefabricated construction techniques to accelerate the deck erection. Prefabricated bridge decks (PBES), which is one of the accelerated bridge construction (ABC) applications, can enhance constructability issues, offer higher quality, provide accelerated and safer construction, and minimize traffic disruption. The prefabricated bridge deck elements are usually connected on-site using field joints. These joints can be classified into two main types. Transverse joints that run perpendicular to the traffic flow direction and longitudinal joints that run along the longitudinal axis of the bridge, i.e. parallel to the traffic direction. Currently, ultra-high performance concrete (UHPC) has gained a great significance and reputation as a bridge deck joint material

Ultra-high performance concrete (UHPC) is a new class of advanced construction materials with enhanced mechanical and durability properties due to steel fiber reinforcement, low water to binder ratio, and optimized particle packing density (Holschemacher and WieBe, 2005; De Larrard and Sedran, 1994; Resplendino, 2011). UHPC typically consists of a well-graded mixture of Portland cement, silica fume, ground quartz, high-range water reducer (HRWR), fine sand, and discontinuous steel fiber reinforcement (Russell et al., 2013; Graybeal, 2006). Typical compressive strength of UHPC may exceed 21.7 ksi (150 MPa) with sustained post-cracking tensile strength of at least 0.72 ksi (5 MPa) (Graybeal, 2011). The unparalleled properties of UHPC have motivated the bridge engineering community to implement it in various applications, such as accelerated bridge construction (ABC) field joints, over the past two decades (Wang et al., 2015). However, most of the current implementations of UHPC worldwide use mostly commercial proprietary UHPC (P-UHPC) products, and until few years ago, there was even only one commercial product available in the United States (Graybeal, 2013).

The proprietary nature of UHPC along with the high cost and limited availability of the material have motivated transportation agencies along with academic and industrial research to find other alternative materials for ABC field joints (e.g. Abokifa and Moustafa, 2021 a). Some other research efforts focused on making UHPC more accessible and less expensive through the

development of non-proprietary UHPC (NP-UHPC) mixes using locally available materials. Former studies (e.g. Wille et al., 2011) demonstrated that it is possible to develop NP-UHPC with a compressive strength greater than 30 ksi (200 MPa) without requiring any special treatment conditions. Due to the high number of these research efforts, a FHWA report was published to summarize some of these research findings to accelerate the use of NP-UHPC and promote more resilient US transportation infrastructures (Graybeal, 2013).

Many state departments of transportation (DOTs) have funded research on developing and testing of several NP-UHPC mixes using locally available materials in their states for use in different bridge applications (e.g. El-Tawil et al., 2016; Berry et al., 2017; Hernandez, 2016). A major contribution in this area is the recent multi-institutional collaboration work between five consortium universities within the ABC university transportation center (ABC-UTC) in the US (Abokifa and Moustafa, 2021 b; Shahrokhinasab and Garber, 2021). The ABC-UTC effort aims at facilitating the use of NP-UHPC for common bridge applications through developing several NP-UHPC mixes using different locally available material sources from at least five different regions across the country. A team from the University of Oklahoma (OU) has expanded their recent work (Looney et al., 2019) and led the ABC-UTC NP-UHPC mix design and basic material characterization. The final mix design has been shared among other ABC-UTC universities to establish the large-scale implementation of the mix using different material sources around the nation. Figure 1-1 shows the overall organization of the project. For example, the University of Nevada, Reno (UNR) has investigated the use of the final shared mix design using local materials on the west coast inside the bridge deck field joints. The work reported in this report is part of this multi-institutional collaboration project and this study aimed at replicating the base line shared mixed design using the local available materials in the Nevada and California states for use in the bridge deck field joints.

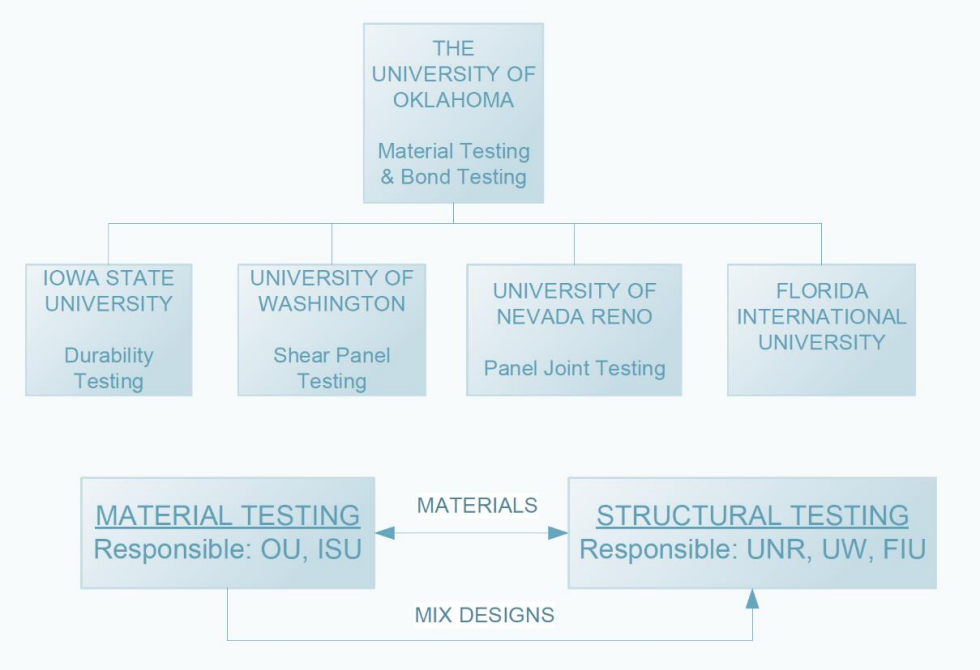

Figure 1-1: Overall organization of the ABC-UTC project and information sharing

1.2 Research Objectives

The main objective of this study is to investigate the structural performance of a recently developed NP-UHPC mixes for precast bridge deck joints under static vertical loading. The initial objective of this study was to provide full mechanical characterization of the developed NP-UHPC mixes to allow for future replication and use of this material for different bridge applications as well as modeling purposes. Then, investigate the effect of material sourcing and variability, such as fine aggregate types and particle gradation, on the main mechanical properties of the material. Finally, proof-test the developed NP-UHPC mixes in transverse and longitudinal field joints of the precast bridge decks. The core of this study is an experimental program that consists of material characterization testing of the developed NP-UHPC mixes and testing of four full-scale bridge deck specimens with NP-UHPC transverse and longitudinal field joints.

1.3 Research Approach

The research discussed herein focuses on the mechanical characterization of the developed NP-UHPC mixes and evaluating the structural performance of such mixes inside the field joints of the precast bridge decks. In addition, the experimental results of the proposed systems were compared with the overall performance of similar reference specimens with proprietary UHPC (P-UHPC) joints. Bridge deck specimens with transverse and longitudinal field joints were fabricated and tested under static wheel patch loading up to failure. This approach was successfully fulfilled through a set of sequenced research steps.

- Review of relevant literature studies, experimental and analytical test results of the bridge decks which are connected using field joints and other information related to the development and characterization of the NP-UHPC mixes.
- Develop several material characterization tests of the developed NP-UHPC mixes to allow for future replication and use of this material for different bridge applications as well as modeling purposes. The material tests included flowability tests, compression, flexure, and direct tensile tests of the NP-UHPC mixes.
- Establish a parametric study which included five different NP-UHPC mixes to investigate the effect of the material sourcing and variability, such as fine aggregate types and particle gradation, on the main mechanical properties of the material.
- Develop a detailed experimental plan, which include testing a total of four full-scale specimens under static vertical loading, with variables including joint orientation (transverse versus longitudinal), reinforcement splice types inside the joint, joint width, and closure joint materials (NP-UHPC with different dosage of steel fibers). The experimental program included three transverse specimens with different details that represent subassemblies of full-scale bridge decks with full-depth transverse joints. This was in addition to a single longitudinal specimen that represents parts of the top flanges of the DBT girders which were connected using full-depth longitudinal joints.
- Test precast bridge deck specimens with transverse and longitudinal field joints for flexure under static loading. The specimens were simply supported over two seat beams and loaded at the middle to allow for a single way bending of the specimens. The vertical static load was applied through a simulated typical wheel patch which was placed adjacent to the field joint.

The specimens were loaded to failure to study the structural behavior of the specimens, performance of the field joints, and damage schemes. Therefore, to come up with a conclusion of whether the joints were able to effectively emulate the anticipated performance from a monolithic deck.

- Establish a comparison between the experimental results and structural performance of the test specimens with NP-UHPC joints and similar reference specimens with P-UHPC field joints.
- Perform a detailed discussion of the experimental test results, and evaluation of the performance. The structural response of the test specimens is evaluated for initial stiffness, peak strength, deflection, damage schemes, reinforcement and concrete strains, and Joint performance at the specified AASHTO load levels. Final conclusions and recommendations were proposed.

1.4 Outline of the Report

The remainder of this report is organized as follows. Chapter 2 presents the development and mechanical characterization tests of the NP-UHPC mixes which were used in this study. Chapter 3 presents the experimental program and test results of the test specimens with transverse field joints. Chapter 4 presents the experimental program and test results of the test specimens with longitudinal field joints. Chapter 5 provides a summary of the study and summarizes the significant conclusions of this research.

2. Development of NP-UHPC mixes

2.1 Introduction

Ultra-high performance concrete (UHPC) is a new class of advanced construction materials with enhanced mechanical and durability properties due to steel fiber reinforcement, low water to binder ratio, and optimized particle packing density (Holschemacher and WieBe, 2005; De Larrard and Sedran, 1994; Resplendino, 2011). UHPC typically consists of a well-graded mixture of Portland cement, silica fume, ground quartz, high-range water reducer (HRWR), fine sand, and discontinuous steel fiber reinforcement (Russell et al., 2013; Graybeal, 2006). Typical compressive strength of UHPC may exceed 21.7 ksi (150 MPa) with sustained post-cracking tensile strength of at least 0.72 ksi (5 MPa) (Graybeal, 2011). The unparalleled properties of UHPC have motivated the bridge engineering community to implement it in various applications, such as accelerated bridge construction (ABC) field joints, over the past two decades (Wang et al., 2015). However, most of the current implementations of UHPC worldwide use mostly commercial proprietary UHPC products, and until few years ago, there was even only one commercial product available in the United States (Graybeal, 2013). The proprietary nature of UHPC along with the high cost and limited availability of the material have motivated transportation agencies along with academic and industrial research to find other alternative materials for ABC field joints (e.g. Abokifa and Moustafa, 2021 a). Some other research efforts focused on making UHPC more accessible and less expensive through the development of non-proprietary UHPC (NP-UHPC) mixes using locally available materials. Former studies (e.g. Wille et al., 2011) demonstrated that it is possible to develop NP-UHPC with a compressive strength greater than 30 ksi (200 MPa) without requiring any special treatment conditions. Due to the high number of these research efforts, a FHWA report was published to summarize some of these research findings to accelerate the use of NP-UHPC and promote more resilient US transportation infrastructures (Graybeal, 2013).

Many state departments of transportation (DOTs) have funded research on developing and testing of several NP-UHPC mixes using locally available materials in their states for use in different bridge applications (e.g. El-Tawil et al., 2016; Berry et al., 2017; Hernandez, 2016). A major contribution in this area is the recent multi-institutional collaboration work between five consortium universities within the ABC university transportation center (ABC-UTC) in the US (Abokifa and Moustafa, 2021 b; Shahrokhinasab and Garber, 2021). The ABC-UTC effort aims at facilitating the use of NP-UHPC for common bridge applications through developing several NP-UHPC mixes using different locally available material sources from at least five different regions across the country. A team from the University of Oklahoma (OU) has expanded their recent work (Looney et al., 2019) and led the ABC-UTC NP-UHPC mix design and basic material characterization. The final mix design developed by OU, which is the base for the work reported herein, was used as a closure joint materials for the bridge deck field joints as will be shown in the next chapters. The full-scale testing, as will be shown in the next chapters, demonstrated that the developed ABC-UTC NP-UHPC mixes can be efficiently used for such ABC connections, which motivated this study to provide a reference baseline comprehensive mechanical characterization of the ABC-UTC NP-UHPC.

The ABC-UTC NP-UHPC mix design is based on previous work by OU (e.g. Looney et al., 2019) as previously mentioned and as explained in the next section. Thus, this study is not concerned with the mix development. Nonetheless, one of the two main goals of this part of study is to characterize the main physical and mechanical properties of the ABC-UTC NP-UHPC mix when produced using different materials from various regions of the US (mostly Western US). The documented work herein provides confidence in reproducing desired UHPC mix characteristics and mechanical behavior from different materials that vary from original development. Material characterization repeatability and mix reproducibility is needed for expanding future implementation of NP-UHPC mixes for ABC applications and field joints. The main physical and mechanical characterization investigated in this study considered flow tests of the fresh mixes and compression, flexural, and direct tension tests of hardened UHPC at different ages. For full documentation, this part delivers the necessary information on the mix design, sourcing of the material ingredients, and mixing procedure of the developed NP-UHPC mixes. The second goal of this part of study is to investigate the variability effects of using different materials and sources, i.e. using different fine aggregate (sand) types and particle grading, on the main mechanical properties of the developed NP-UHPC mixes. Results from all mechanical tests of the varying NP-UHPC mixes are also used in this study to check the validity of existing mechanical behavior equations, which have been mostly developed using commercial UHPC mixes, for representing NP-UHPC.

In the next section, detailed literature review and background on the development of NP-UHPC, mix design, material sourcing, and mixing methodologies are provided. Next, the variability study is explained and followed by the experimental test results and discussion of the various material characterization tests conducted at different ages. Finally, a brief summary of the work done in this part of study is provided.

2.2 Background on Developing Non-proprietary UHPC

This section provides an overall literature review with special focus on the work done by OU on the development of the ABC-UTC NP-UHPC mix. The reviewed topics include mix designs, proportioning, material constituents, and mixing methodologies.

2.2.1 Mix Design

Among the various recent NP-UHPC development efforts, a research team from OU was funded to develop a NP-UHPC mix for Oklahoma DOT using their local materials to replace the need for using expensive and proprietary UHPC. The final NP-UHPC mix design (Looney et al., 2019) was developed after establishing a wide parametric study that included evaluation of the particle packing density of large number of different mix designs and comparison with the optimum packing curve generated from the Modified Andreasen and Andersen particle packing equation (Funk and Dinger, 2013). The design of the NP-UHPC mixes should conform to optimizing the particle packing to minimize voids and ensure high strength, low permeability, and self-consolidation properties (Lowke et al., 2012; Yu et al., 2015). The mix design process investigated the effect of using different mixing proportions and combinations of various material ingredients. The study selected three different mixes of NP-UHPC which have the good potential to satisfy the

desired performance for further flow tests and compression and flexure testing by applying variable heat curing schemes. The final mix design included the replacement of the high cement ratio with almost 30% cement slag by weight to reduce the overall NP-UHPC mix cost. Research at OU used the final mix design in precast bridge deck joints and demonstrated acceptable behavior when compared to commercial UHPC formulations (Looney et al., 2021).

The final NP-UHPC mix developed by OU and demonstrated for bridge joints was then selected as the main candidate for the ABC-UTC NP-UHPC initiative. Figure 2-1 in the next section provides the mix design in the form of components and mixing proportions, but the reader is referred to (Looney et al., 2019; Looney et al., 2021) for more details on the mix design. It is worth noting that complementary research at various ABC-UTC institutions is ongoing to characterize varying UHPC mixes using several material and durability tests such as: flowability, compressive strength, modulus of elasticity, flexural strength, splitting tensile strength, direct tensile strength, drying shrinkage, creep, setting time, freeze-thaw resistance, and rapid chloride ion penetration in addition to bar pullout and beam splice tests. As part of the ABC-UTC collaborative effort, one task we undertook at the University of Nevada, Reno (UNR) is to reproduce the original OU mix using the locally-sourced Oklahoma set of materials, then identify and employ comparable materials from western US regions such as Nevada and California. This part presents the several NP-UHPC mixes sampled and produced at UNR along with results from the selected mechanical tests for comparison and assessment purposes.

2.2.2 Mixture Proportions

The mixing proportions of the baseline NP-UHPC mix using 1% and 2% steel fibers by volume are shown in Figures 2-1 a and 2-1 b, respectively. As a reference to the developed mixes and for further comparisons, the composition of a typical commercial UHPC product that incorporates 2% steel fibers by volume, as obtained from FHWA report (Russell et al., 2013), is shown in Figure 2-1 c. Figure 2-1 d shows the range of the mixing proportions of the seven different NP-UHPC mix designs which were recommended by the FHWA for the Northeast, upper Midwest, and Northwest regions (Graybeal, 2013). It is noted that the mixing proportions of these seven mixes were proposed without the addition of steel fibers, and in turn, should be adjusted when fibers are added.

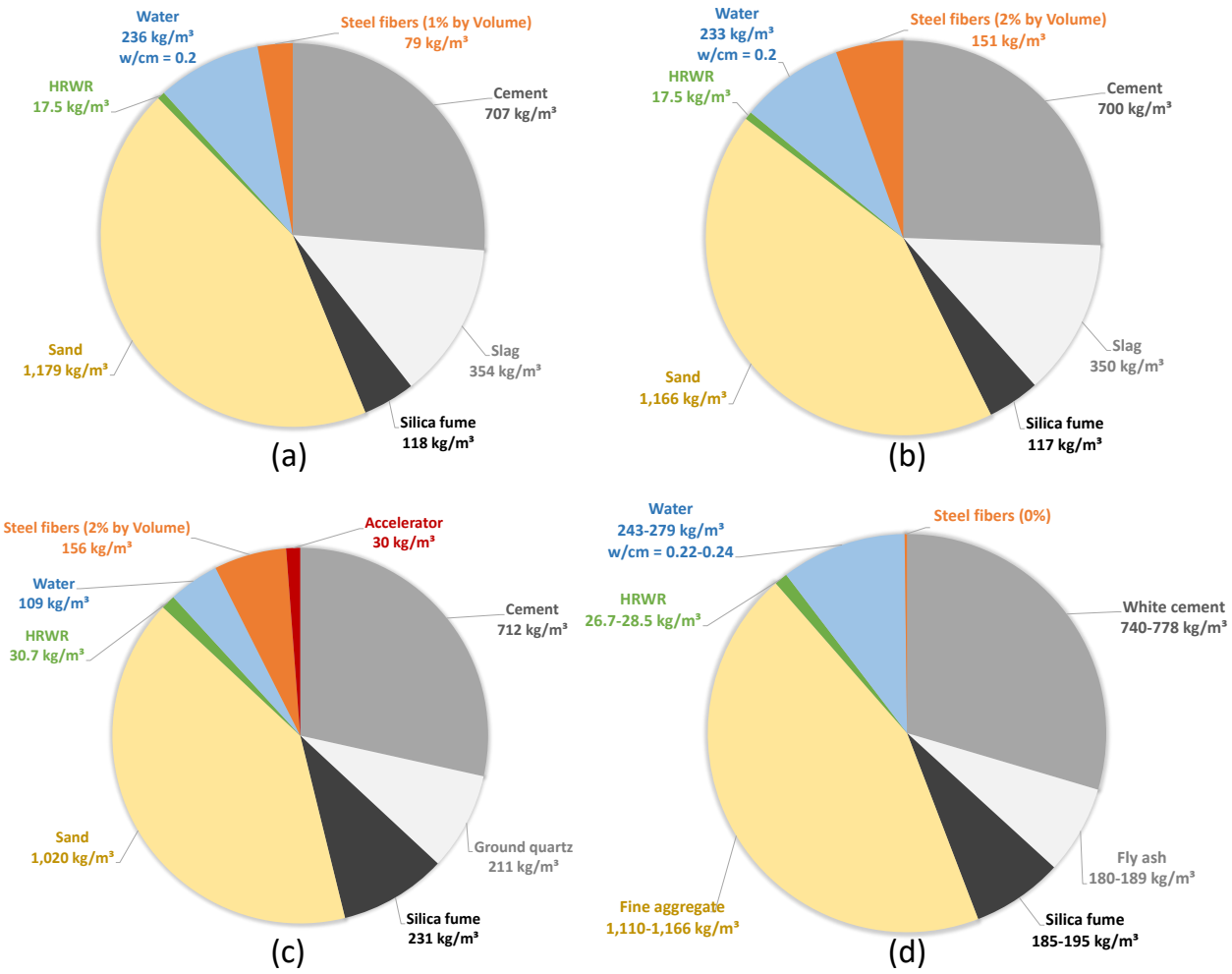

Figure 2-1: Mixing proportions of: (a, b) ABC-UTC NP-UHPC baseline mix with 1% and 2% steel fibers, (c) typical commercial UHPC mix reported in (Russell et al., 2013), and (d) FHWA NP-UHPC mixes reported in (Graybeal, 2013)

2.2.3 Material Constituents

Most of the NP-UHPC mixes reported in the literature were developed through the mixing and proportioning of six or more main ingredients. A brief overview of each ingredient and its use in previous studies is provided in this section.

Cement is a primary ingredient of any NP-UHPC mix as it acts as the main binder in the UHPC matrix. At least 20% of the total volume of UHPC is cement (Mendonca et al., 2020). The typical volume of the cementitious paste in the UHPC mixes ranges from 50% to 75% (Russell et al., 2013; El-Tawil et al., 2016; Park et al., 2008). Many previous studies investigated the effect of using different types of cement (e.g., Types I, I/II, II/V, III and V Portland cement, white cement, and oil-well cement) on the flow properties and compressive strength of the developed NP-UHPC mixes (Graybeal, 2013; Park et al., 2008; Alkaysi et al., 2016). Most of the work recommended the use of type I/II Portland cement due to its low content of C_3A that can reduce the required amount of water, decrease the developed hydration heat, and provide better performance for UHPC

(e.g. Wille et al., 2011; Mendonca et al., 2020; Shi et al., 2015). Because of the low water to cement ratios (w/c) in the typical UHPC mixes, the cement amount in the mix is not fully hydrated. Hence, the remaining un-hydrated cement particles act only as a filler material. As a result of this behavior and because of the high cement cost, many researchers have investigated the effect of replacing a percentage of cement with diverse supplemental cementitious materials (SCMs) and fillers such as silica fume, slag cement, fly ash, and quartz powder (Mendonca et al., 2020). SCMs reduce the overall NP-UHPC cost, enhance the particle packing density, and increase the strength due to the pozzolanic reactions (Mendonca et al., 2020). The present study included a 40% replacement of the cement amount with slag cement (30%) and silica fume (10%) to reduce the cost and increase the particle packing density.

Silica fume is one of the byproducts of the production of the Ferrum-silicon alloy and it is a common SCM used in the fabrication of UHPC. Due to the very fine particle size of the silica fume (0.4 micrometer), it is used in the UHPC mixtures as a micro filling material to physically fill the gaps between the mixture particles and generally improve the packing density of the mixture. Silica fume requires a relatively higher demand for water to increase the workability of the UHPC mixes due to its high surface area. Many researchers have investigated the effect of varying the percentage of silica fume on the flow properties and strength of the NP-UHPC mixes. In various NP-UHPC mix design guidelines, the content of silica fume ranges from 21% to 50% of cement weight (e.g. Russell et al., 2013; El-Tawil et al., 2016; Berry et al., 2017). However, in some of the cases, the high content of silica fume has resulted in more entrapped air voids because of the lower flowability (Mendonca et al., 2020). Consequently, other research efforts have optimized silica fume dosage to only 14% (Mendonca et al., 2020) and 20%-30% (Park et al., 2008) by cement weight. The silica fume content used in the present study is approximately 17% of the cement mass.

Slag cement is another SCM that is byproduct of steel industry and known as ground granulated blast furnace slag (GGBS). A major benefit of using slag cement in the UHPC mixture is that it undergoes pozzolanic reactions that result in a denser UHPC matrix (Meng et al., 2017; Kosmatka et al., 2002). The literature (e.g. ACI, 2011) proved that partial replacement of cement with slag has enhanced the workability of the fresh UHPC mixes, delayed the early strength gain while improved the later age strength, and reduces permeability and carbon footprint. One study (Kim et al., 2016) showed that slag replacement could reduce the 28-day compressive strength of UHPC if half the cement is partially substituted by slag cement. Meanwhile, other studies (e.g. Yazici et al., 2010) showed that adding a limited amount of slag cement results in a less flowable fresh mix and reduced strength due to the less particle packing density of the developed mixes. Due to its wide range of effects, some studies focused on optimizing the dosage of slag cement and recommended it to be somewhere between 20% (Yazici et al., 2010) and 30% (Mendonca et al., 2020). The present study, i.e. ABC-UTC NP-UHPC, uses a 30% replacement of the used cement with slag cement.

A key component of UHPC that is responsible for various aspects of the unparalleled mechanical properties such as higher tensile strength and ductility, is steel fibers. Steel fibers increase the UHPC toughness, enhance pre- and post- cracking tensile strength, and increase the durability

through better cracking control (Russell et al., 2013; Graybeal, 2006; Mendonca et al., 2020). Various shapes and dimensions of steel fibers are available in the market, however, the straight type of steel fibers with 0.2 mm diameter and 13 mm length are the most frequently used as they could provide the best performance (Graybeal, 2013). Since the steel fibers are the most expensive component of UHPC mixes, its dosage should be carefully controlled and optimized to provide attractive and less expensive alternative NP-UHPC mixes. Nonetheless, engineering the steel fiber ratio should be associated with functionality and consequent design parameters. The ABC-UTC NP-UHPC has implemented the usage of 2% steel fibers by volume but also considers efficient and cost-effective NP-UHPC mix solutions with only 1% steel fibers. For example, in an ongoing study, the authors are investigating the behavior of 8-in wide field joints with 1% steel fiber ratio versus 6-in joints with 2% fibers.

HRWR is a chemical admixture that is added to UHPC mixes to enhance workability and is also known as a superplasticizer. HRWR is mainly added to account for the significantly less water content typically used in the UHPC formulations to ensure adequate flow properties and self-consolidation of the fresh mix. The most common type of HRWR, which have been frequently reported in the literature (e.g. Berry et al., 2017; Mendonca et al., 2020; Schrofl et al., 2008) in the development of NP-UHPC and in turn, is used herein, is the polycarboxylate ether-based HRWR. The required amount of HRWR is usually adjusted based on the w/c to provide the desired workability of the fresh mix. For example, it is recommended to use 1% by cement weight polycarboxylate ether-based HRWR when combined with 0.22 w/c ratio (Schrofl et al., 2008). For the ABC-UTC NP-UHPC, a 1.5% by cement weight HRWR is used in combination with 0.20 w/c ratio.

Water is typically added to the dry UHPC mixture to produce the cementitious paste before adding the steel fibers. The typical range of w/c ratio for the developed NP-UHPC mixes in the literature varies from 0.16 to 0.28 depending on the accompanying HRWR dosage (e.g. Russell et al., 2013; Graybeal, 2013; Park et al., 2008; Allena and Newtson, 2011). As reported in the state-of-the-art FHWA report (Russell et al., 2013), it was recommended to use a w/c ratio of about 0.22 for developing UHPC with commercially available materials. The FHWA has recommended using less water amount for the NP-UHPC matrices with coarse aggregate than the ones with fine aggregates (Graybeal at al., 2013). The high content of dry materials and low water content in UHPC commonly lead to higher temperature of the fresh UHPC and in turn, higher levels of autogenous shrinkage (Xie et al., 2018). Hence, many studies have recommended partial or full replacement of water with crushed ice in case of mixing UHPC at temperatures that exceeded 25°C (Russell et al., 2013; Aboukifa et al., 2019; Teichmann and Schmidt, 2002).

The last major component of UHPC is aggregate. Most of the developed NP-UHPC mixes use a high percentage of fine aggregates or coarse aggregates (Graybeal, 2013; Qiao et al., 2016; Teichmann and Schmidt, 2002; Collepardi et al., 1997). Natural fine sand is the most commonly reported type of UHPC fine aggregate in the literature. The optimum binder to the aggregate ratio for the typical NP-UHPC mixes found in the literature is 1 or 1.1 (Graybeal, 2013; Xie et al., 2018). These optimal values were suggested to reduce the shrinkage of the developed NP-UHPC mixes

(Xie et al., 2018) and provide adequate volume and cost-effective NP-UHPC mixes. A binder to the aggregate ratio of 1.0 is adopted for the ABC-UTC NP-UHPC in the present study.

2.2.4 Mixing Methodology

The mixing and placing procedures of UHPC can affect its mechanical properties and must be appropriately coordinated to achieve consistency of the developed mixes. The mixing of UHPC usually requires a time-specific procedure to maintain the uniformity of the mixed constituents in the UHPC mix. The over-mixing or under-mixing of the UHPC should be avoided. The mixing methodology adopted in this study for the ABC-UTC NP-UHPC includes the initial mixing of all the dry components, i.e. cement, sand, silica fume, and slag, for 10 minutes. Afterwards, the required amount of water is mixed with half the superplasticizer amount and gradually added to the mix over the course of 2 minutes and mixing continues for another minute. Next, the other half amount of the superplasticizer is added over the course of one minute and mixing continues for an additional 5-10 minutes until the mix turns flowable and more like a paste. Finally, the steel fibers are gradually added over the course of 2 minutes and mixing continue for another 2 minutes before the NP-UHPC batch is ready for casting. For this study, all the NP-UHPC mixing was done at UNR using a high shear mixer (Imer 360), which has a total capacity of 0.145 m^3.

2.3 Variability Study

As mentioned earlier, one of the main objectives of the present experimental work is to reproduce and understand the variation in the ABC-UTC NP-UHPC mechanical properties when using different materials. The sought variability had two components: (1) material sourcing variability associated with utilizing different material sources from different regions of the country, and (2) aggregate type and grading variability through the using of fine masonry sand or sieved and non-sieved crushed aggregate sand in the NP-UHPC mixes. Accordingly, five different NP-UHPC mixes were produced and used in this study. More details on the two components of the variability along with a summary of the five different mixes utilized herein are provided in this section.

2.3.1 Material Sources Variability

Different sets of materials for the ABC-UTC NP-UHPC mix were acquired using the locally available materials in the Midwest/South region (as provided by our collaborators from OU) versus what we identified and procured in the Western region. All mixing proportions followed the same baseline AB-UTC NP-UHPC mix (see Figure 2-1 above). The main objective of this part of the study again is two-fold. The first part is to verify the repeatability of baseline mix and mechanical characteristics if independently produced by different team using different equipment and in a different setting. The second part is investigating the reproducibility of the baseline mix using a whole different set of materials locally supplied in the NV and CA regions. Verifying repeatability or reproducibility was established by relating and comparing various mechanical properties as discussed in the next section. Table 2-1 shows a list of the material suppliers and material types used in for both reproducibility and repeatability of the ABC-UTC NP-UHPC using materials from Western US (acquired by UNR) and Midwest/South US (provided by OU), respectively.

Table 2-1: Material constituents and local suppliers of the NP-UHPC mixes used in this study

Material	Acquired by UNR		Provided by OU	
	Type/Name	**Supplier**	**Type/Name**	**Supplier**
Cement	Type I/II	Nevada Cement, Reno-NV	Type I	Ash Grove, Chanute-KS
Silica Fume	MasterLife® SF100	BASF	Norchem	Norchem, Marietta-OH
Slag	Slag Cement	Lehigh Hanson, Sacramento-CA	Lafarge Slag	LafargeHolcim, South Chicago-IL
Steel Fibers	Dramix® OL 13/0.2	Bekaert	Dramix® OL 13/0.2	Bekaert
HRWR	MasterGlenium®7920	BASF	MasterGlenium®7920	BASF
Aggregate	Crushed Aggregate Sand	Martin Marietta, Sparks-NV	Fine Masonry Sand	Metro Materials, Norman-OK
Water	Potable Water	N/A	Potable Water	N/A

2.3.2 Aggregate Types and Grading Variability

For most of the NP-UHPC constituents, these are commercial products that satisfy respective ASTM standards and follow rigorous quality control through production. However, for sand and fine aggregates, there are thousands of types available in the US market and their properties differ from one region to another. Hence, there are high levels of uncertainty associated with the random particle size gradation and variation of sand or aggregate types, which could significantly affect the characteristics of a certain NP-UHPC mix. Thus, the objective of this part of the study is to investigate whether the characteristics of the ABC-UTC NP-UHPC, originally designed using fine masonry sand for fine aggregate, can be reproduced using other locally available types of sand in the west, especially in NV. If successful, this investigation will provide a foundation for the wide future implementation of NP-UHPC mixes across different regions of the country using different sand types and gradation. The type of sand acquired by UNR is a blend of well-graded small-size crushed aggregates added to fine and medium sand. The maximum size of the crushed aggregates is less than 4.76 mm. The crushed aggregate sand is locally known as concrete as it is usually used in the production of conventional concrete.

In the literature, many types of sand and aggregates have been used in the development of local NP-UHPC mixes such as masonry sand, river sand, silica sand, quartz sand, basalt, limestone, and volcanic rock as mentioned before. In general, fine sand has been the most common type. However, using coarse aggregate or mix of various aggregate sizes in NP-UHPC mixes have been widely considered to study its effect on strength. The FHWA study (Graybeal, 2013) showed that the NP-UHPC matrices with fine aggregated exhibit a slightly higher compressive strength than the course NP-UHPC matrices, but yet, allows the use of fine and coarse aggregates up to a maximum particle size of 9.5 mm (Graybeal, 2013). (Collepardi et al., 1997) showed that an equal volume replacement of fine ground quartz with a natural coarse aggregate with a maximum size of 8 mm did not affect the compressive strength. Another study by (Arora et al., 2019) showed that it is possible to achieve a higher packing density and high compressive and flexural strengths for the NP-UHPC mixes using a combination of three different coarse aggregate sizes (6.25 mm, 4.75

mm, and 2.36 mm) and two fine aggregate sizes (0.6 mm and 0.2 mm). Nevertheless, the large number of studies in the literature reported sizes between #8 (2.36 mm) and #18 (1 mm), which guided our selection at UNR. It is noted that the crushed aggregate sand used in the present study was also used in a former study at UNR to develop a NP-UHPC mix for seismic ABC connections for California DOT (Caltrans) (Aboukifa et al., 2020; Subedi et al., 2019). In that previous work, the acceptable aggregate consists of sand particles that pass the ASTM No. 30 (0.6 mm) sieve and is retained at the No. 200 (0.075 mm) sieve.

Careful sieving of crushed aggregate sand could be beneficial for enhancing the NP-UHPC mix strength, but it is also time- and labor-consuming and may prohibit scalability for large-scale applications. Thus, one other motivation of this study is to explore the use of raw crushed aggregate sand and establish a comparison between NP-UHPC mixes with and without the sieving procedure noted above. Accordingly, three types of sand were used in this study (see Figure 2-2) as follows: (1) Type A denotes non-sieved crushed aggregate sand acquired by UNR; (2) Type B denotes sieved crushed aggregate sand acquired and processed by UNR; and (3) Type C denotes the fine masonry sand provided by OU. Before any mixing, all sand types were carefully dried in controlled oven temperature of 250°C for 24 hours then left to cool down on-site for at least 48 hours. Sieve analysis according to ASTM C136 (ASTM C136/C136M-14, 2014) was also done for the three sand types to evaluate and report the sand particle size distribution to allow for the future replication of the NP-UHPC mixes using similar sand types from other local sources. Figure 2-2 provides the particle size distribution curves of the three sand types used in this study.

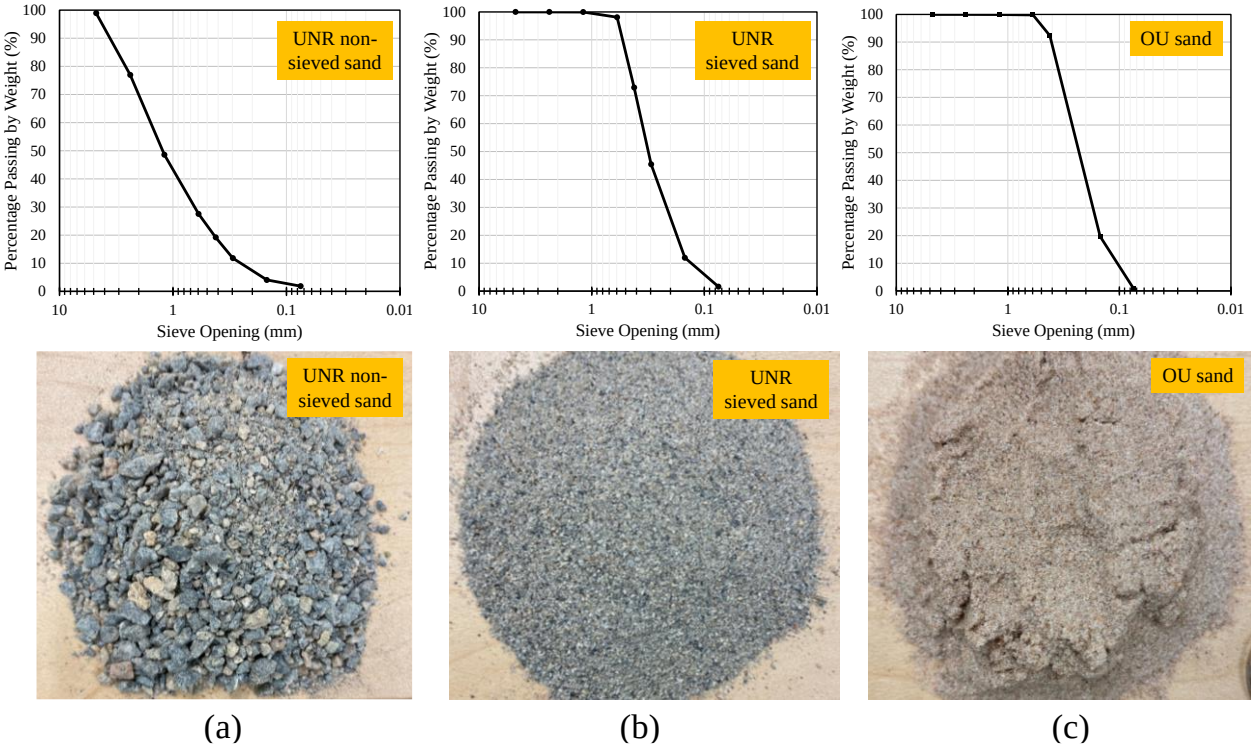

Figure 2-2: Different sand types used in the various NP-UHPC mixes in this study: (a) UNR non-sieved crushed aggregate sand, (b) UNR sieved crushed aggregate sand, and (c) OU fine masonry sand.

2.3.3 NP-UHPC Mixes Summary

Based on the material and aggregate variability explained above, five NP-UHPC mixes were considered and experimentally tested through this study as shown in Table 2-2. It is noted that the steel fiber content was also considered as an additional variable.

Table 2-2: Summary of five different NP-UHPC mixes used in this study

Notion	Prescriptive Batch ID*	Local materials acquired by	Steel fiber content (% by volume)	Sand type (as per Figure 2-2)
B1	B1 – UNR – 2% – NS	UNR	2 %	Type A
B2	B2 – UNR – 2% – S	UNR	2 %	Type B
B3	B3 – UNR – 1% – NS	UNR	1 %	Type A
B4	B4 – UNR – 1% – S	UNR	1 %	Type B
B5	B5 – OU – 2% – NS	OU	2 %	Type C
**"NS" denotes non-sieved sand or raw sand, and "S" denotes sieved sand*				

2.4 Test Results and Discussion

This section provides the material and mechanical characterization test results of all five studied NP-UHPC mixes. For verifying repeatability, respective results from OU selected tests are used. Four types of tests were conducted and discussed here: flow tests, compression tests, flexural tests, and direct tension tests. The section also provides a detailed assessment of how the NP-UHPC test results relate to strength prediction equations available in the literature, which have been mostly developed based on commercially-available proprietary UHPC mixes.

2.4.1 Flow Tests

UHPC is a highly flowable material that does not require special considerations such as tamping or vibration during placing or casting processes. Thus, the assessment of the flow properties of fresh mixes is one of the important criteria in developing NP-UHPC mixes with optimized particle packing density. The optimization of the mixture paste is usually associated with adequate flowability of the fresh mix and high compressive strength, which makes these two main properties the basic qualifiers for NP-UHPC mix development. The FHWA study (Graybeal, 2013) evaluates the efficiency of the newly developed NP-UHPC mixes based on a unitless efficiency parameter E, which is calculated based on the flowability, compressive strength, and material cost of the mixes. According to the ASTM C1856 (ASTM C1856/C1856M-17, 2017) and previous studies, the flow of the freshly mixed UHPC is frequently assessed using the test method in ASTM C1437 (ASTM C1437, 2006), while the mold and flow table shall comply with the requirements specified in the ASTM C230 (ASTM A., 2014). Only few literature studies have followed another standard to measure the flowability of the UHPC such as the ASTM C1611 (ASTM A., 2014) which is used to measure the slump of the self-consolidating concrete. In this study, flow table tests have been used following the procedures of the ASTM C1856 (ASTM C1856/C1856M-17, 2017) along with ASTM C1437 (ASTM C1437, 2006) without tamping to evaluate the rheology of the fresh NP-UHPC mixes.

For typical flow tests, a sample of the fresh NP-UHPC mix was taken immediately after mixing, then poured into the flow cone mold to the full capacity. The cone was then removed gently upward one minute after the mixing completion to allow the paste to flow over the 255 mm diameter table. Then, the mortar was left to spread over the table for two minutes according to the ASTM C1856 standards (ASTM C1856/C1856M-17, 2017) or until the flow become steady to measure the static flow of the mix. Finally, the flow table was dropped 25 times in 15 sec to measure the dynamic flow. The static and dynamic flows of the NP-UHPC mortars were calculated based on the average of the measured maximum and minimum diameters (ASTM C1856/C1856M-17, 2017).

The ASTM C1856 specifies a flow limit between 200 and 250 mm, while different state DOTs and the FHWA require a flow of 179 to 250 mm (Mendonca et al., 2020). However, based on the work at OU (Looney et al., 2021), it was found that a flow target of 250 mm can lead to steel fibers segregation as the fibers would not stay suspended at the flow, and hence, the study recommended a target flow values of 175 to 195 mm for the developed NP-UHPC mixes. Based on above, the assessment criteria followed here considers the mix appropriate if the static flow diameter is between 190 to 225 mm and the dynamic flow diameter is around 250 mm. It is noted that the flow of the NP-UHPC mixes can be greatly affected by the type and degree of fineness of sand. Thus, it is recommended to always test the flow properties of future mixes replication to ensure consistency and validity. If needed, a slight modification in the dosage of the HRWR based on the different sand types is also permitted to ensure that the flow of the NP-UHPC mixes is satisfying the recommended flow values.

The static and dynamic flow values of the five considered NP-UHPC mixes are shown in Figure 2-3. Photos of the static flow of the fresh NP-UHPC mixes are shown in Figure 2-4. The average of both static and dynamic flow measurements of the fresh NP-UHPC mixes fall within the specified flow requirements of the FHWA and ASTM C1856. It is noted that some of the mixes required slight adjustments to the HRWR to ensure consistent flow properties. The applied adjustments varied between −15% to +10% of the actual doses (see Figure 2-1) of the HRWR specified weights. The static flow measurements were typically within the 190-225 mm recommended flow limits, except for B3 and B4. All the dynamic flow measurements were around the recommended value of 250 mm. The photos in Figure 2-4 show that the fresh mixes with fine sands had a consistent steel fibers distribution over the flow spread. Oppositely, the fresh mixes with non-sieved sand (i.e. B1 and B3) are shown to have an accumulation of the steel fibers around the bigger particle sizes of the crushed aggregates in the mix. This accumulation is very clear in the B1 with the 2% steel fiber amount, while it is negligible in B3 with the 1% steel fiber amount.

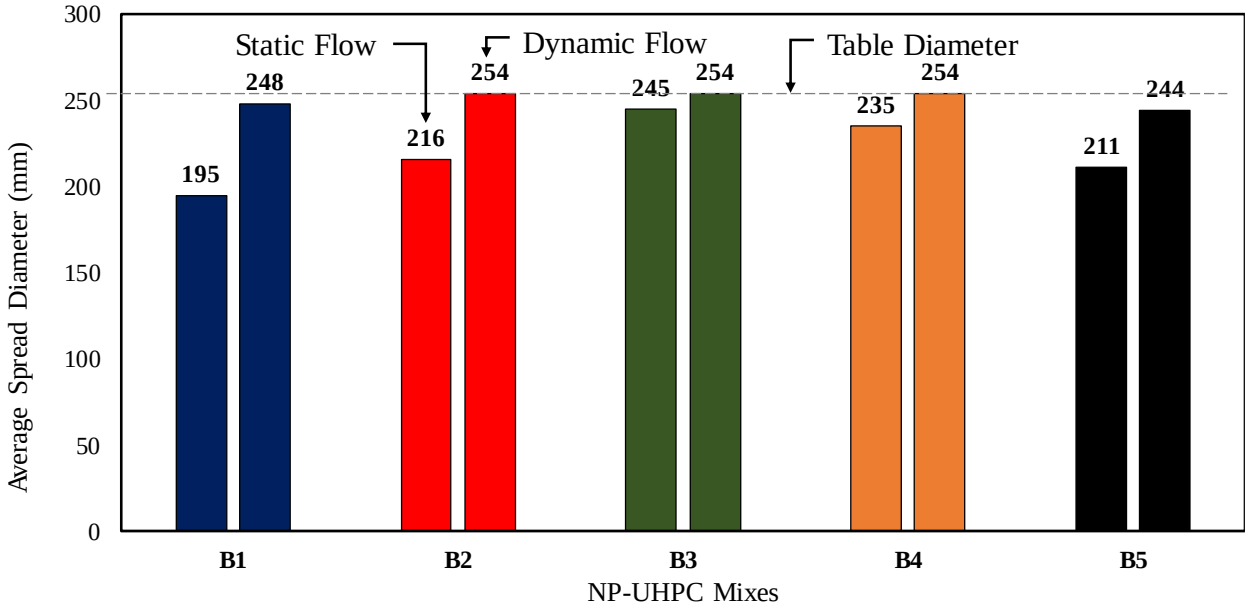

Figure 2-3: Static and dynamic flow table measurements of the five different fresh NP-UHPC mixes.

Figure 2-4: Static flow of the fresh NP-UHPC mixes.

2.4.2 Compression Tests

UHPC is known for its superior compressive strength which is almost 5-6 times that of the conventional concrete. Research studies, reports by FHWA and different state DOTs, and ASTM commonly specify minimum compressive strength values to categorize a material as UHPC. For example, the minimum 28-day compressive strength is specified by ASTM C1856 (ASTM C1856/C1856M-17, 2017) and FHWA (Graybeal, 2013) to be 117 and 150 MPa, respectively to define UHPC. However, for emerging NP-UHPC mix development, more economic mixes based on the application might not require a very high compressive strength. For the ABC-UTC NP-UHPC mix, the main goal is to provide a robust material for ABC field joints. Thus, a target compressive strength of about 120 MPa was set for such development. Meanwhile, it is also important to keep in mind that for ABC applications, emerging guidelines (e.g. California Department of Transportation, 2015) do not recommend opening the bridge for traffic or removing formwork unless the UHPC reaches a minimum compressive strength of 97 MPa.

2.4.2.1 Test procedure and specimens preparation

According to the test standards ASTM C1856 (ASTM C1856/C1856M-17, 2017), it is recommended to use a modified version of the ASTM C39 (ASTM C39, 2012) to determine the

compressive strength of the UHPC. The modification includes testing of 3×6 in cylinders under a rate of loading of 1 MPa/s. Note that increasing the loading rate has a negligible effect on the measured strength (Graybeal, 2015). Moreover, the test cylinders should be prepared by grinding the ends to a certain tolerance in lieu of capping or other sample preparation methods. Some studies recommend using ASTM C109 (ASTM C109, 1992) to test cubes instead of cylinders, to relax the challenging and time-consuming UHPC cylinders preparation process, and propose some conversion factors for the compressive strength obtained from different shapes and dimensions of the UHPC samples (Graybeal, 2015; Kusumawardaningsih et al., 2015). In this study, previous expertise among the research team and dedicated equipment (Aboukifa et al., 2019; Naeimi and Moustafa, 2021) have been leveraged to carefully prepare and use cylinders for compressive testing as explained later. The compressive strength of the various NP-UHPC mixes was determined at different ages including 3, 7, 28, and 56 or 230 days (a consequence of COVID-19 full shut down in April 2020). Three 3×6 in UHPC cylinders were prepared and tested at each age from each NP-UHPC mix. A SATEC compression machine with a loading capacity of 500 kips (2220 kN) was used at a rate of approximately 150 psi/s for all tests (see Figure 2-5 a).

Previous studies (e.g. Russellet al., 2013) have investigated the effect of various curing conditions such as steam curing at elevated temperatures, high moisture conditions, and ambient-cured conditions on the compressive strength of UHPC. Special curing like steam curing is not always practical for real bridge applications and the ambient curing conditions are more feasible and appropriate for many applications (Graybeal and Stone, 2012). Thus, in the present study, all test cylinders were left in fabrication yard for one day after mixing before transferring them to a temperature-controlled room with normal humidity and room temperature of about 73 ^{o}F (~ 23 ^{o}C). The test specimens were continuously subjected to the described curing conditions up to approximately two hours before compression testing to allow some time for cylinders preparation. Cylinders preparation aimed at removing the weak top layer, which could lead to underestimating the compressive strength of UHPC cylinders if not removed, then grinding the two ends as per ASTM C1856 (ASTM C1856/C1856M-17, 2017) provisions to ensure perpendicularity and planeness. A saw cutting machine was used to remove the top weak crust of the UHPC cylinders and a special hydraulic grinding machine was used for end grinding as shown in Figure 2-5 b. The test cylinders had a final length to diameter ratio after preparation between 1.86 and 1.93. Figure 2-5 c shows photos of the NP-UHPC cylinder ends following the previously mentioned sequence.

Figure 2-5: Compression testing of NP-UHPC cylinders: (a) test setup; (b) grinding machine for cylinder preparation; and (c) views of typical NP-UHPC cylinder through preparation sequence.

2.4.2.2 Compressive strength gain

The measured compressive strength versus age of the NP-UHPC mixes is plotted in Figure 2-6. Each data point in the curves represents the average measured compressive strength obtained from three test cylinders at a certain age. Many efforts in the literature have investigated the compressive strength gain of commercial UHPC products, and they recommended equations to predict the strength of UHPC cured at laboratory temperature 73 °F based on the age of concrete (Graybeal, 2006; Graybeal and Stone, 2012). These equations are yet to be verified for emerging NP-UHPC mixes such as the ones presented in this study. Two equations proposed by Graybeal (Graybeal, 2006; Graybeal and Stone, 2012) were selected for assessment and plotted in comparison with the measured strength of the NP-UHPC mixes in Figure 2-6. The first equation (Equation 2-1 below) was initially proposed by Graybeal (Graybeal, 2006) based on regression analysis of the compression test results of commercial UHPC cured under standard laboratory conditions for any time after 0.9 days (Graybeal, 2006). Graybeal (Graybeal and Stone, 2012) then revised the equation with focus on readily available UHPC for ABC field connections. The updated equation (Equation 2-2) can be used for UHPC cured at three different temperature conditions, i.e. 105 °F, 73 °F, and 50 °F, and provides relationship between the compressive strength, curing temperature, and age. For such, Equation 3 can be used to determine the time to initiation of the strength gain.

$$f'_{c,t} = f'_c\left[1 - exp\left(-\left(\frac{t-0.9}{3}\right)^{0.6}\right)\right] \quad (2\text{-}1)$$

$$f'_{c,t} = f'_c\left[1 - exp\left(-\left(\frac{t-t_{start}}{a}\right)^{b}\right)\right] \quad (2\text{-}2)$$

$$t_{start} = {}^{2.8}/_{\sqrt{T}} \quad (2\text{-}3)$$

where, $f'_{c,t}$ is compressive strength at age "t" days after mix initiation; t is time after casting in days; f'_c is UHPC compressive strength at 28 days; t_{start} is time of initiation of strength gain in days; a is a fitting parameter in days (for 23 ^{o}C, a = 1.0 day); and b is a dimensionless fitting parameter (for 23 ^{o}C, b = 0.3).

Figure 2-7 shows the results of the compressive strength gain of the NP-UHPC mixes along with its comparison against two other commercial UHPC mixes reported in the literature (Graybeal and Stone, 2012). Both mixes represented the commercial product Ductal JS1100RS (rapid strengthening UHPC) but the premix materials had different age at the time of casting. Both mixes had steel fibers of 2% by volume and added accelerator admixture and were cured at 73 ^{o}F. From the figures, it is observed that all the NP-UHPC mixes satisfied the minimum compressive strength of 117 MPa, which was specified by the ASTM C1856. Most of the mixes also reached the 97 MPa compressive strength limit after approximately 7 days; the threshold recommended for opening bridges for traffic or removing formwork. Both equations were able to closely predict the compressive strength gain of the developed mixes at the early ages and up to around 56 days. It is clearly shown that Equation 2-3 slightly overestimates the strength of the NP-UHPC during the first week as this equation is mainly developed for the UHPC mixes that use accelerator admixtures or agents in their mixtures.

The NP-UHPC mixes with 2% steel fibers have very comparable compressive strength and strength gain over time, while the mixes with 1% steel fibers are more scattered with around 20 MPa difference. This concludes that the compressive strength of the mixes with 2% steel fibers is less sensitive to the variability in the aggregate type or the source of the materials. While the compressive strength of the mixes with 1% steel fibers is more dependent on the type of aggregate used in the mix. The NP-UHPC mixes with local materials sourced by UNR and non-sieved sand (i.e. B1 and B3) have a higher compressive strength and more rapid early strength gain. B3 has the highest compressive strength among all the developed NP-UHPC mixes, hence it is recommended for future implementation in large-scale applications.

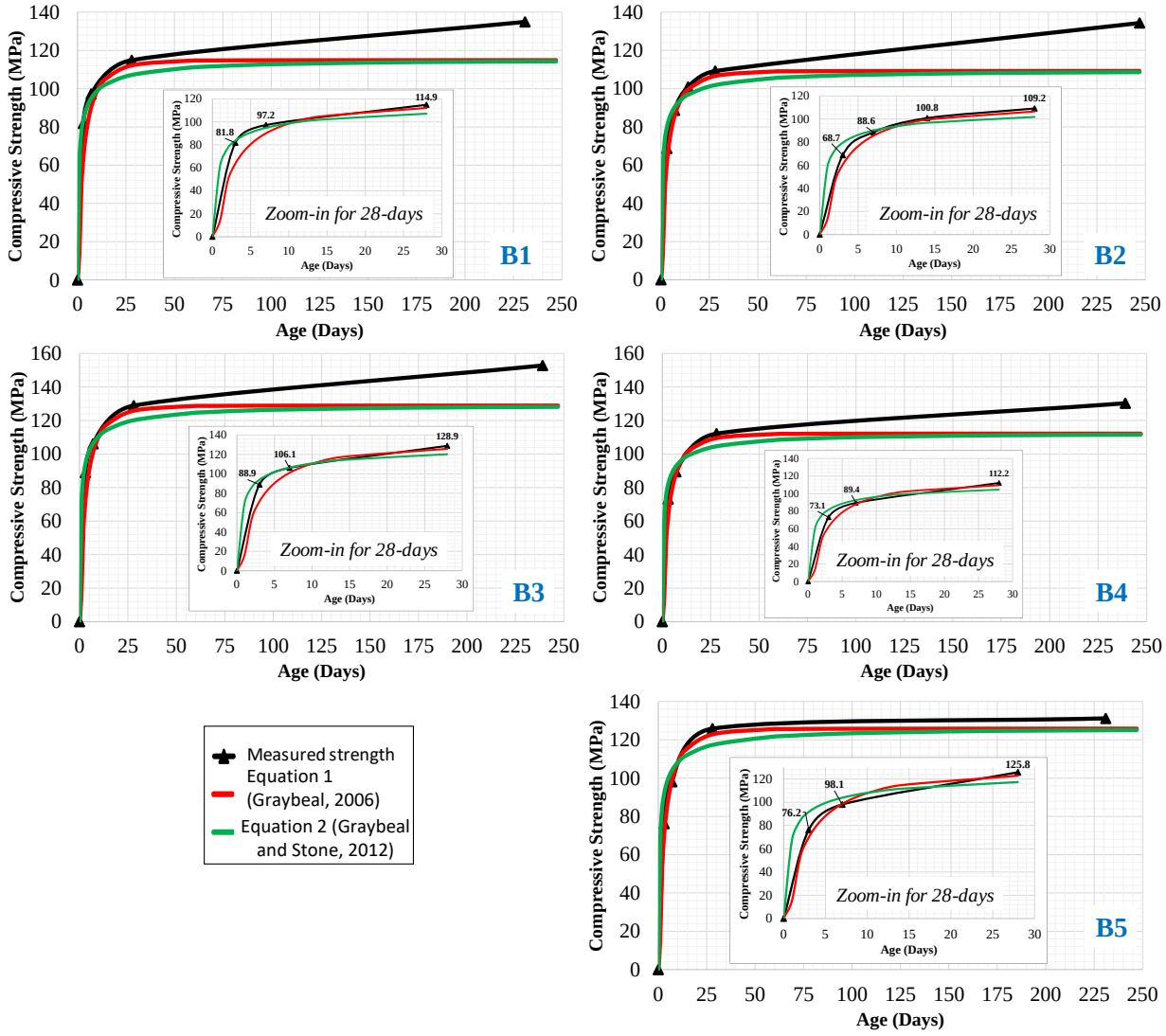

Figure 2-6: Compressive strength gain of NP-UHPC mixes in comparison with prediction equations (Graybeal, 2006; Graybeal and Stone, 2012).

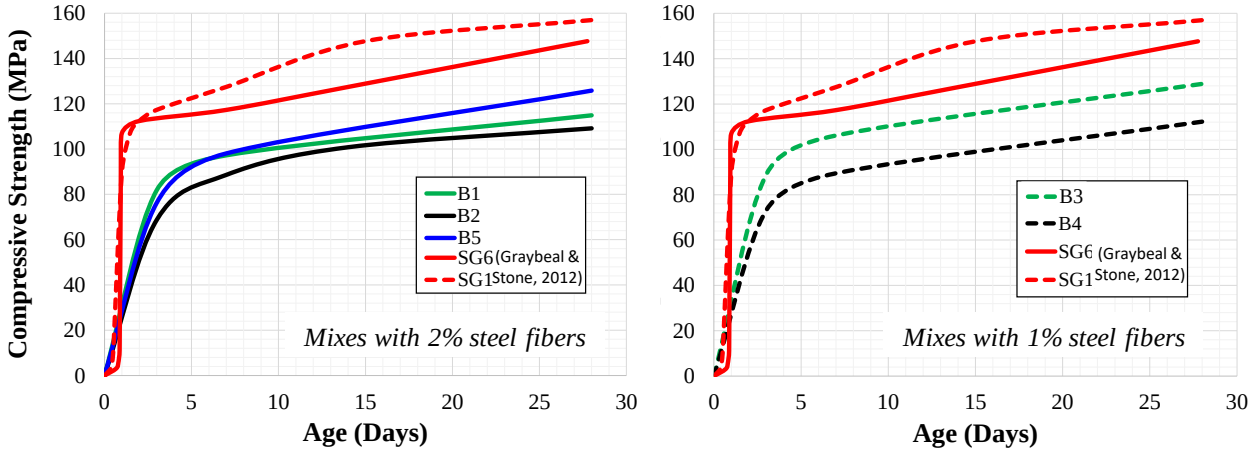

Figure 2-7: Compressive strength versus time for mixes with 2% (left) and 1% (right) steel fibers.

2.4.2.3 Full compression stress-strain behavior

The full compressive stress-strain behavior and elastic modulus of the NP-UHPC cylinders were determined according to the ASTM standards C469 (ASTM C469/C469M-14, 2014) along with ASTM C1856. It is noted that only few studies have reported full stress-strain curves for commercial UHPC (e.g. Naeimi and Moustafa, 2021), and much less even considered NP-UHPC. Thus, this study also fills a knowledge gap in this area by providing sufficient information about full compression and tension behavior of NP-UHPC, which is crucial for modeling (Joe and Moustafa, 2016; Naeimi and Moustafa, 2020) and future expansion of UHPC use. The curing and preparation of the test samples followed the same procedure used before for the compressive strength testing. The test samples were tested using the Tinius Olsen testing machine at ages between 231 and 247 days and fully instrumented using three displacement transducers (LVDTs) to determine the full stress-strain relationship of the different mixes. Figure 2-8 shows the test setup and instrumentation. The same loading rate of approximately 1 MPa/s was applied throughout all the tests.

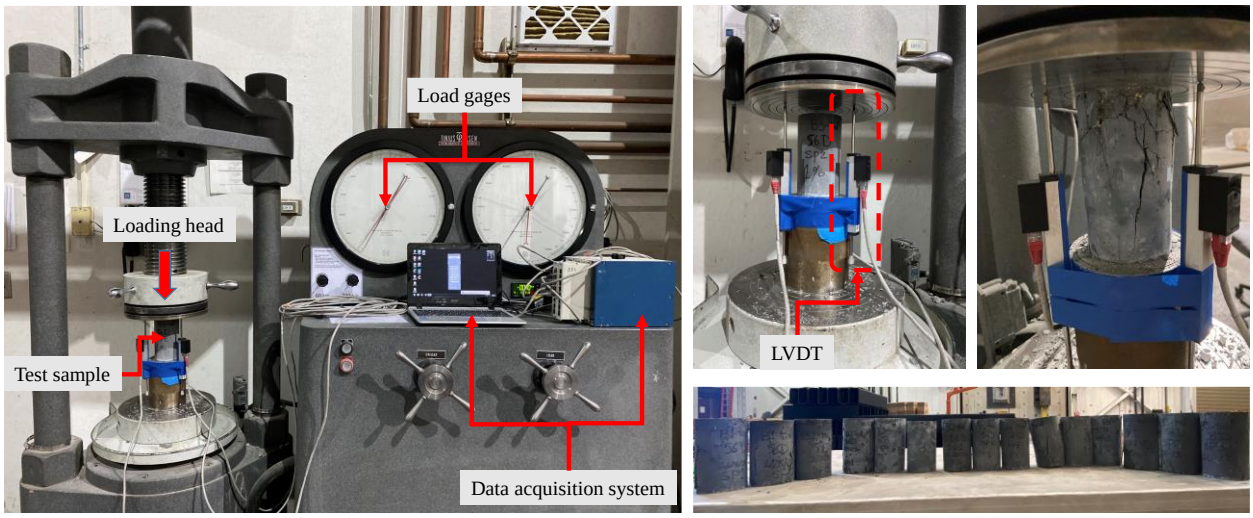

Figure 2-8: Test setup of the compressive stress-strain behavior test.

Figure 2-9 shows the average compressive stress-strain response of the developed NP-UHPC mixes in comparison to the previously proposed constitutive stress-strain equations (Equations 2-4 to 2-6 below) reported in the literature (Graybeal, 2007; Haber et al., 2018). The constitutive stress-strain relationship of the UHPC is determined based on the deviation from the linear elastic response as shown in Equation 2-4 (Graybeal, 2007).

$$f_c = \varepsilon_c E(1-\alpha) \quad (2\text{-}4)$$

$$\alpha = a\, e^{\frac{\varepsilon_c E}{b f_c'}} - a \quad (2\text{-}5)$$

$$\alpha = a \left(\frac{\varepsilon_c E}{f_c'}\right)^b \quad (2\text{-}6)$$

Where f_c is compressive stress; ε_c is compressive strain; E is modulus of elasticity; and α is linearity deviation parameter that is determined based on Equations 2-5 (Graybeal, 2007) or 2-6 (Haber et al., 2018). The linearity deviation parameter α usually varies depending on the different types of

UHPC and different curing regimes and is calculated based on the fitting parameters (i.e. *a* and *b*). Based on (Graybeal, 2007), the values for *a* and *b* for untreated regime are 0.011 and 0.44, respectively. However, (Haber et al., 2018) suggested Equation 2-6 for calculating α with values for *a* and *b* are 0.106 and 2.754 at 23 ºC, respectively, which was based on data from six different commercial UHPC products.

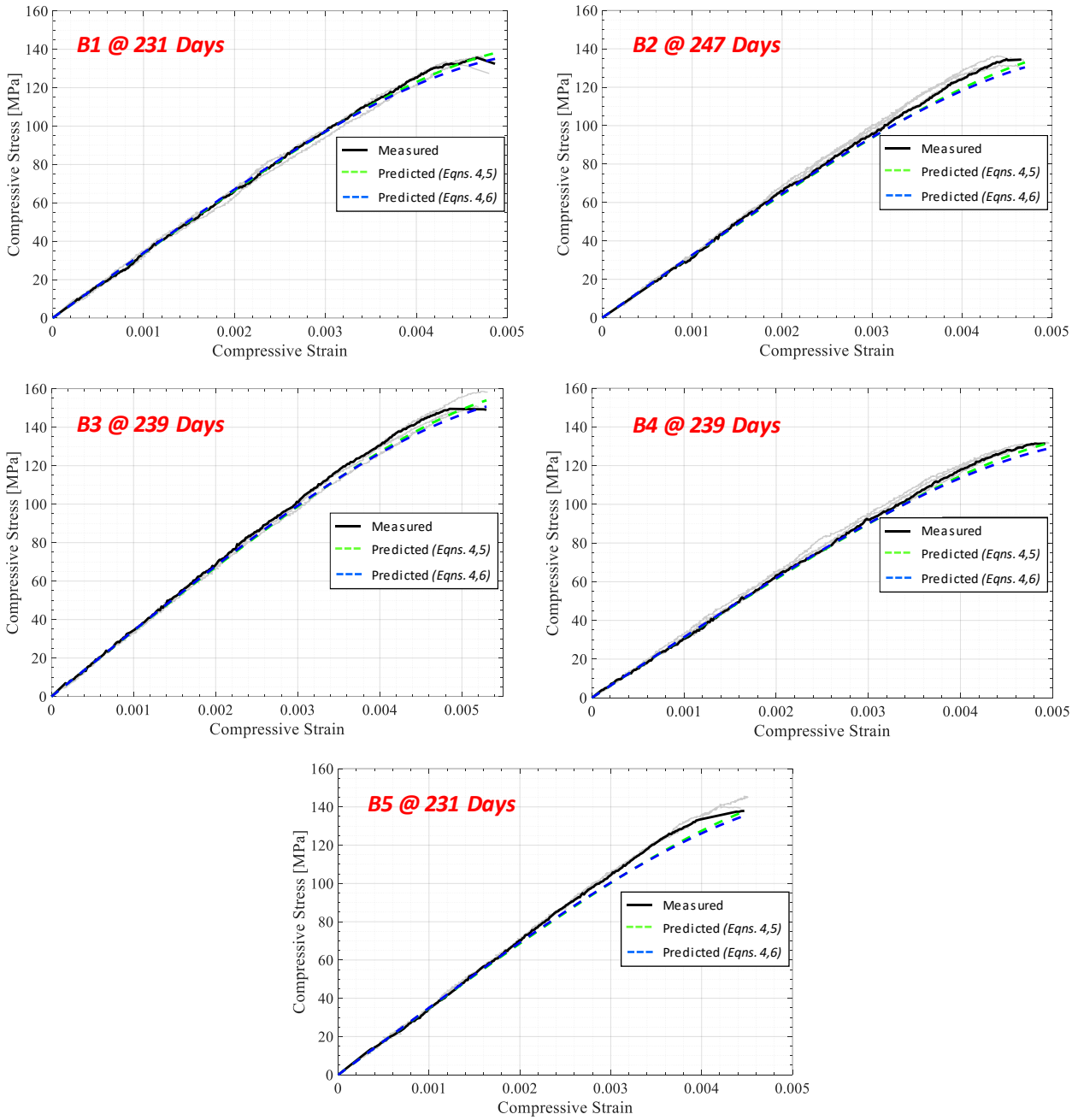

Figure 2-9: Compressive stress-strain relationships of the five tested NP-UHPC mixes.

As seen in Figure 2-9, the compressive stress-strain behavior of the developed mixes is almost linear up to approximately 50% of the maximum stress. A minor nonlinear response was observed

when approaching the failure of the specimens, which is consistent with FHWA previous studies (Graybeal, 2007). Moreover, the results from both equations are closely matching with the average response of the tested NP-UHPC mixes with slight underestimation of compressive strength prior to failure.

Figure 2-10 shows the average compressive strains measured at the peak stress of the NP-UHPC mixes. The measured strains at the peak of all the developed mixes are very comparable as they ranged from 0.00432 (B5) to 0.00512 (B3). It was also observed that the strains of B3 and B4 with 1% steel fibers were slightly higher than the rest of the mixes with 2% steel fibers. It is noted that the reported strains in Figure 2-10 are comparable to the range of the strains reported in the literature. For example, the strains at peak compressive stress for the six commercial UHPC products tested by (Haber et al., 2018) ranged between 0.00274 and 0.00524.

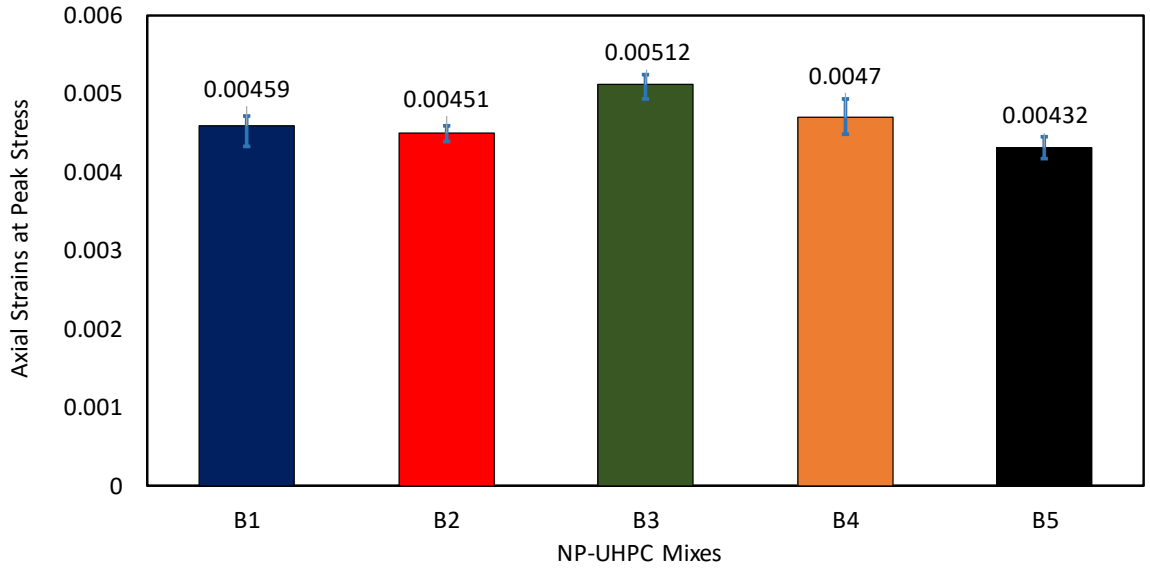

Figure 2-10: Average axial strains measured at peak compressive stresses.

2.4.2.4 Modulus of elasticity (E_c)

The compressive elastic modulus was calculated based on the linear best-fit approximation of the stress-strain relationship between 10% and 40% of the peak compressive stress. The relationship between the compressive strength and the elastic modulus of the UHPC has been previously investigated by many researchers and consistently reported as a multiplier of the square root of the compressive strength f_c'. (Graybeal, 2007) proposed a multiplier of 3,840 (when f_c' under the root is in MPa) based on results of commercial UHPC products. He also proposed another multiplier of 4,070 based on the results of a commercial rapid strengthening UHPC product (Graybeal and Stone, 2012). More recent work at the FHWA (Haber et al., 2018) provides a multiplier of 3,760 based on the results of six commercial UHPC products. It is noted that all these equations were developed for commercial UHPC products. Thus, it is of interest to check the validity of these equations for predicting the modulus of elasticity of the tested NP-UHPC mixes. Figure 2-11 shows the comparison between predications based on the various aforementioned equations, i.e. $E_c = 3840\sqrt{f'c}$ or $4070\sqrt{f'c}$ or $3760\sqrt{f'c}$ and the measured experimental values. The comparison

shows that all previously developed equations extensively overestimate the modulus of elasticity of the NP-UHPC mixes. Hence, a new equation is proposed herein to better estimate the modulus of elasticity of NP-UHPC as $E_c = 2{,}860\sqrt{f'c}$ (for f'_c in MPa). The results from the new proposed equation are also listed in Figure 2-11 for comparison.

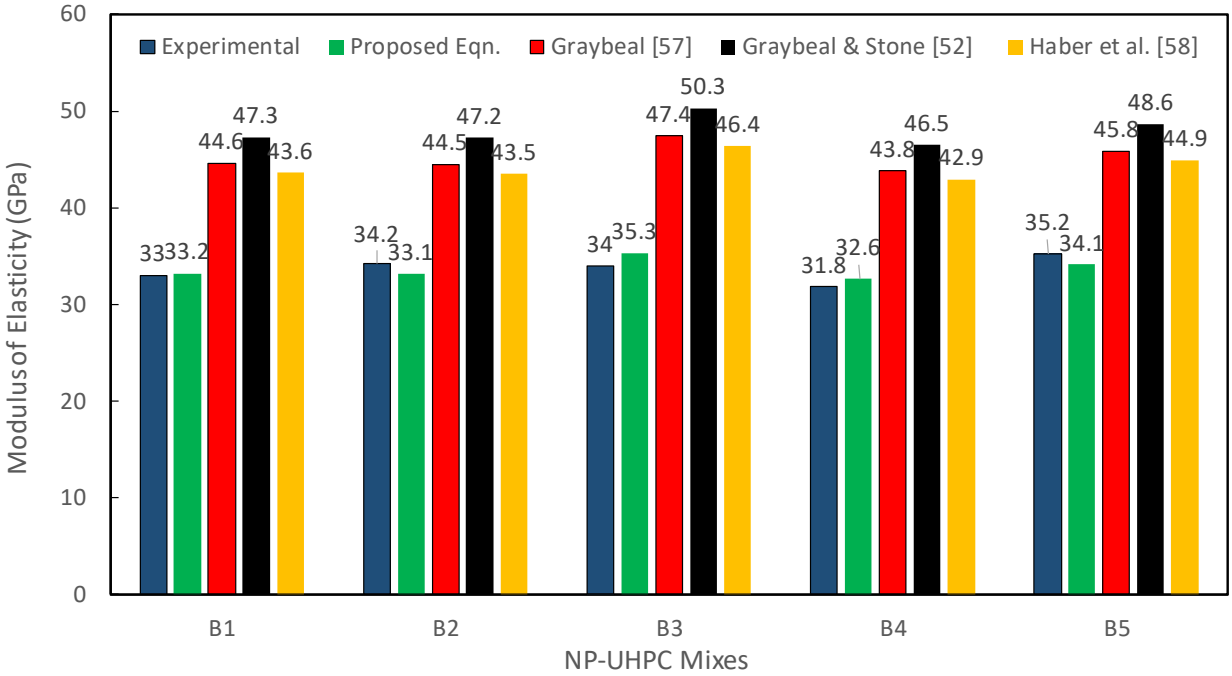

Figure 2-11: Measured modulus of elasticity for the various NP-UHPC mixes and comparison against different predictions using selected equations from the literature and a new proposed equation.

2.4.3 Flexure Tests

Due to importance of characterizing the UHPC tensile behavior, several methods have been used such as flexure tests, splitting tension tests, and direct tension tests. Ongoing research efforts in the US is aiming at developing a future standard direct tension test exclusive for UHPC. However, until such test methodology is established, standard flexure tests along with non-standard direct tension tests are commonly considered for UHPC, which were both done in this study and reported in this section and the next one, respectively. The ASTM C1856 recommended testing UHPC prisms according to the ASTM C1609 to determine the flexural strength.

2.4.3.1 Test procedure and specimens preparation

Flexural strength tests were conducted on 76 × 76 × 280 mm prisms with a 229 mm simple span. The loads were applied at third points according to ASTM C1609 (ASTM C1609/C1609M-07) along with ASTM C1856. An Instron testing machine with a maximum capacity of 250 kN was used to test the NP-UHPC samples at age of 7 and 28 days as well as other later ages dictated by COVID-19 related laboratory shutdown and operation resumption. A sampling rate of 10 Hz was used to collect data from the tests. The load was controlled by the mid-span displacement of the specimen. A displacement rate of 0.076 mm/min was used up to 0.254 mm mid-span vertical displacement, then the rate was increased to 0.127 mm/min until the end of a given test. The mid-

span deflection of the beams was measured using a laser extensometer device. The laser extensometer reads the extension between two fixed laser targets as one target was attached at the middle of the beam and the other was attached at a fixed point over the bending table as shown in Figure 2-12. The curing of the test specimens followed the same procedure used for the compression cylinders where the prisms were covered with plastic sheets and left in the fabrication site for one day after casting. Then, the samples were demolded on the second day and left to cure on 73 ^{o}F (~ 23 ^{o}C) up to the testing day. The bending prisms do not require special preparation or grinding as the prisms were aligned on their flat sides during the flexure testing.

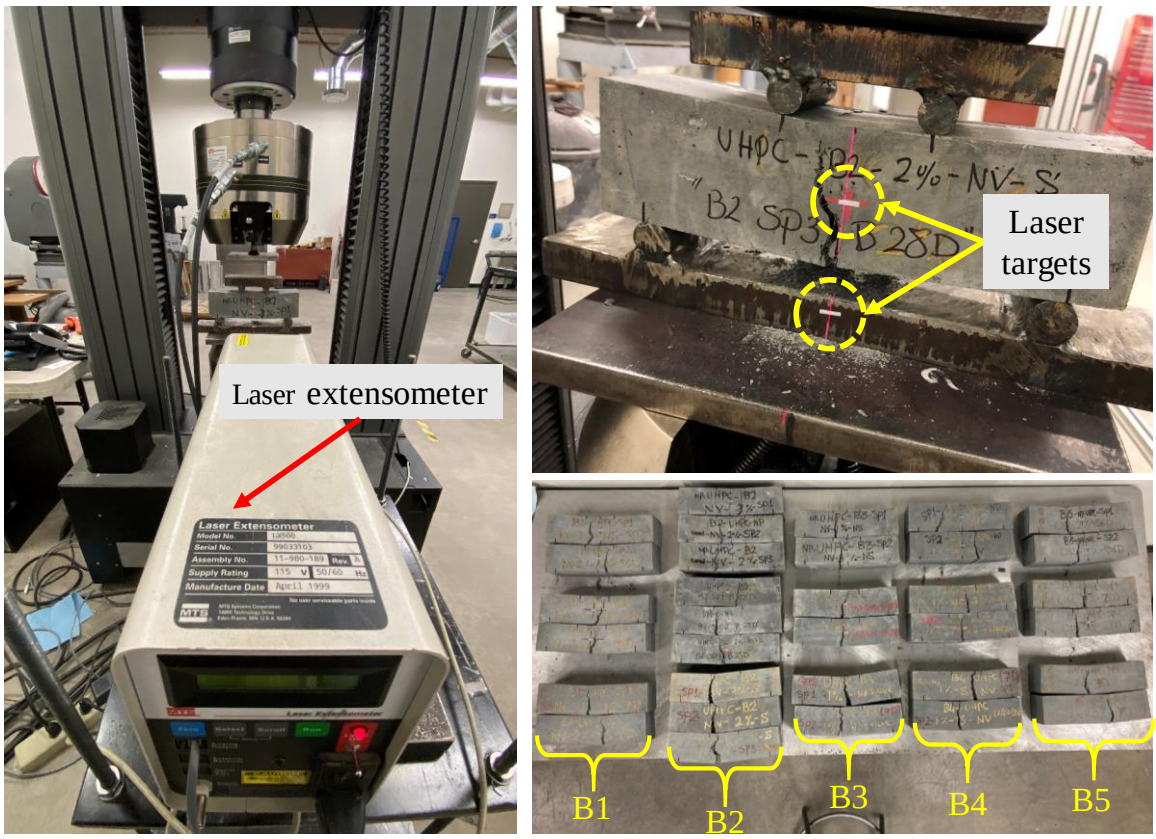

Figure 2-12: Flexural testing and instrumentation of the NP-UHPC prisms.

2.4.3.2 Flexural strength

The flexural strength measured at different ages for the NP-UHPC mixes is shown in Figure 2-13. The flexural strength of the specimens was calculated based on the maximum bending moment and the final beam dimensions after testing assuming a linear-elastic behavior. The results of the flexural strength confirm that the NP-UHPC mixes with 2% steel fibers have higher flexural strengths than that of the mixes with 1% steel fibers as expected. The use of half the amount of steel fibers (i.e. 1% versus 2%) has led to a reduction of the 28-day flexural strength of about 12% and 31% for the NP-UHPC mixes with sieved and non-sieved sand, respectively. As seen in Figure 2-13, the flexural strength of B5 is very comparable to that of B1 and B2 and the difference between all the results is within 15% only. Hence, it can be concluded that the flexural strength of the proposed NP-UHPC mixes with 2% steel fibers is only slightly affected by the change in

material sources. B1 with non-sieved sand had a higher early flexural strength compared to B2, while the flexural strength of B2 exceeded that of B1 at later ages. This was anticipated because the NP-UHPC mixes with fine particle gradation usually require more time for the hydration process to gain strength compared to the mixes with coarse sand. B3 had a lower flexural strength than B3. Thus, it can be concluded that using coarse sand may slightly decrease the flexural strength of the NP-UHPC mixes because of the less homogeneity of the fibers as they may accumulate around the bigger sand particles as previously shown in the flow test photos in Figure 2-4. The flexural strength of the NP-UHPC mixes reached approximately 90% of the 28-days strength after one week and then slightly increased by only 10% between 28 and about 235 days age.

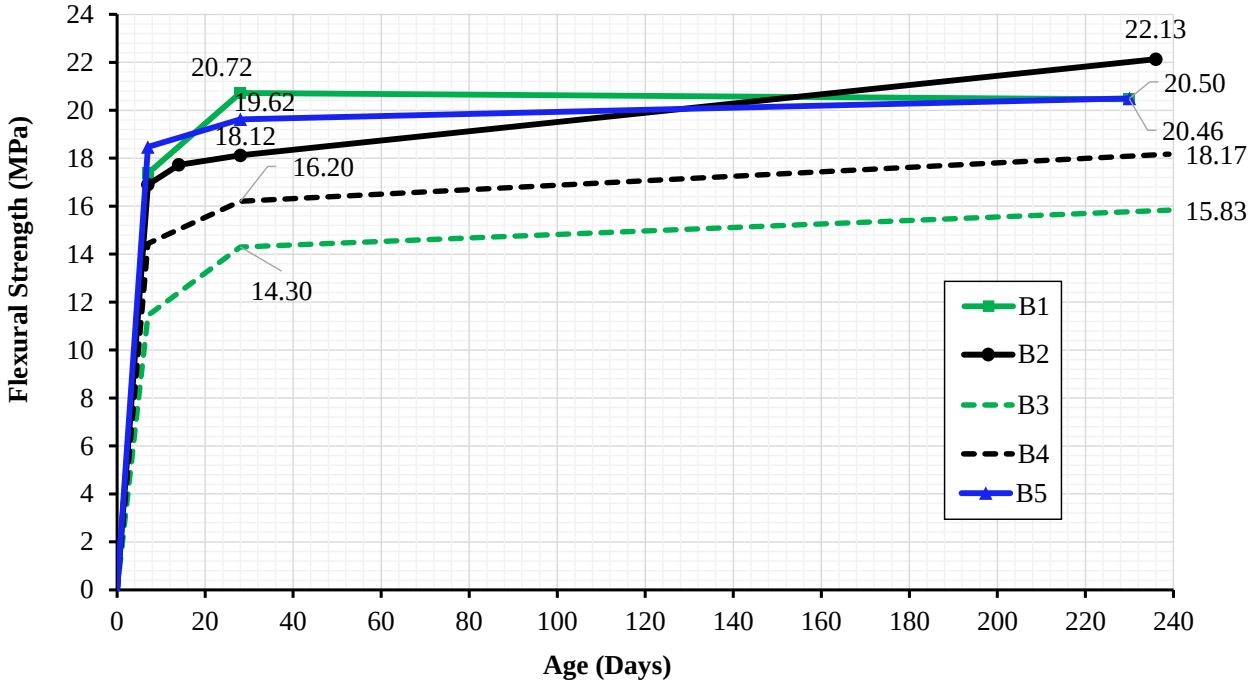

Figure 2-13: Flexural strength versus time for the NP-UHPC mixes.

2.4.3.3 Flexural behavior

The relationships between the flexural stress and the middle deflection of the NP-UHPC prisms are shown in Figure 2-14 for the different ages. The flexural behavior of NP-UHPC beams was linearly elastic up to the initiation of the first crack at approximately 50% of the flexural strength. Then, more micro-cracking took place leading to a slight inelastic behavior. During this stage, the composite action of the steel fibers that bridge across the cracks has led to sustained strain hardening and more ductile behavior through failure. The NP-UHPC prisms reached their peak strength after the propagation of significant cracking across the weakest section at the middle third of the beam. Afterwards, a gradual decline in strength was observed due to the pullout of the steel fibers. The flexural behavior of all the NP-UHPC mixes is very comparable and they all feature sustained strain hardening without brittle or sudden failure. This indicates that the use of sieved or non-sieved sand does not affect the full range of flexural behavior. It is also noted that as the age

increases, the flexural strength increases but the sustained load capacity at the peak load decreases, and the rate of the decline in strength through failure would slightly increase.

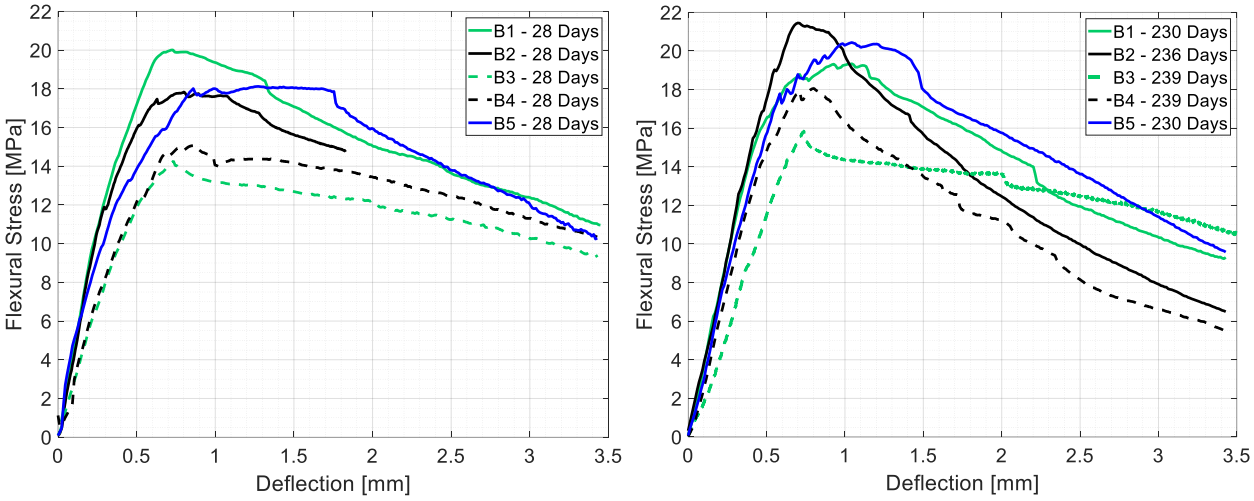

Figure 2-14: Flexural stress versus middle deflection for the NP-UHPC prisms tested at different ages.

2.4.4 Direct Tension Test

Although flexure tests are more convenient, they still overestimate the actual tensile strength of UHPC because of the non-uniform stress distribution across the beam and the dependence on boundary conditions or prism dimensions. Hence, it is more essential to determine the exact tensile strength of UHPC in general, and the NP-UHPC for this study as well, using direct tension testing. Dog-bone shape specimens have been commonly used for direct tension tests with varying dimensions and sizes. The tensile stress distribution over the reduced cross-section of the dog-bone specimen is more uniform compared to the flexural prisms. The direct tensile strength and full stress-strain behavior of the NP-UHPC mixes were investigated and reported in this section. Because of the lack of standard test procedures for the direct tensile testing of UHPC, many studies in the literature have recommended testing of different specimen shapes and sizes under different loading procedures to capture the post-cracking tensile behavior of the UHPC. However, due to the convenience of simpler tests like flexure, other studies have established correlations between the flexural and tensile behavior of UHPC such as a recent FHWA study (Graybeal and Baby, 2019).

2.4.4.1 Test procedure

The direct tensile strength of the NP-UHPC mixes was determined based on testing of dog-bone shaped samples with a nominal cross-section at the reduced section of 2.54 cm × 2.54 cm dimensions. The length of a typical specimen is 28 cm with a gauge length of 6.35 cm. Instron testing machine was used to test the samples at 7 and 28 days. A sampling rate of 50 Hz was used to collect the data of the test. A displacement-controlled loading rate of 0.127 mm/min was used throughout most of the test up to the post-peak drop to 90% of the observed peak load, then the displacement rate was increased to 1.27 mm/min until the test was terminated. The tensile strains were captured during the test using a laser extensometer device that typically reads the extension

between two shiny targets attached at the end of the reduced section of the dog-bone specimen. Figure 2-15 shows the direct tension test setup for one of the dog-bone specimens tested at UNR. Note that all dog-bone specimens were fabricated using plastic molds and cured following the same procedure as flexural and compression test specimens.

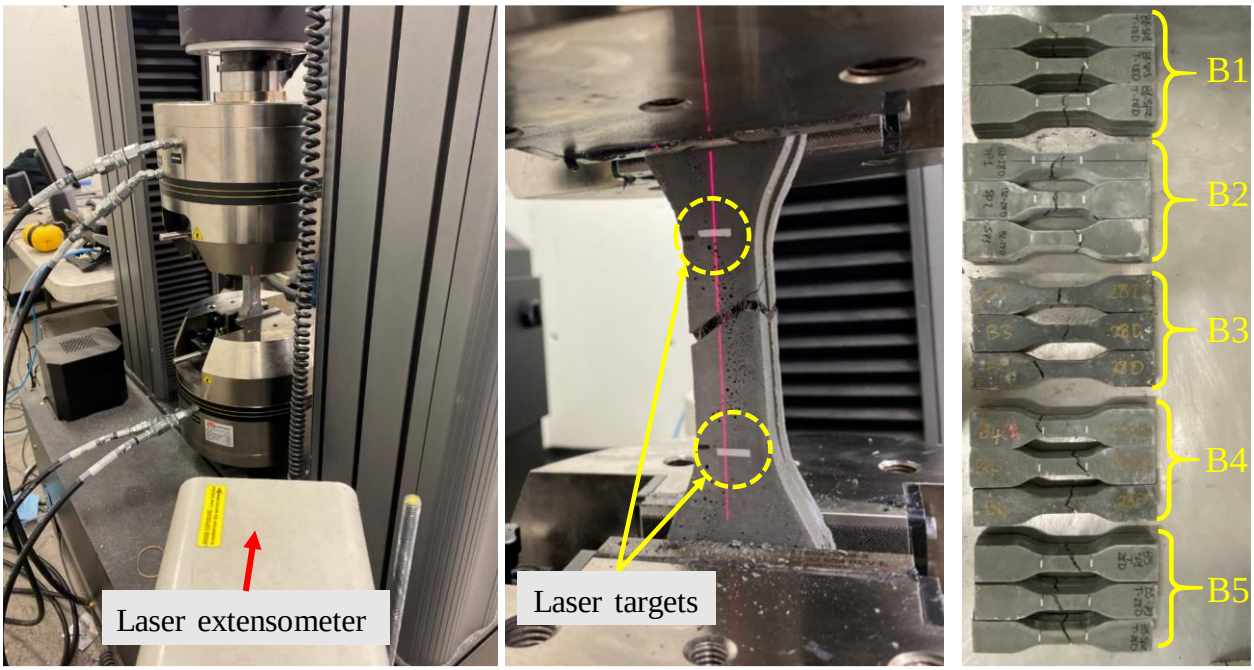

Figure 2-15: Direct tension testing of NP-UHPC dog-bone specimens.

2.4.4.2 Tensile strength

The relationships between the direct tensile strength versus the age for the different NP-UHPC mixes are shown in Figure 2-16. The results show that B2 has the highest tensile strength while B3 has the lowest tensile strength among all the proposed mixes. The use of 1% steel fiber amount in B3 instead of the 2% used in B1 has resulted in a decrease in the 28-days tensile strength by approximately 15%. B4 also had 28% less 28-day tensile strength than that of B2. It is also noted that the change in the material sources between mixes B2 and B5 has resulted in a slight increase in the 28-days tensile strength of about 10%. Hence, it is possible to replicate the mixes using different material sources without severely affecting the tensile strength of the material. At 28 days, it is indicated that the use of non-sieved sand instead of the fine sieved sand has resulted in less tensile strength of the mixes for both 1% and 2% steel fiber cases. This behavior is consistent with the results from the flexural tests and attributed to the homogeneity and dispersion of the steel fibers across the cross-section.

2.4.4.3 Tensile behavior

Robust UHPC mixes exhibit a high tensile capacity and sustained post-cracking strength, which is desired to verify for the emerging NP-UHPC mixes used in this study. Many research efforts that focused on the tensile behavior of UHPC (e.g. Graybeal and Baby, 2019) suggest that the tensile behavior of UHPC can be idealized and divided into four regions of behavior. The first region is

the linear elastic behavior before the initial cracking. The second region indicates the initiation of non-linearity through the multi-cracking. The third region is the crack straining which includes the engagement of steel fibers in carrying the internal tensile forces between the cracks and this behavior is usually called bridging action. The last region is mainly the failure or the crack localization and this is usually associated with the pullout of the steel fibers. The tensile stress-strain relationships for the NP-UHPC mixes at 7 and 28 days are shown in Figure 2-17. The results indicate that all the NP-UHPC mixes exhibited the desired prolonged and ductile behavior through failure. The 28-days tensile behavior of B2 and B5 are very comparable, which is an important conclusion again that the tensile behavior of the NP-UHPC mixes is not dependent on the variation of the material sources.

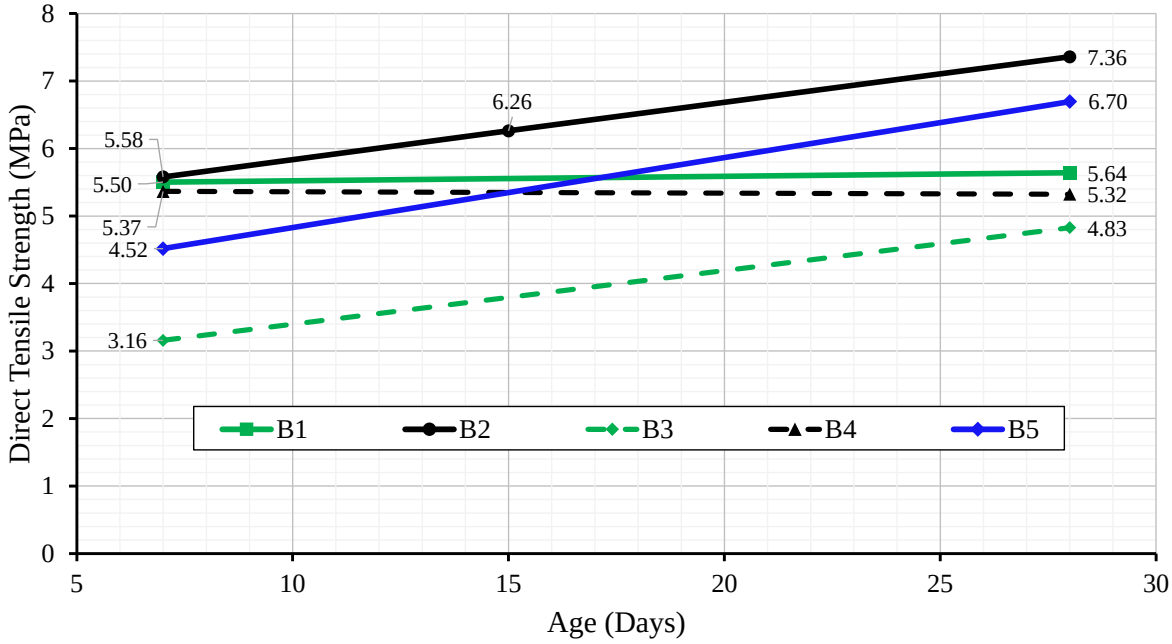

Figure 2-16: Direct tensile strength versus time of the NP-UHPC mixes.

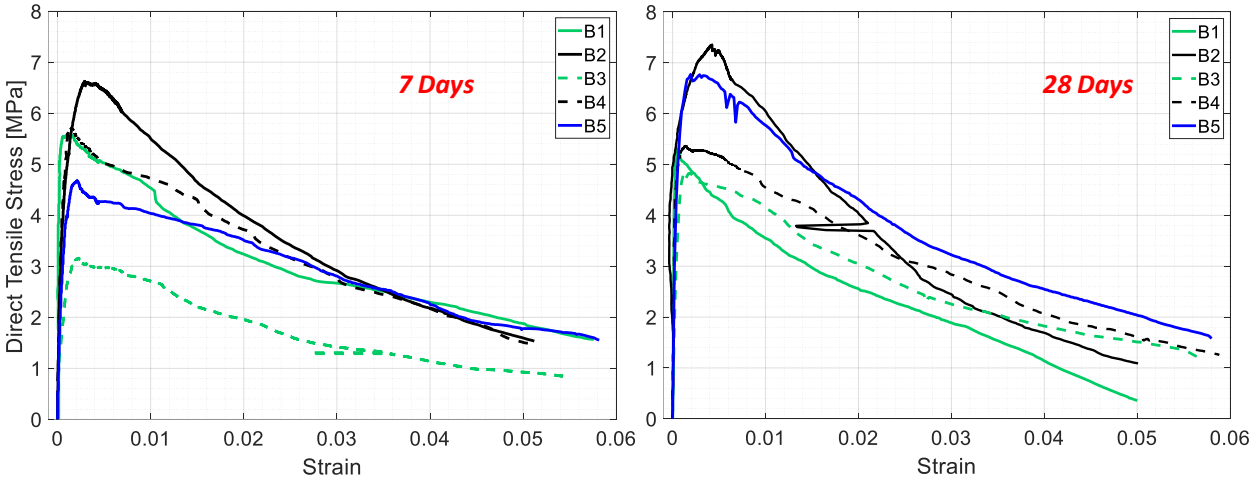

Figure 2-17: Direct tension stress-strain relationships of all NP-UHPC mixes tested at 7 and 28 days.

2.5 Summary

This chapter presented the implementation of an emerging class of NP-UHPC for ABC field joints. The ABC-UTC NP-UHPC mix has been designed at OU and this part of study investigated the repeatability and reproducibility of a baseline mix using local materials from Western US. The NP-UHPC mixes using Western US materials have been successfully tested in transverse and longitudinal bridge deck joints, which motivated this study to provide mechanical characterization and behavior relationships that can be used for future modeling and larger applications. A total of five NP-UHPC mixes have been considered to investigate the effect of varying material sources as well as aggregate types and nominal sizes on the main mechanical properties. The flow properties of the developed mixes were tested and compared with the recommended flow values. Moreover, different sets of testing were conducted on the developed mixes to test the compressive, flexural, and direct tensile strength and full behavior of the different NP-UHPC mixes. The results reported in this chapter provide guidance for bridge and field engineers and researchers to further replicate the proposed NP-UHPC mixes by establishing the baseline mechanical properties for assessment and modeling.

3. Experimental Testing: Transverse Field Joints

3.1 Introduction

Cast-in-place (CIP) construction techniques have been widely used for many years in construction of the bridge decks around the nation. The reason for the wide implementation of these CIP systems was because they are relatively cheaper than other systems and easier to construct. However, these systems showed lack of performance, degradation in strength and less durability after spending many years in service. As a result, nearly 56,000 US bridges are considered in poor condition on the records of the American Road and Transportation Builders Association (ARTBA, 2020). Since that bridge decks deteriorate faster than the other bridge components, more than $8 billion are spent annually on repairing or replacing these deteriorated decks (ARTBA, 2020). Approximately 85% of the US daily commuters travel on state-owned bridges, which makes it more difficult to use the traditional construction techniques or cast-in-place (CIP) methods in the replacement or rehabilitation of the deteriorated decks. This has paved the way to a wider implementation of the prefabricated construction techniques to accelerate the deck erection. Prefabricated bridge decks (PBES), which is one of the accelerated bridge construction (ABC) applications, can enhance constructability issues, offer higher quality, provide accelerated and safer construction, and minimize traffic disruption. The prefabricated bridge deck elements are usually connected on-site using field joints. These joints can be classified into two main types. Transverse joints that run perpendicular to the traffic flow direction and longitudinal joints that run along the longitudinal axis of the bridge, i.e. parallel to the traffic direction. Figure 3-1 shows both field joint types in a typical precast bridge deck system.

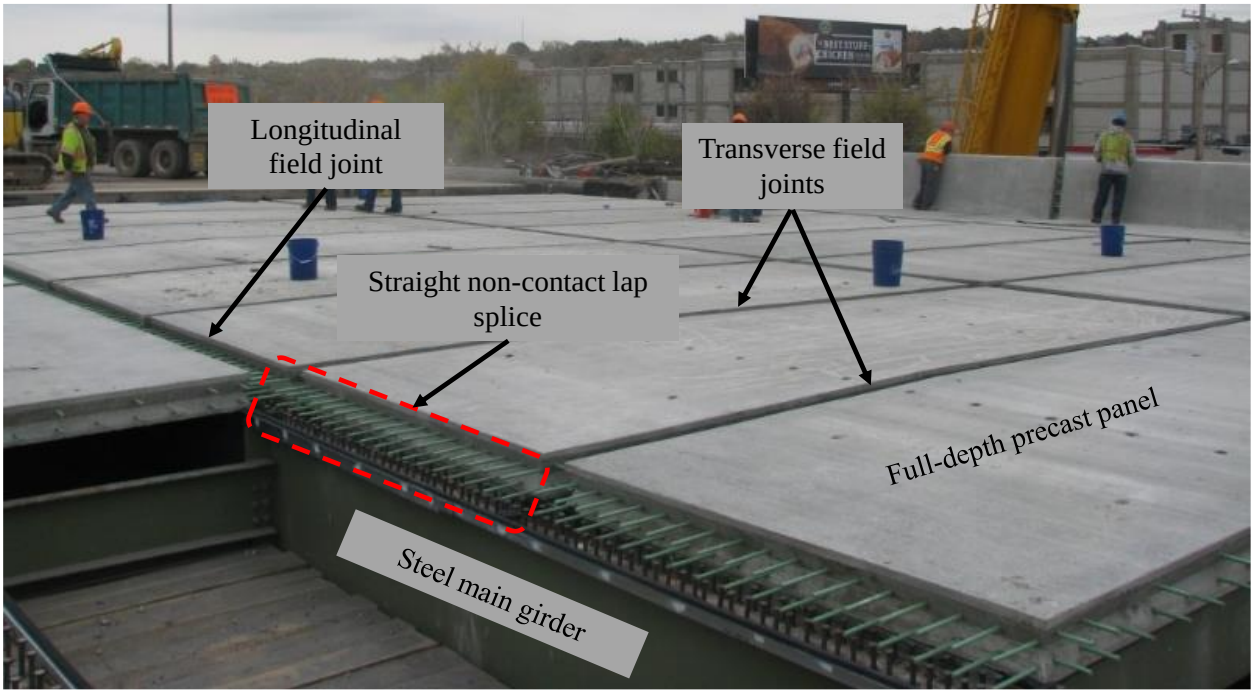

Figure 3-1: Types of field joints in a typical prefabricated bridge deck system.

Currently, ultra-high performance concrete (UHPC) has gained a great significance and reputation as a bridge deck joint material. Many research studies demonstrated that the ideal UHPC field joint has a diamond-shaped shear key, 15.2–20.3 cm joint width and traditional straight or loop splices. These typical joint details are sufficient in transferring shear and bending across the prefabricated deck elements (Graybeal, 2010 a; French et al., 2011; Perry et al., 2014; Sritharan et al., 2012). However, the use of UHPC comes with several challenges. First, the commercial UHPC products are very expensive as they are 20 times more expensive than conventional concrete. Nonetheless, UHPC is proprietary and it is only supplied by limited number of suppliers. This often limits state DOTs that are trying to avoid sole-sourcing among other bidding issues to use UHPC. Hence, there is a growing interest from various state DOTs and research agencies in developing non-proprietary UHPC (NP-UHPC) mixes to be used for different bridge applications. These research efforts have sought to make UHPC more accessible and less expensive through using the local available materials in the NP-UHPC mixtures (Qia et al., 2016; Graybeal, 2013; Aboukifa et al., 2020; Aboukifa et al., 2021; Berry et al., 2017; Alsalman et al., 2017; Willie et al., 2011). One major contribution to this field of study is the recent research work done by the five consortium universities within the ABC university transportation center (ABC-UTC) in the US (Abokifa and Moustafa, 2021; Shahrokhinasab and Garber, 2021). As mentioned earlier, OU has led this project by developing the mix design and material testing of the baseline NP-UHPC mix (Looney et al., 2019). The information regarding the base line mix design was shared with the other universities to examine the viability of using this NP-UHPC mix in various ABC applications. The experimental work covered in this study, which was part of this wider collaboration project, was conducted by the University of Nevada, Reno (UNR). The main role for UNR in this project was to extend the use of the shared NP-UHPC mix design to develop NP-UHPC mixes using locally available materials in Nevada (NV) and California (CA). Then, conducting experimental testing of full-scale precast bridge deck panels connected using transverse and longitudinal field joints which was filled with the developed NP-UHPC mixes. This chapter only covered the experimental results of the transverse joint specimens to provide a detailed discussion of the structural behavior and analysis of the joint performance.

As previously mentioned, the overall objective of this part of study is to investigate the structural performance of the prefabricated deck elements with NP-UHPC transverse filed joints. Other objectives of this part of study included engineering and optimization of the NP-UHPC mixes and joint details to provide efficiently equivalent systems at a cheaper cost. The engineering solutions used in this study included the optimization of the amount of steel fibers in the NP-UHPC mixes, varying the joint width, using different joint splices, and varying the distribution of the overlapped reinforcement. Three full-scale specimens were experimentally tested in this part of study under static vertical loading. This chapter includes several sections that present a discussion of the development of the mix, results from a similar precedent study, details of the experimental program, test results and discussion, and summary.

3.2 Reference Specimen with P-UHPC Joint

This section provides detailed information about the experimental test results of a similar bridge deck specimen with proprietary UHPC (P-UHPC) transverse field joint. This test specimen (i.e.,

reference specimen) was tested by the authors in a precedent study (Abokifa and Moustafa, 2021; Abokifa et al., 2020), while the main test results obtained from this reference specimen are shown in this section to allow for further comparisons with the NP-UHPC specimens which were tested in this study.

As mentioned earlier, the reference specimen was tested as a part of a comprehensive experimental study which included testing of five large scale bridge deck specimens with transverse and longitudinal field joints. The main aim of this precedent study was to compare and investigate the structural performance of bridge deck specimens with polymer concrete and P-UHPC field joints (Abokifa and Moustafa, 2021; Abokifa et al., 2020). The reference specimen has an overall planar dimensions of 2.44 * 2.74 m and a thickness of 20.3 cm. A P-UHPC transverse field joint, which has a width of 15.24 cm and diamond shaped shear key, is located at the middle of the specimen. The details of the P-UHPC joint was proposed based on real bridges practical implementations and results of many research projects. These typical joint details have been demonstrated to develop sufficient shear and bending capacities to provide integrity between the joined deck panels. The design details of this reference specimen is typical to that of the first specimen which is tested in this study. The specimen was simply supported and loaded at mid-span with static vertical load. The results of the load versus mid-span deflection relationship of the reference specimen is shown in Figure 3-2 a. Figure 3-2 b shows the load versus the reinforcement strain readings of the bottom transverse bars (i.e., main reinforcement) of the P-UHPC specimen. The results shown here will later be used for the comparison and assessment of similar specimens with NP-UHPC transverse specimens.

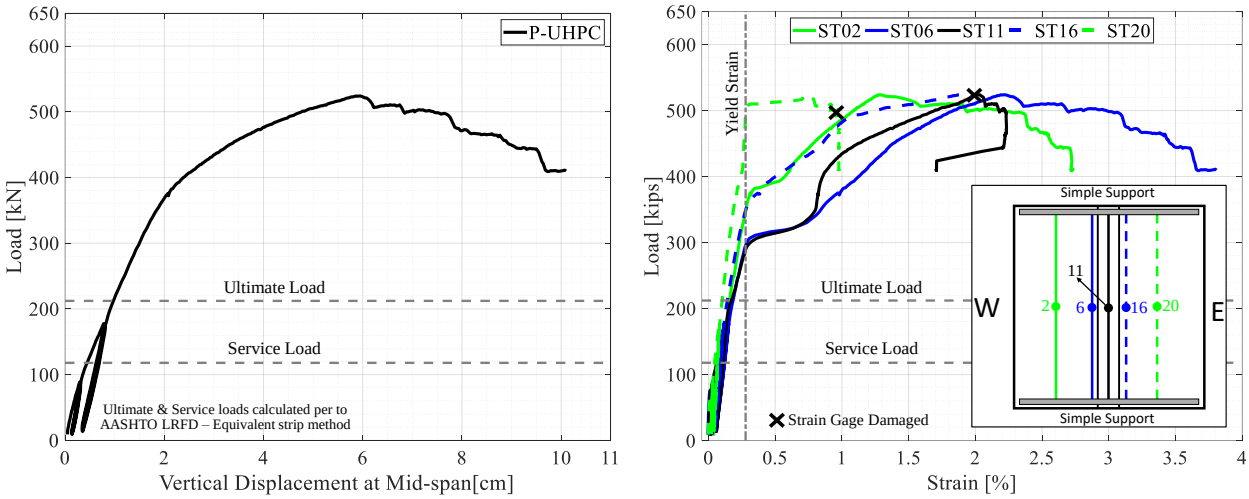

Figure 3-2: Experimental test results of the reference P-UHPC specimen: (a) Load versus mid-span deflection; (b) Load versus tensile strains at the middle of the bottom transverse reinforcement.

The peak load capacity of the reference specimen was 524.5 kN at which 5.92 cm mid-span vertical displacement was measured. The failure of the specimen was dominated by flexure as it included yielding of the main reinforcement followed by the crushing of concrete at the top of the precast panels. It was observed that no interface cracks or bond slippage has happened up to the peak load capacity of the specimen. Moreover, the specimen has remained essentially elastic in which no

reinforcing bars has yielded up to the AASHTO LRFD ultimate load level as shown in Figure 3-2 b.

3.3 Experimental Program

This section provides information regarding the design and structural details of the test specimens, fabrication process, experimental test setup, loading methodology, and instrumentation plan.

3.3.1 Specimens Design and Test Matrix

The experimental program presented in this section included testing of three full-scale bridge deck specimens with transverse NP-UHPC field joints. Each specimen consists of two precast deck panels which were cast using conventional concrete with specified compressive strength of 34.5 MPa. The precast panels were joined together in the transverse direction of the bridge (i.e., perpendicular to the direction of motion of traffic) using NP-UHPC full-depth field joints. Each panel has a protruded longitudinal reinforcement which was spliced at the field joint location to provide continuity of load transfer across the panels. The experimental program included testing of different parameters such as different types of reinforcement splices, splice lengths, joint materials, and reinforcement configurations. While all specimens have the same overall dimensions and top and bottom transverse reinforcement (i.e., main reinforcement). Non-contact lap-splices were utilized in this study, but they vary in their length and type. Table 3-1 shows the test matrix and test variables of three tested specimens in addition to the P-UHPC reference specimen which is referred by as "S0".

Table 3-1: Experimental test matrix and specimen design details

Specimen Name	Transverse Reinforcement		Longitudinal Reinforcement		Field Joint Material	Lap Splice type	Lap Splice Length (cm)
	Top	Bottom	Top	Bottom			
S0	#16 @ 17.8cm	#16 @ 17.8cm	#13 @ 38.1cm	#16 @ 25.4cm	P-UHPC 2%	Straight	12.7
S1-Str-2%			#13 @ 29.6cm	#16 @ 25.4cm	NP-UHPC 2%	Straight	12.7
S2-Lop-2%			#13 @ 17.8cm	#13 @ 17.8cm	NP-UHPC 2%	Loop	11.4
S3-Str-1%			#13 @ 29.6cm	#13 @ 17.8cm	NP-UHPC 1%	Straight	17.8

Abbreviations; Str: Straight splice, Lop: Loop splice.

The first specimen "S1-Str-2%" has a straight splice with 12.7 cm length, while the second specimen has a loop splice with 11.4 cm length. The loop splice can provide less splice length compared to the straight splice because of the bearing effects at the bend. The use of loop splices inside the field joints was shown to provide a better joint performance and better load transfer across the precast panels (Abokifa et al., 2020). A smaller bar diameter (i.e., #13 versus #16) has been selected for the longitudinal reinforcement of specimen "S2-Lop-2%" to accommodate the bend diameter requirements in the ACI 318 provisions (ACI, 2008). The NP-UHPC mixes, which were used in both specimens, have a 2% (i.e., by volume) steel fibers amount.

As mentioned earlier, one of the objectives of this part of study is to engineer and optimize the materials in the field joints. Hence, a NP-UHPC mix with only half the amount of steel fibers (i.e., 1%) was used for the third specimen "S3-Str-1%". This was mainly done to reduce the cost of the material as the steel fibers is the most expensive component in the NP-UHPC composition. On the other side, the authors has proposed an increase of the lap splice length of this specimen by 40% to be 17.8 cm. This increase in the splice length was suggested to compensate for the expected lower strength of the NP-UHPC with 1% steel fibers compared to that of the 2% steel fibers which may require a slightly longer development length. The bottom longitudinal reinforcement of specimen "S1-Str-2%" includes #16 bars which were spaced at 25.4 cm. The authors have also suggested to use the same amount of steel for the bottom longitudinal reinforcement of the third specimen while using #13 bars at 17.8 cm spacing. The choice of using a smaller bar diameter has resulted into narrower spacing between the reinforcement inside the joint which was proved to enhance the field joint performance and overall load distribution over the specimen (Abokifa et al., 2020). In summary, the joint material of the third specimen was optimized to include only half the steel fibers amount. While the splice length was increased and the spacing of the bottom longitudinal reinforcement was decreased to compensate for the lesser strength of the NP-UHPC.

The design of the specimens has followed the same design provisions of the cast-in-place (CIP) bridge decks in the AASHTO LRFD Bridge Design Specification (AASHTO, 2014). This design procedure does not account for the deck discontinuity and the field joint effects. The moments demands were calculated based on the AASHTO equivalent strip method. This method takes into account the largest moment values imposed on the bridge decks from the numerous live loading conditions. The cross-section of the bridge example used to design the test specimens has five steel girders spaced at 3.65 m on center and a 20.3 cm thick concrete deck slab. A grade 60 reinforcing steel has been used for the reinforcement of the test specimens. The precast deck panels has a 2.54 cm and 5.08 cm bottom and top concrete covers, respectively. To facilitate the bridge deck erection and casting of the joints, non-contact lap splices, which were arranged in a staggered formation, have been used inside the joint. No adhesive coatings or surface preparation have been used for the surface of the diamond shaped shear keys. This was done mainly to examine the weakest possible interface between the joint and the panels and to minimize the time and labor required for this task in the real field implementations. All specimens has a general outside concrete dimensions of 2.74 m x 2.44 m x 20.3 cm. The structural design details of all test specimens are shown in Figure 3-3.

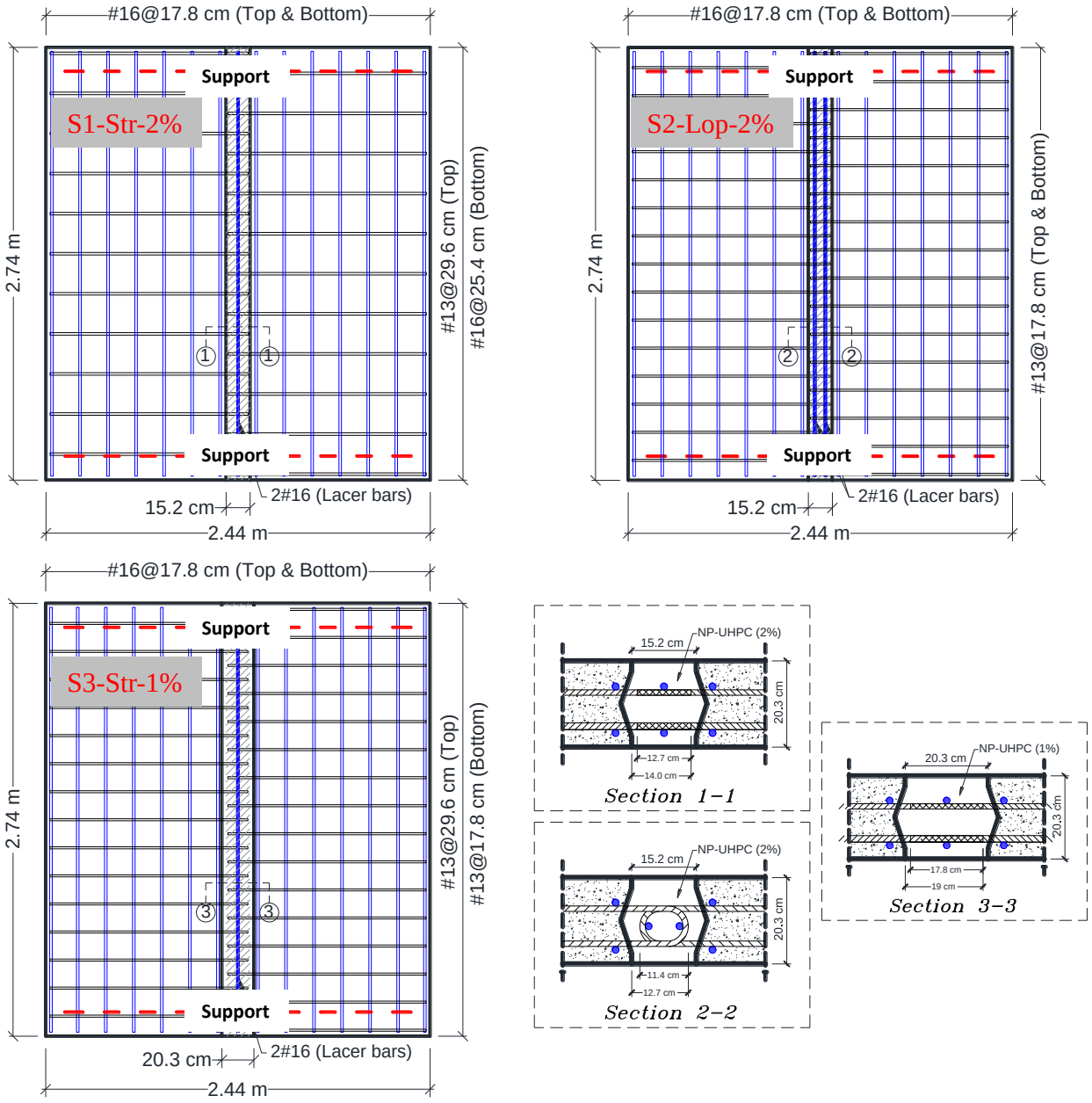

Figure 3-3: Overall dimensions and structural design details of the test specimens.

3.3.2 Test Setup and Instrumentations

The experimental testing of the test specimens was done at the Earthquake Engineering Laboratory (EEL) at UNR. The test specimens were simply seated over two seat beams and loaded with a vertical static loading from a 980 kN hydraulic actuator at the middle (i.e., three point bending). Elastomeric rubber bearings were used on the top of the steel seat beams to allow a zero moment or free rotation at supports. Since the test setup was not designed to provide fixity at the ends to mimic the real bridge deck case scenario, the span length of the specimens were set up based on the estimated distance between the bending inflection points. As mentioned earlier, the bridge example has a 3.65 m spacing between the main beams. For ideal uniform load distribution over

the bridge deck, negative moments are expected near the main beam locations while a positive moment is expected at the middle. The distance between the seat beams is adopted to represent the effective span length or the distance between the bending inflection points where the bending span length is adopted to be 2.44 m. This distance represents almost two-thirds of the 3.65 m main beams spacing from the utilized bridge example. The mid-span vertical load was applied at the edge of the field joint to test the largest possible shear stresses at the interface between the joint and the precast panels. Figure 3-4 shows a schematic drawing and a photograph of the test setup used in this study. Many instrumentation devices were used to monitor deflections, concrete cracks, and reinforcement and concrete strains throughout the test. Figure 3-5 shows some of the instrumentation devices used in this study. Figure 3-5 also shows the locations of the string potentiometers which were used to measure the deflections of the test specimens.

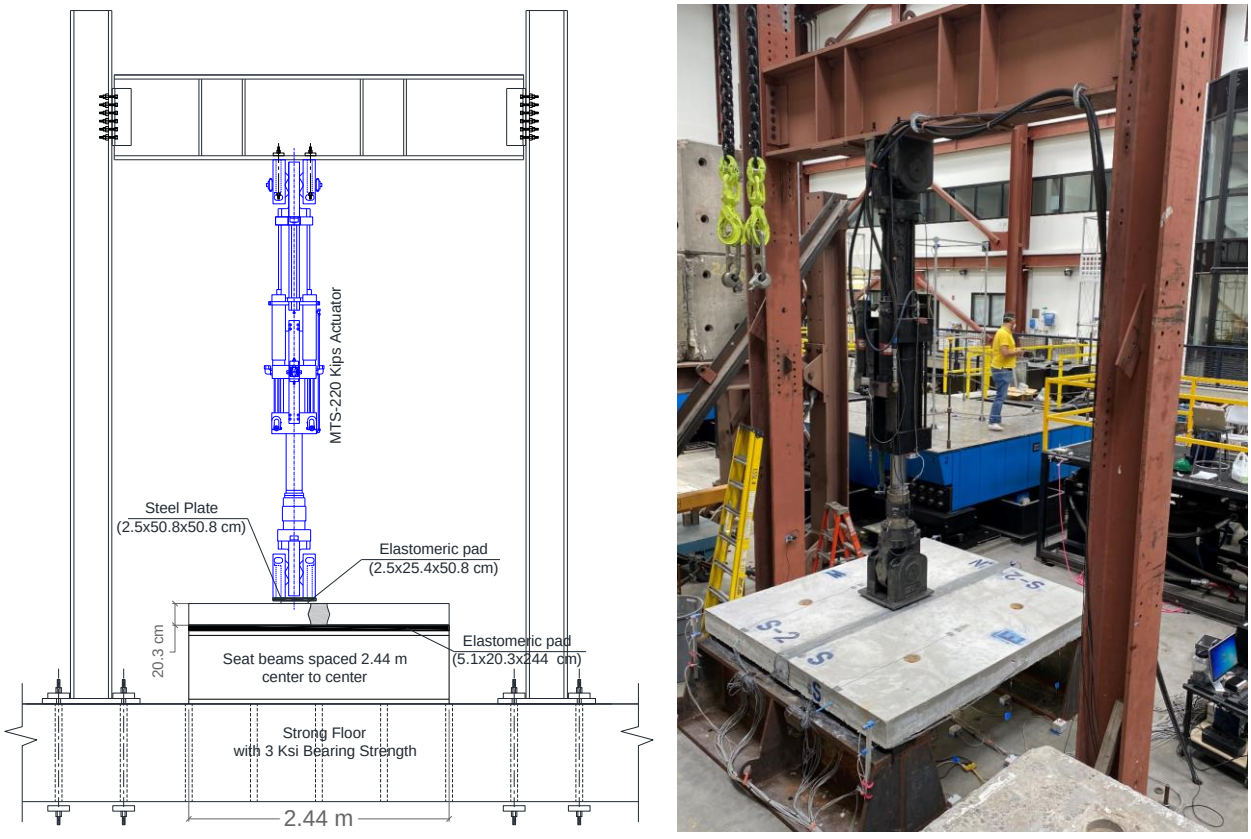

(a) (b)

Figure 3-4: Experimental test setup (a) schematic drawing of the test setup, and (b) photograph of the actual test setup at UNR.

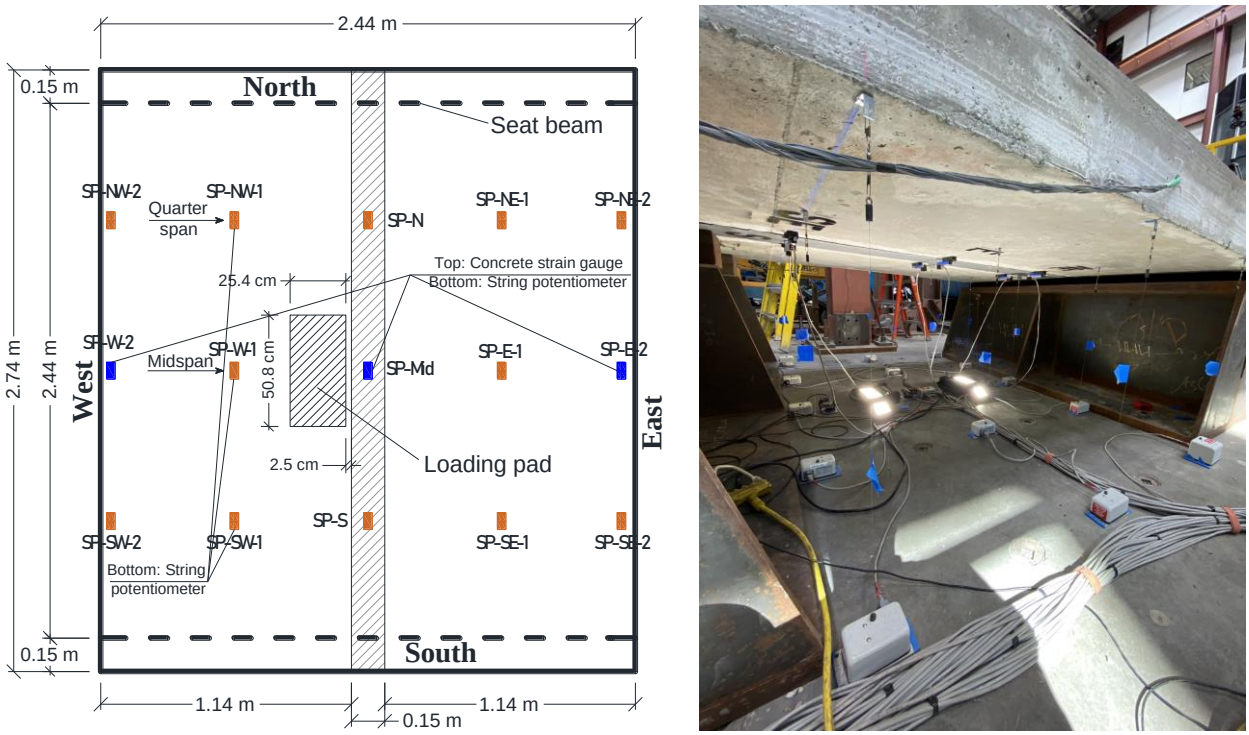

(a) (b)

Figure 3-5: Instrumentation plan (a) plan view for the locations of the string potentiometers, and (b) photograph of the instrumentations.

3.3.3 Loading Protocol

The loading procedure used in the present study, and was also used to test the control specimen with P-UHPC, consisted of four cycles of loading and loading at small load levels. These cycles were followed by a static monotonic loading up to the failure of the specimen. The purpose of establishing these initial cycles was to study the performance of the test specimens under representative service loads. The initial cycles included two 89 kN cycles, then other two 178 kN cycles. A loading and unloading at a rate of 22.24 kN/min were used during the first four cycles, while the last cycle was controlled by the mid-span deflection at a rate of 1.9 mm/min up to failure.

3.3.4 Fabrication of Test Specimens

The construction of the test specimens has followed three main phases as shown in Figure 3-6. First, two precast panels were fabricated for each specimen using conventional concrete from a single ready mix batch. The conventional concrete has a compressive strength of 27.5 MPa at 15 days and 52.4 MPa at test days. After two weeks, every two panels were aligned together leaving a middle gap to pour the field joints. Finally, the field joints were poured using the NP-UHPC mixes with 2% and 1% steel fibers. The measured compressive strengths at test days of the 2% and 1% NP-UHPC mixes were 146.4 MPa and 125.7 MPa, respectively. The P-UHPC reference specimen was fabricated using conventional concrete with 35.8 MPa compressive strength measured at the day of test. While the P-UHPC had a compressive strength of 191.7 MPa at the day of test.

Figure 3-6: Photographs to illustrate the sequence of construction of the test specimens.

3.4 Test Results and Discussion

This section shows the experimental test results of the three tested specimens. This section also provides a discussion of the global behavior of the tested specimens in terms of damage progression, modes of failure and load-deflection relationships. Furthermore, the local behavior of the tested specimens were also reported herein in terms of the load versus the reinforcement and concrete strains. Nonetheless, this section provides evaluation and comparisons of the proposed NP-UHPC systems with the reference P-UHPC specimen to validate the use of the new systems for future applications.

3.4.1 Key Results

A brief summary of the test results is provided in Table 3-2. The table shows the initial stiffness, load capacities, load at which the reinforcement started to yield and middle deflections of the three NP-UHPC specimens in comparison with the results of the reference P-UHPC specimen. It is known that the bridge decks are designed to remain essentially elastic under the code specified service and ultimate loads. While, the testing of the specimens continued up to failure in order to understand the structural behavior and joint performance at such higher loads and to determine if the whole system will remain intact or the field joint or the joint interface would be the weakest links.

Table 3-2: Summary of key experimental test results

Specimen Name	Peak Load (kN)	Load @ 1st Yield (kN)	Mid-span Deflection (cm)			Initial Stiffness, (kN/cm)
			@ Peak Load	@ Service Load	@ Ultimate Load	
S0	524.5	≈ 290	5.920	0.444	0.975	420.3
S1-Str-2%	592.0	≈ 320	6.217	0.349	0.811	510.6
S2-Lop-2%	598.1	≈ 298	6.697	0.345	0.805	545.3
S3-Str-1%	581.0	≈ 281	6.183	0.437	0.992	460.1

The peak load capacities and initial stiffness of the NP-UHPC specimens are higher than that of the reference specimen with P-UHPC. This behavior is attributed to the higher compressive strength of the precast panels of the NP-UHPC specimens (i.e., 52.4 MPa) compared to 35.8 MPa for specimen S0. The three NP-UHPC specimens have very comparable behaviors. However, specimen S3-Str-1% has slightly less initial stiffness and load capacity because of the lower strength of the NP-UHPC with 1% steel fibers. This has resulted into larger deflections at the AASHTO service and ultimate loads. To be able to compare the results of specimen S1-Str-2% with the reference specimen S0, the compressive strength of both specimens were normalized since there is a difference between the compressive strength of the precast panels and the field joints of both specimens. Each specimen was fabricated from two different components (i.e., concrete panels and UHPC joints). The weighted compressive strength of specimen S0, depending on the width and compressive strength of the two components, is 45.54 MPa. While specimen S1-Str-2% has a weighted compressive strength of 58.27 MPa. Hence, specimen S1-Str-2% has a 28% higher compressive strength than specimen S0. The 28% higher compressive strength has resulted in a 21% increase in the initial stiffness and only 12% increase in the load capacity of specimen S1-Str-2%.

3.4.2 Global Behavior of Specimens

The global behavior of the tested specimens was evaluated herein in terms of the damage progression, modes of failure and load versus deflection relationships.

3.4.2.1 Damage progression and mode of failure

The observed modes of failure of the test specimens were almost similar, as such flexural members are usually designed to be tension controlled. In this case, the cross section of the deck specimens are under reinforced which forces the main reinforcement to yield before the concrete crushing. Hence, the common observed mode of failure for all test specimens is yielding of the bottom transverse reinforcement due to bending followed by crushing of the conventional concrete at the top of the precast panels. Figure 3-7 shows the damage schemes at the bottom and top sides of the test specimens.

The crushing of concrete was initially observed near the applied load location just before the failure of the specimens at approximately 570 kN. Then the crushing propagated through the across the width of the west and east precast panels. While it was observed that specimen S1-Str-2% had crushing at the west precast panel only. This was due to the interface crack (See figure 3-7) that happened at the top and bottom of the specimen between the east precast panel and the field joint. This interface crack was the main reason for the interruption of the load transfer path from the loaded west panel to the east panel that resulted in crushing of the west panel only. This damage is similar to the damage of the reference specimen and unlike that of the other two NP-UHPC specimens as there were no interface cracks observed. It is noted that specimens S2-Lop-2% and S3-Str-1% have a denser longitudinal reinforcement which were overlapped inside the joint compared to specimen S1-Str-2%. This denser reinforcement inside the joint may enhance the interface and prevent interface separation between the joint and the precast panels. This may suggest that, besides the option of using sand blasting and roughing the inner side of the panels

before pouring the closure joint material, it is also possible to use more overlapped reinforcement inside the field joint to avoid interface cracking and to ensure better load distribution across the precast panels.

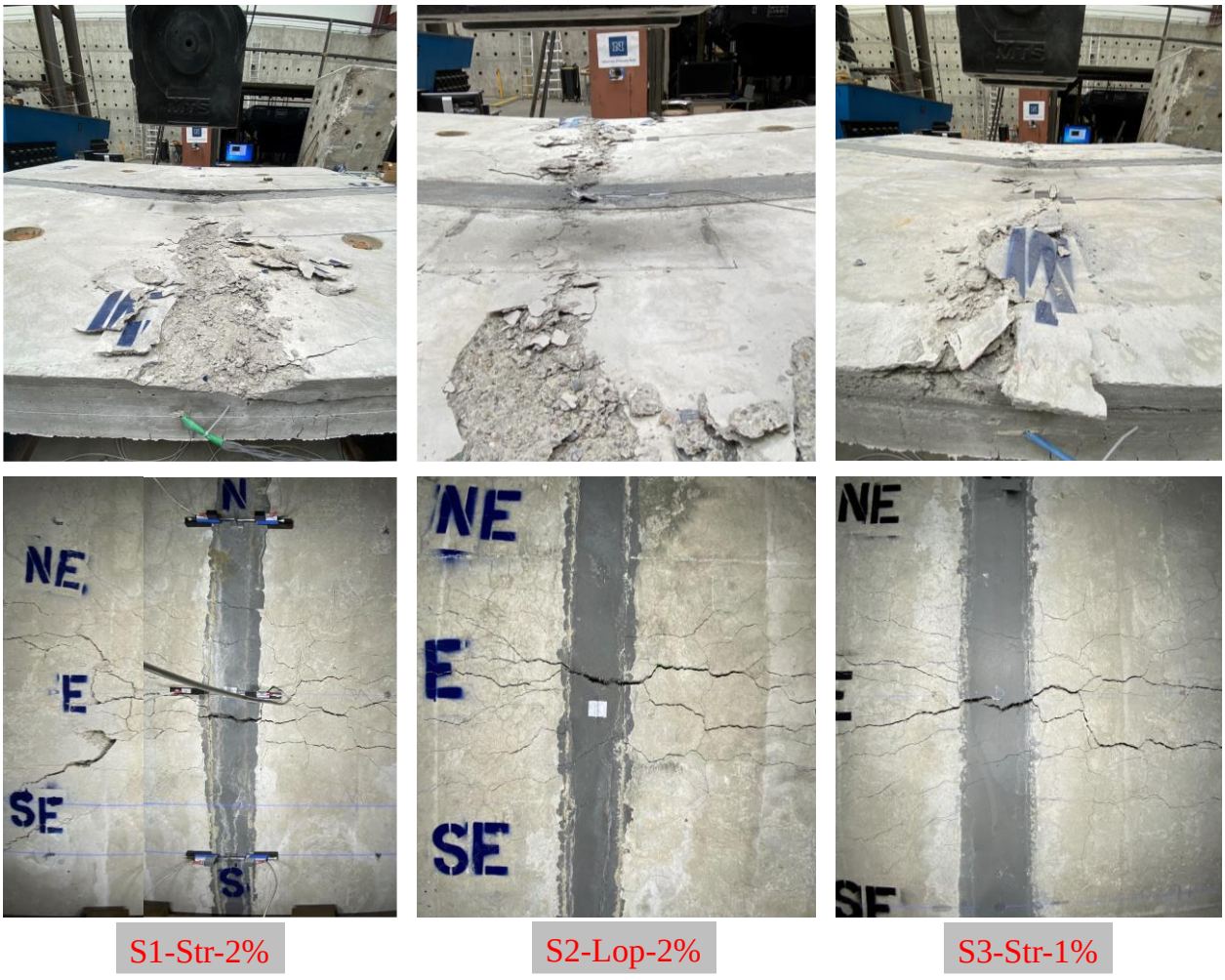

Figure 3-7: Crack pattern, damage and modes of failure at the top and bottom of the test specimens.

Since bridge decks are mainly designed to elastically sustain the AASHTO service and ultimate load levels, it is important to evaluate the damage of the specimens at these specified load levels. At the AASHTO ultimate load, only limited and narrow flexural cracks were observed at the bottom of the precast panels. While no flexural or interface cracks were observed on any of the joints at this load level because of the high tensile strength of the NP-UHPC and its higher bond strength with the precast panels. The field joints of specimens S1-Str-2% and S2-Lop-2% were cracked at around 335 kN. While the field joint of specimen S3-Str-1% was cracked at earlier load (i.e., 260 kN) because of the less tensile strength of the NP-UHPC with 1% steel fibers compared to the 2% steel fibers. On the other hand, the first interface crack was observed at 335, 445, and 400 kN for specimens S1-Str-2%, S2-Lop-2% and S3-Str-1%, respectively. These interface cracks were located mainly at the middle bottom of the specimens between the field joint and the east precast panel as shown in Figure 3-7. More importantly, the effect of these cracks were minor and

they did not dominate the failure of the specimens as all specimens failed in pure flexural behavior. One more observation for the tested specimens is that there is no obvious visual signs for bar slip for the lap splices within the joints throughout the test. This means that the proposed lap lengths was adequate to transfer the forces between both precast panels up to failure loads. The test was stopped when a specimen lose 20% of the observed peak load capacity.

3.4.2.2 Load-deflection relationship

The global behavior of the test specimens was also evaluated based on the load versus middle deflection relationships. In this section, the load versus deflection relationships of the three test specimens were compared together. The main aim of this section is to investigate the effect of varying the test parameters on the flexural behavior of the specimens. Nonetheless, the overall behavior of the NP-UHPC specimens was also compared with that of the reference P-UHPC, which was provided in section 3.2. Figure 3-8 a shows the load versus mid-span deflection relationships of the three test specimens. Figure 3-8 b illustrates the different stages of behavior on the load versus deflection relationship of specimen S1-Str-2%. The flexural behavior of the tested specimens is almost typical. Hence, the stages of the flexural behavior of specimen S1-Str-2% is shown here as a sample. The AASHTO LRFD limit states, shown in Figure 3-8, were calculated using the Equivalent strip method. This method takes into account the largest possible moment values of the deck slabs with respect to the different loading conditions.

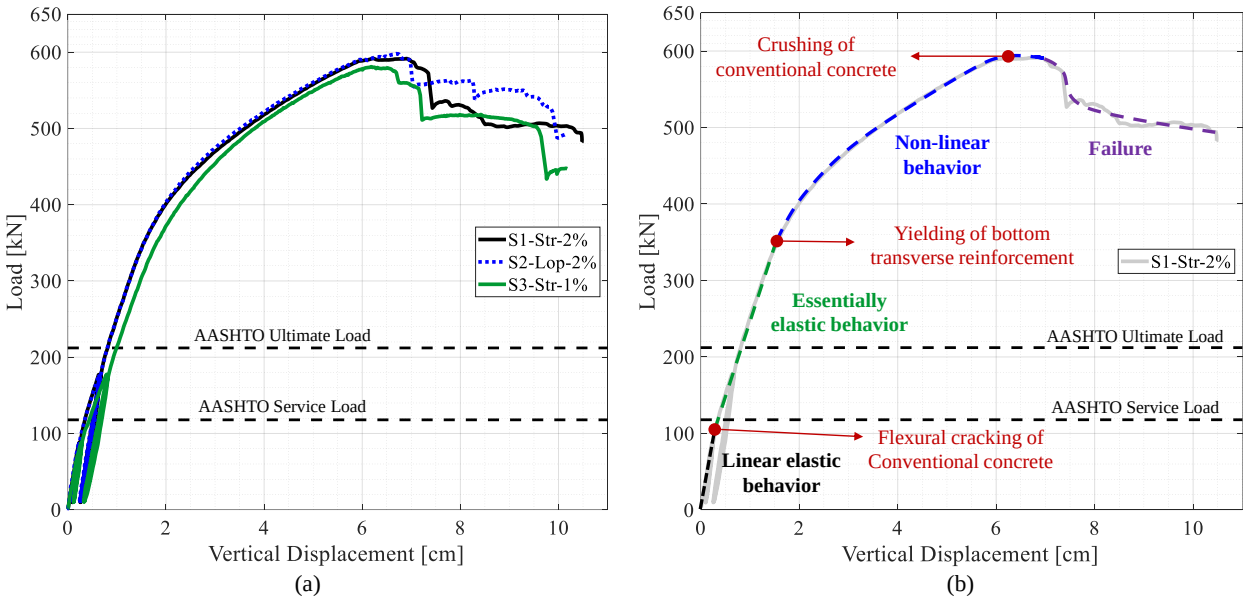

Figure 3-8: Global Behavior of the NP-UHPC specimens: (a) Load versus mid-span deflection relationships of the tested specimens; (b) Stages of the flexural behavior of specimen S1-Str-2%.

In general, the flexural behavior of the test specimens is very comparable no matter the variation of the test parameters. While, it is shown that specimen S3-Str-1% has a slightly softer behavior due to the less in stiffness aroused from the use of a NP-UHPC mix with only 1% steel fibers. The flexural capacity of the tested specimens has far exceeded the specified AASHTO LRFD ultimate limit state. There are many reasons for this large difference such as the limit states were calculated

based on the nominal steel yielding value of 410 MPa and nominal concrete compressive strength of 35 MPa. While the actual steel yielding value is 480 MPa and the actual compressive strength is 52.4 MPa. Moreover, at the design stage of the test specimens, a moment reduction factor of 0.9 was used to magnify the moment demand and increase the required bottom transverse reinforcement. Nonetheless, the AASHTO design procedure does not count for the contribution of the top layer of reinforcement that usually yields into more required bottom reinforcement. The behavior of the tested specimens is similar to that of the P-UHPC specimen and the failure was dominated by flexure of the deck slabs without any major joint or joint interface failure or slippage of rebar lap splices inside the joints. Therefore, the NP-UHPC mixes used in this study with the proposed joint details can be considered as viable solutions for the transverse bridge deck field joints. As they can fulfill the target behavior of the conventional cast-in-place bridge decks in terms of strength and flexure dominated failure.

The typical flexural behavior of the tested specimens, as shown in Figure 3-8 b, is divided into four main regions. The flexural behavior started with a linear elastic response up to approximately 100 kN in which the applied load was less than the cracking load of the specimens. The second region is defined by the essential elastic behavior in which the conventional concrete was cracked in tension while the reinforcement was not yet yielded. The concrete cracking has resulted in a slight decrease in the flexure stiffness compared to the initial stiffness reported in Table 3-2. The initiation of yielding of the bottom transverse reinforcement was observed at the end of this stage which was associated with flexural and in some cases interface cracking of the field joints. This has resulted in a non-linear flexural response of the specimens in which significant reduction of stiffness was observed. This reduction in flexural stiffness was mainly due to a combination of factors including the aggressive tensile cracking of concrete, continued yielding of reinforcement, and, to less extent, the interface cracking of the joints. Finally, the failure of the specimens were observed after the crushing of the conventional concrete at the applied load location. This has resulted in a global stiffness degradation in which the load capacity of the specimens decrease with increasing the applied vertical displacements.

3.4.3 Local Behavior of Specimens

The local behavior of the tested specimens was evaluated in this section in terms of the load versus the tensile strains of the transverse and longitudinal reinforcement in addition to the load versus the concrete compressive strains.

3.4.3.1 Transverse reinforcement strains

The load versus the measured tensile strains of the bottom transverse reinforcement at mid-span (i.e., maximum moment location) are shown in Figure 3-9. The figure also includes schematic drawings of the test specimens, location of the instrumented reinforcing bars and locations of the installed strain gages. It is noted that some of the strain gages were damaged, especially at larger strain levels. The damaged strain gages were also noted on Figure 3-9.

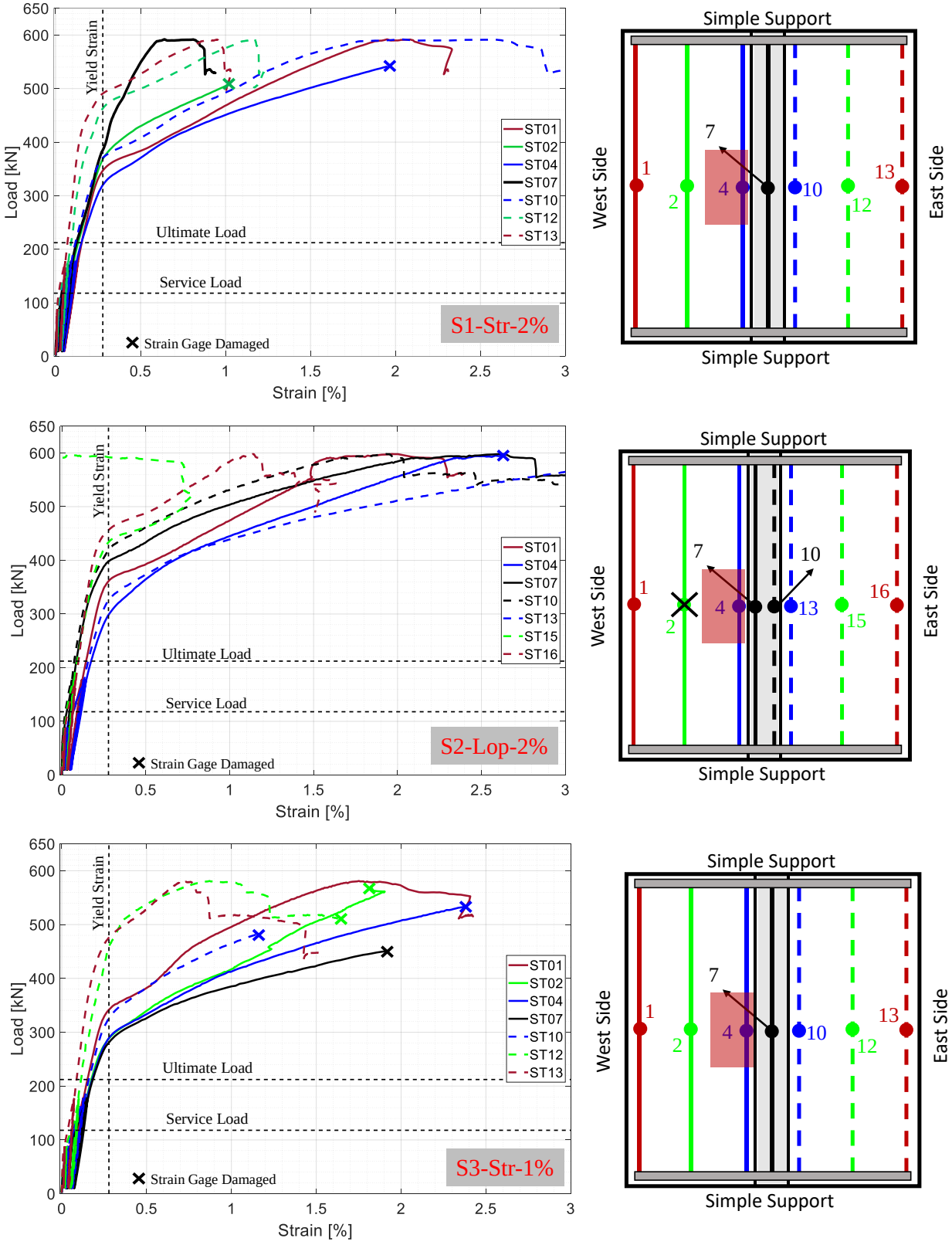

Figure 3-9: Load versus tensile strains of the bottom transverse reinforcement measured at mid-span.

The main observation from Figure 3-9 is that the main reinforcing bars have not yielded before reaching the AASHTO LRFD ultimate load. This observation supports the fact that the specimens remained essentially elastic up to and slightly beyond the code allowable limit. This behavior was expected because of many reasons such as the use of the nominal values for concrete compressive strength (i.e., 35 MPa) and steel yielding strength (i.e., 400 MPa) to calculate the AASHTO ultimate load. While the actual strength values usually surpass these nominal values. Other reason belongs to the use of a reduction factor of 0.9 during the design stage, which increases the moment demand on the cross-section and consequently increases the required reinforcement. However, this behavior verifies the acceptable performance of the NP-UHPC mixes as a closure joint materials for the field joints of precast bridge decks. The yielding was initially observed whether in the reinforcing bars which were located inside the field joints or adjacent to the west side of the joints. The first yield in the main reinforcing bars was observed at approximately 320, 298, and 281 kN for specimens S1-Str-2%, S2-Lop-2% and S3-Str-1%, respectively. The onset of yielding was followed by a sequence of yielding of the adjacent bottom transverse reinforcement. The excessive yielding of reinforcement has resulted in global softening of specimens and consequently change of the flexural behavior to the non-linear response (see Figure 3-8 b). It is also noted that the reinforcing bars which were located on the west precast panel were more stressed than the bars on the east side panel. This is attributed to the eccentricity of loading in the east-west direction as the load was applied on the west side of the field joint (see Figure 3-4). The two middle bars which were located inside the field joint of specimen S2-Lop-2% are usually called lacer bars. These bars are usually used to connect the inner tip of the loop splices (see Figure 3-3) to enhance the bearing reactions of the splices and increase ductility. As a result of the location of these lacer bars which were not located at the outermost surface of the joint, the tensile strains of these bars were found to be slightly lower than the other adjacent bars outside the joint.

3.4.3.2 Longitudinal reinforcement strains

The previous section covered the tensile strains of the bottom transverse reinforcement (i.e., main flexural reinforcement). While this section focuses on the tensile strains of the longitudinal reinforcement (i.e., secondary flexural reinforcement) which were overlapped inside the joints. The strain gages were attached to the longitudinal bars near the two sides of the interface between the field joint and the precast panels as shown in Figure 3-10. The location of the strain gages was chosen based on two main reasons. First, the strain readings from both strain gages were to be compared together to anticipate if there is slippage of the reinforcement splices inside the joint. Second, the strain readings of the strain gages which were installed inside the joints (marked in red in Figure 3-10) were to be verified with the yield strain to determine if the development length was sufficient to yield the bars inside the joint. The two ways of verification may indicate if the proposed joint details and the utilized NP-UHPC mixes are sufficient to transfer the load from the west to the east precast panels. In this case, the proposed multi component deck system can be considered equivalent to the monolithic cast in place bridge decks. Figure 3-10 shows results of the load versus the tensile strains of selected bottom longitudinal reinforcement. Figure 3-10 shows the maximum strain values of the longitudinal bars. It is noted that many of the strain gages were damaged during the construction of the specimens and field joints. Hence, the maximum strain results of the longitudinal bars of specimen S3-Str-1% were not shown in Figure 3-10.

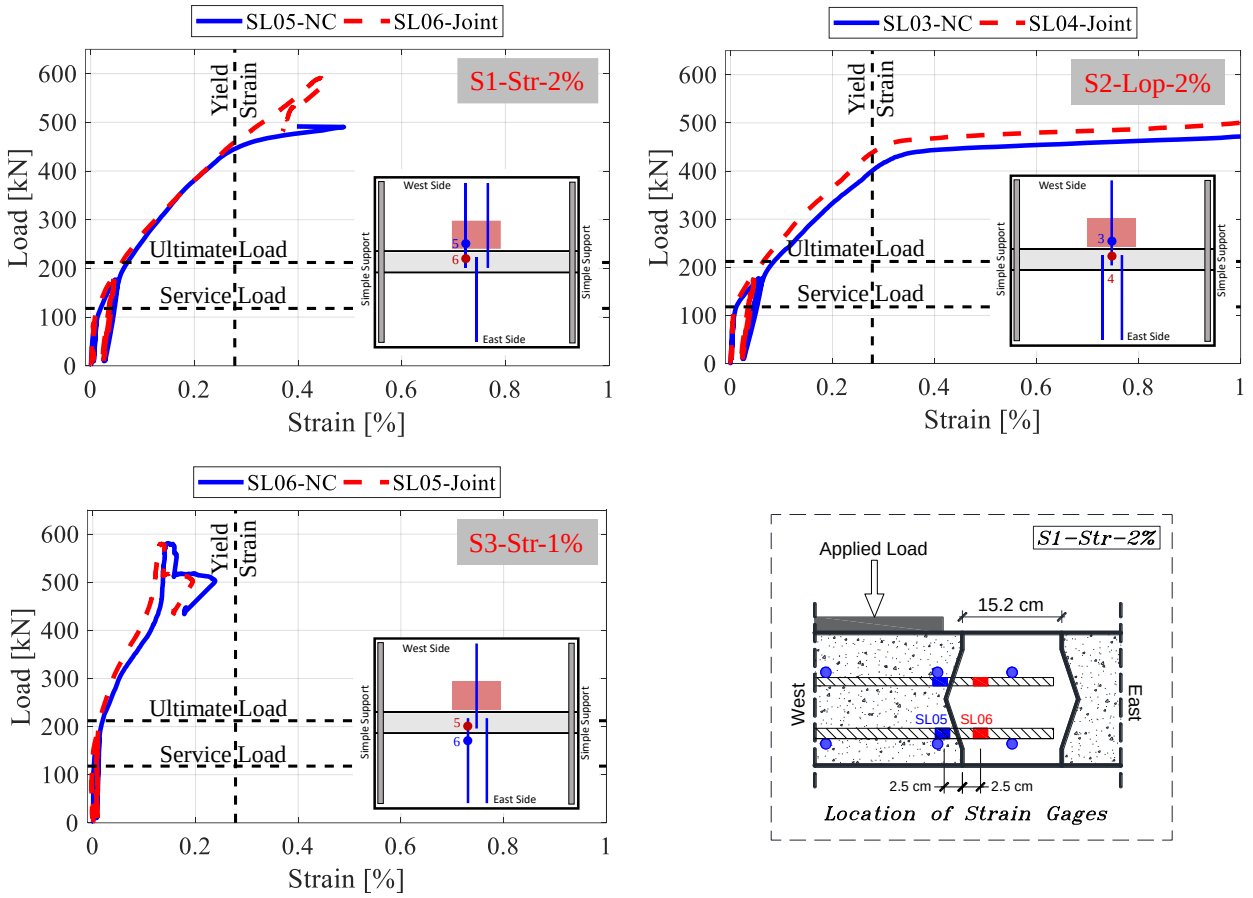

Figure 3-10: Load versus tensile strains of selected bottom longitudinal reinforcement.

It was observed that the measured tensile strains of inside and outside the field joint were almost typical with no signs of bar slippage that has occurred up to the peak load. Nonetheless, the measured strain values of the longitudinal bars inside the joint for specimens S1-Str-2% and S2-Lop-2% has exceeded the yield strain of reinforcement. This confirms that the proposed overlap length was sufficient to develop yielding of reinforcement inside the joints. At the AASHTO ultimate load, the measured tensile strain values were typically far below the yield strain. This could be informed that the demand on the field joints within the AASHTO design loads does not dictate the need for the full development length of the bars inside the joints. However, the use of the full development length may be required if the deck slabs were to be subjected to more demand loads than the specified AASHTO ultimate loads.

3.4.3.3 Concrete compressive strains

While the previous section was focused on the tensile strains of the transverse and longitudinal reinforcement, the load versus compressive strain readings of the conventional concrete and NP-UHPC are presented in Figure 3-11 for completeness. The concrete strain gages were placed at mid-span (maximum moment location) to measure the maximum compressive strength at the extreme concrete compression fibers of the precast panels and the field joint. The measured strain values were compared with the strains at which crushing of the conventional concrete and NP-

UHPC are expected to happen. The crushing of the unconfined conventional concrete and NP-UHPC are expected to happen at compressive strains of approximately 0.003 and 0.005, respectively (Abokifa and Moustafa, 2021; ACI, 2008; AASHTO, 2014). Hence, Figure 3-11 includes shaded areas, highlighted in blue color, to show boundaries of the concrete crushing strain values. Some of the concrete strain gages were damaged during the test, especially at higher load values. Figure 3-11 shows when the concrete strain gages were damaged.

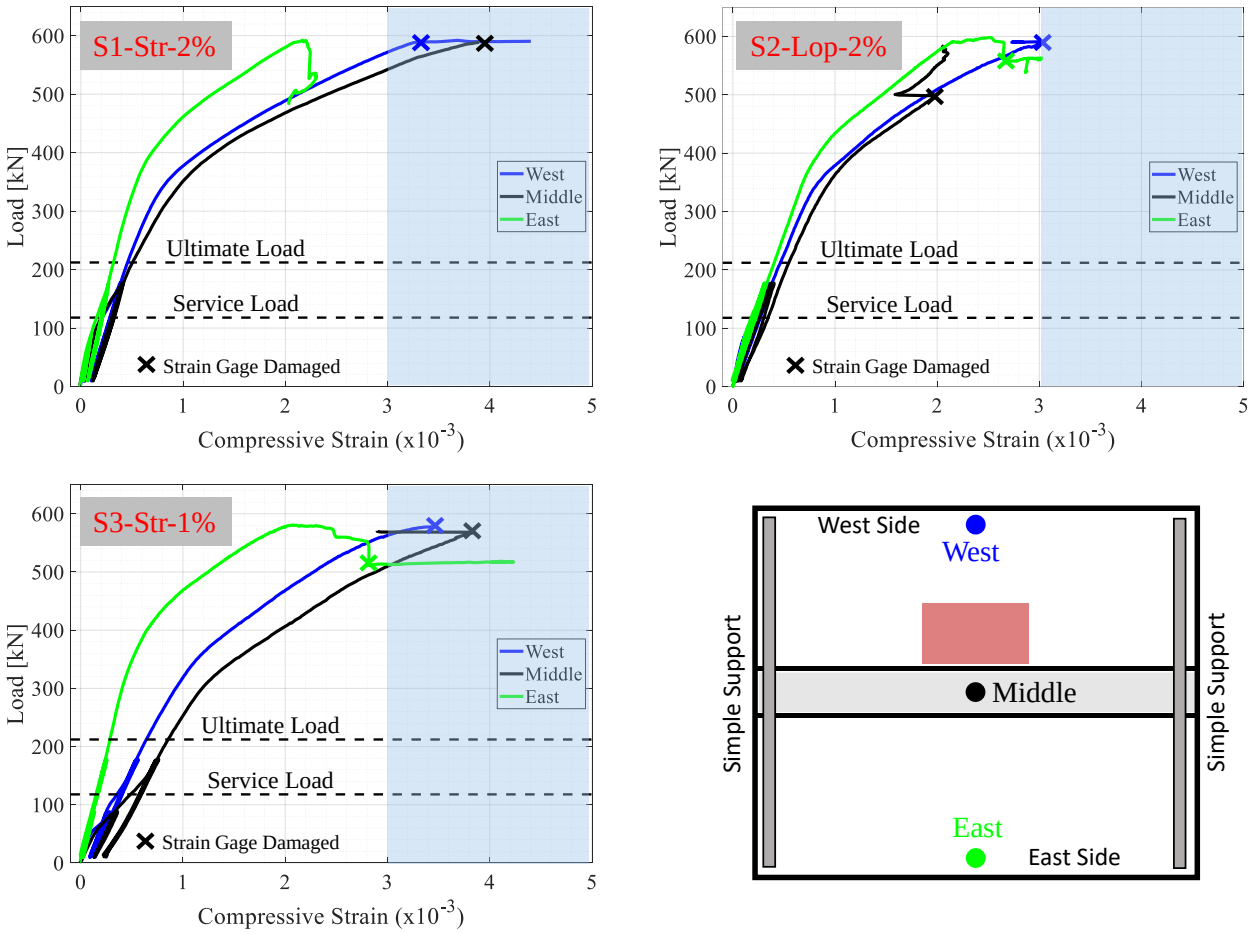

Figure 3-11: Load versus concrete compressive strain measured at mid-span.

As mentioned earlier, crushing of concrete was observed slightly before the failure of the test specimens. Same observation was also shown in Figure 3-11 as the compressive strain readings indicated that most of the concrete strains are slightly more than 0.003 at the peak loads of the test specimens. The crushing of concrete was observed on the east and west precast panels and similarly on the field joints. This behavior was slightly different from that of specimen S1-Str-2% as no crushing was observed in the east precast panel. The compressive strain values of specimen S1-Str-2%, which were measured at the east precast panel, were smaller than the crushing strain values. This is attributed to the interface crack between the field joint and the east precast panel that was the main reason for interrupting the load path from the applied load location to the east panel. The concrete compressive strains of the east precast panel are slightly lower than the strains measured at the west panel and the field joint. This was expected because of the eccentricity of

loading in the east-west direction. It was observed that specimen S2-Lop-2% has a slightly better strain distribution over the cross-section when compared to the other specimens. This indicates that the use of loop splice instead of the straight lap splice has enhanced the load distribution over the specimen cross-section. On the other hand, the dispersion of the concrete strains values of specimen S3-Str-1% may indicate a poor load distribution across the precast panels because of the use of a NP-UHPC mix with only 1% steel fibers.

3.5 Summary

This previous section summarized the main results of the comprehensive large scale experimental testing of representative precast bridge deck panels with NP-UHPC transverse field joints. The section is part of a bigger research project that aims at developing a local NP-UHPC mixes and demonstrating the viability of these mixes for longitudinal and transverse field joints of the precast bridge decks. In this section, two NP-UHPC mixes with ingredients sourced from the western states (Nevada and California States) were used as a closure joint materials. The section initially started with presenting the results of a similar specimen with P-UHPC transverse field joints which was used later as reference specimen for comparison with the experimental results of this study. The experimental program included testing of three full scale bridge deck specimens with transverse NP-UHPC joints. The test parameters included different joint splice details, joint widths, closure joint materials, and longitudinal reinforcement configurations. Finally, this section provided discussion of the structural performance of the test specimens in terms of the global and local behaviors.

4. Experimental Testing: Longitudinal Field Joints

4.1 Introduction

As of April 2020, more than 46,000 bridges across the United States are considered structurally deficient (ARTBA, 2020). Most of these bridges need bridge deck replacement or rehabilitation. The reason for this behavior is that bridge decks are usually susceptible to rapid degradation in their structural performance because of harsh environments where they are more vulnerable to mechanical wear and tear effects. Moreover, the use of dicing salts in very cold weathers has resulted in a rapid reduction in the bridge deck lifetime because of the corrosion of reinforcement. The Accelerated Bridge Construction (ABC) techniques have paved the way to offer viable and rapid solutions for bridge deck replacements. The use of full-depth precast deck panels is one of these rapid solutions that can provide improved quality and durability. Moreover, the use of Deck-Bulb-Tee (DBT) girders has become a more popular application for bridge superstructure replacements especially in remote and rural areas where limited on-site activities are strongly required. DBT girders are prefabricated and shipped to the bridge site where they can be quickly assembled. Therefore, DBT girders can provide fast erection for bridge superstructures and hence less traffic disruption.

DBT girders can provide an integrated system that combines the typical I-section pre-stressed concrete girders with the top bridge deck layer. The integral DBT girders have top wide flanges that are connected on-site using longitudinal field joints as shown in Figure 4-1 (Haber and Graybeal, 2018). Connecting the adjacent top flanges of the DBTs can provide a continuous multi-span bridge deck layer across the width of the bridge. Such DBTs longitudinal field connections between the top flanges of adjacent girders are the focus of this paper. Despite the major benefits of using the DBT systems, some state departments of transportation (DOTs) have limited their use because of the inadequate construction methods of the longitudinal field joints which were used in the past. In the past, welded clips and grouted joints were used in the longitudinal joints, which resulted in less durable joints due to the observance of interface cracking along the joint that may lead to leakage (Qiao et al., 2016). Thus, emerging research efforts investigated the applicability of using modern advanced materials such as ultra-high performance concrete (UHPC) for such joints to maintain simpler joint configurations in addition to increased durability (Graybeal, 2010 a).

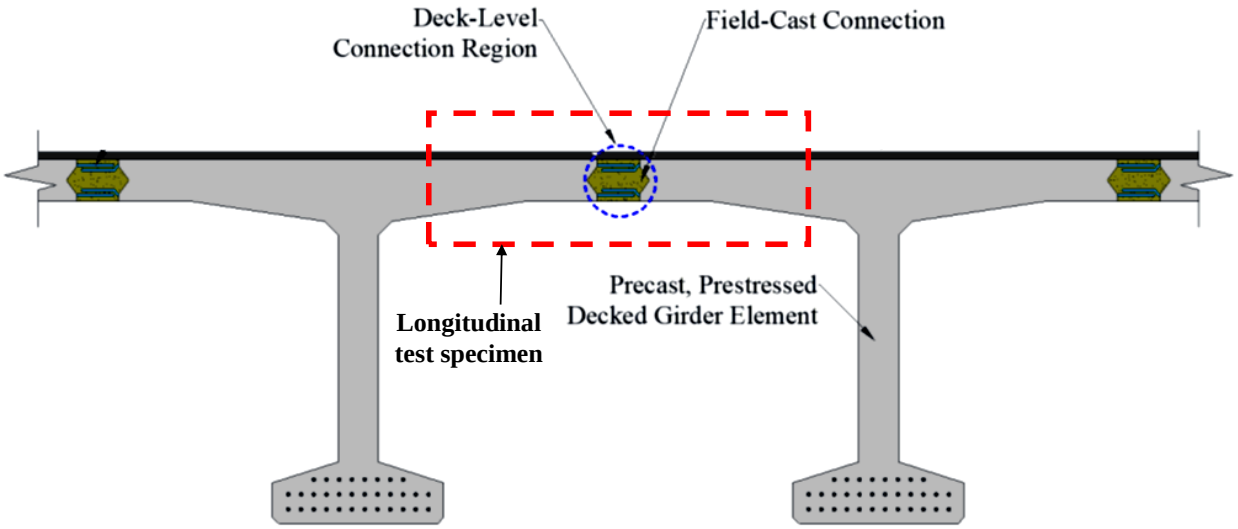

Figure 4-1: DBT girders with full-depth longitudinal field joints [2].

UHPC is an advanced construction material that was developed in the late 20th century. It is a cementitious material with steel fibers and a low water-to-cement (w/c) ratio. The compressive strength of UHPC is typically 4-6 times higher than the normal strength concrete (NSC) in addition to other superior mechanical properties. Accordingly, many researchers examined the use of UHPC in many structural applications especially the use of UHPC in bridge field joints to connect different precast members. Examples of the research studies that focused on the use of UHPC in bridge deck field joints include, but are not limited to, the work done by (Graybeal, 2010 a; Peruchini et al., 2017; Hartwell, 2011; Hwang and Park, 2014; Coufal et al., 2016; Abokifa et al., 2021; Abokifa and Moustafa, 2021). The earlier research studies examined the use of conventional construction materials for such joints as advanced grouts, high-performance concrete (HPC), and HPC with steel fibers (Zhu et al., 2012; Li and Jiang, 2016; Verger-Leboeuf et al., 2017). However, special reinforcement requirements such as mechanical splices and post-tensioning along with relatively wider joints have been associated with the use of these conventional materials inside the field joints. Many of these previously provided solutions require more on-site work in addition to higher labor costs that are not viable for ABC.

When using UHPC, several research studies reported a typical UHPC field joint that has a diamond-shaped shear key and a 6 to 8 in (15.2 to 20.3 cm) width without reinforcement post-tensioning and with traditional straight or loop splices. These typical details of the UHPC field joint demonstrated acceptable structural performance in transferring shear and bending across different precast panels in addition to significantly providing higher durability under cyclic loading (Graybeal, 2010 a; French et al., 2011; Perry et al., 2014; Sritharan et al., 2012). Nonetheless, UHPC is associated with practical challenges as it requires special expertise to mix and place due to steel fibers and has a long mixing time. However, these problems could be easily tackled by increasing the number of research studies that focus on developing large UHPC batches. Additionally, these problems could be solved by having more technical reports that provide better practices for mixing and placing UHPC along with the other solutions for the technical issues reported in various projects. Another major drawback of using UHPC that is also attracting more

interest to resolve is the expensive and proprietary nature of robust UHPC mixes. This usually causes bidding issues among state DOTs that are trying to limit the sole sourcing of materials.

Some state DOTs sponsored research to develop their own non-proprietary UHPC (NP-UHPC) mixes with implementing locally and domestically available materials to avoid the cost and bidding issues associated with the proprietary UHPC (e.g. Qiao et al.,2016; Graybeal, 2013; Wille et al., 2011; Wille et al., 2012; Alsalman et al., 2017; Berry et al., 2017). But only very limited research studies focused on large-scale applications and experimental testing of newly developed and emerging NP-UHPC mixes when used in bridge deck field joints. A recent research project, which was funded by Washington DOT, aimed at developing NP-UHPC using locally available materials and tested the new mix in a hypothetical DBT longitudinal field joints setting (Peruchini, 2017). However, this study tested only a small section of the deck representing actual DBT girders with a width of 2 ft [0.6 m] under static bending to determine the required joint width and splice length. The experimental results showed that a UHPC joint width of 7.11 in [18 cm] and a splice length of 5.11 in [13 cm] are considered sufficient to fracture the bars inside the joint. Moreover, the study concluded that the body of the UHPC joint did not suffer any cracking, while there was a significant interface crack at the cold joint between the UHPC and the adjacent precast members owing to the unprepared flat joint surface. These interface cracks usually allow the ingression of moisture and deicing chemicals that may lead to rapid corrosion of the reinforcement and deterioration of the bridge deck. Hence, it is strongly recommended from some literature studies to use female-female shear keys for such connections instead of the ordinary flat surfaces to facilitate the compression strut transfer of applied loads, instead of relying on dowel action of reinforcing bars (Graybeal, 2014). Looney et al. have also tested representative full-scale bridge deck specimens with proprietary and NP-UHPC longitudinal field joints (Looney et al., 2021). The purpose of this study was to evaluate the behavior of a NP-UHPC mix, which was developed using locally available materials in the state of Oklahoma, as a bridge deck joint material (Looney et al., 2019). The NP-UHPC mix design used in the present study follows the same mix design used in this literature study, but with using different material sources. The study concluded that the NP-UHPC mix performed comparably to the proprietary UHPC. This study has motivated the authors to further replicate the same mix design using local materials available in the western states. However, this study has also used the undesirable flat shear key shape with a relatively wider joint of 11.8 in width and a straight contact lap splice with adding splicing bars. Yuan and Graybeal have recommended the use of non-contact lap splices as they can exhibit higher bond strengths than the contact lap splice inside the UHPC (Yuan and Graybeal, 2015).

To further resolve bidding and sole-source issues, some research efforts also considered identifying other alternative closure materials that can provide the same acceptable performance as proprietary UHPC in bridge deck field joints. For example, in recent work conducted by the authors (Abokifa et al., 2021; Abokifa and Moustafa, 2021), poly-methyl methacrylate polymer concrete (PMMA-PC) was identified as a potential alternative to the UHPC for deck field joints. In a parallel ongoing research project, the authors tested three full-scale specimens with transverse field joints in addition to two other specimens with longitudinal field joints. The study established a direct “apples-to-apples” comparison between the specimens with robust proprietary/commercial UHPC mix and PMMA-PC field joints. It has been concluded that the PMMA-PC joints can

provide the same structural performance as the UHPC joints without any interface cracking or bar slippage (Abokifa et al., 2021; Abokifa and Moustafa, 2021). The reason that project is considered a parallel effort is that the experimental work reported herein leverages and complements the recently completed work through using similar specimen designs and testing setup.

As mentioned above, there are only limited experimental validations for NP-UHPC field joints behavior and implementation. Some of these experimental efforts provided guidance for the potential use of different NP-UHPC mixes in the field joints. However, the tested specimens in those studies had relatively smaller dimensions than the full-scale specimens or un-recommended shear key shapes and joint splices. Hence, this study aims at filling this important knowledge gap and providing a good understanding of the experimental behavior of the commonly used longitudinal field joints in DBT girders. The focus of this chapter is to further extend the use of the ABC-UTC NP-UHPC mix for longitudinal joint specimens. The overall objective of this part of study is to investigate and validate the structural performance of NP-UHPC longitudinal field joints as compared to robust proprietary/commercial UHPC joints. This chapter presents results from two full-scale experimental tests of deck assemblies of representative DBT girder flanges with proprietary and NP-UHPC longitudinal field joints under static vertical loading. The chapter includes several sections that present a discussion on the details of the conducted experimental program, test results comparisons and discussions, and summary.

4.2 Experimental Program

This section provides information regarding the structural design, details, and construction of the test specimens along with the test setup, instrumentation plan, and loading protocol used in this study.

4.2.1 Design and Fabrication of the Test Specimen

The design of the specimens was done according to the provisions of the AASHTO LRFD Bridge Design Specification (AASHTO, 2014). The design procedure assumes a monolithic behavior of the bridge deck without accounting for the deck discontinuity and field joints effects. The bending and shear demands were calculated based on the AASHTO Equivalent strip method that considers the maximum moment and shear values experienced by a bridge deck from infinite loading conditions. The general dimensions of the test specimens were determined based on the dimensions of the top flange of the standard and typical precast DBT girder in addition to the typical test specimens reported in previous research studies. The thickness of the top flange of the typical AASHTO/PCI standard DBTs is 6 in (15.2 cm) (PCI, 2011). In literature, many researchers have conducted experimental testing of narrow strips of the top DBT girder flanges with a middle longitudinal field joint. For example, Haber and Graybeal have tested 6-in (15.2-cm) thick panels with general plan dimensions of 28 in (71.1 cm) width and 107 in (271.8 cm) length and a bending span of 90 in (228.6 cm) (Haber and Graybeal, 2018). Peruchini has tested panels with a width of 24 in (61 cm) and a bending span of 90 in (228.6 cm) (Peruchini et al., 2017). The minimum and maximum centerline to centerline spacing between the DBT girders as specified by WSDOT is 60 in (152.4 cm) and 96 in (243.8 cm), respectively and it has a typical 6 in (15.24 cm) thick top flanges (Peruchini et al., 2017). However, other researchers have conducted large scale testing of

relatively bigger test specimens with plan dimensions that range between 72-96 in (183-244 cm) width and 72-84 in (183-213 cm) length with a bending span of 72 in (183 cm) (e.g. Graybeal, 2014; French et al., 2011). Hence, the general dimensions of the test specimens, as shown in Figure 4-2, were selected to be within the range of dimensions as reported in the previously mentioned literature studies.

As illustrated previously in Figure 4-1, the test specimens represent only a portion of the connected top flanges of the DBT with a longitudinal field joint at the middle of the specimen. The width of this portion was determined based on the likely representative distance between the bending inflection points so that the specimen would see just the expected positive moment part. Since it is hard to determine the exact locations of these inflection points, because of the large number of the expected loading conditions, the width of the specimen was taken as 7 ft (2.13 m) to allow for a 6 ft (1.83 m) positive bending span which is approximately 75% of the maximum centerline to centerline distance between DBT girders.

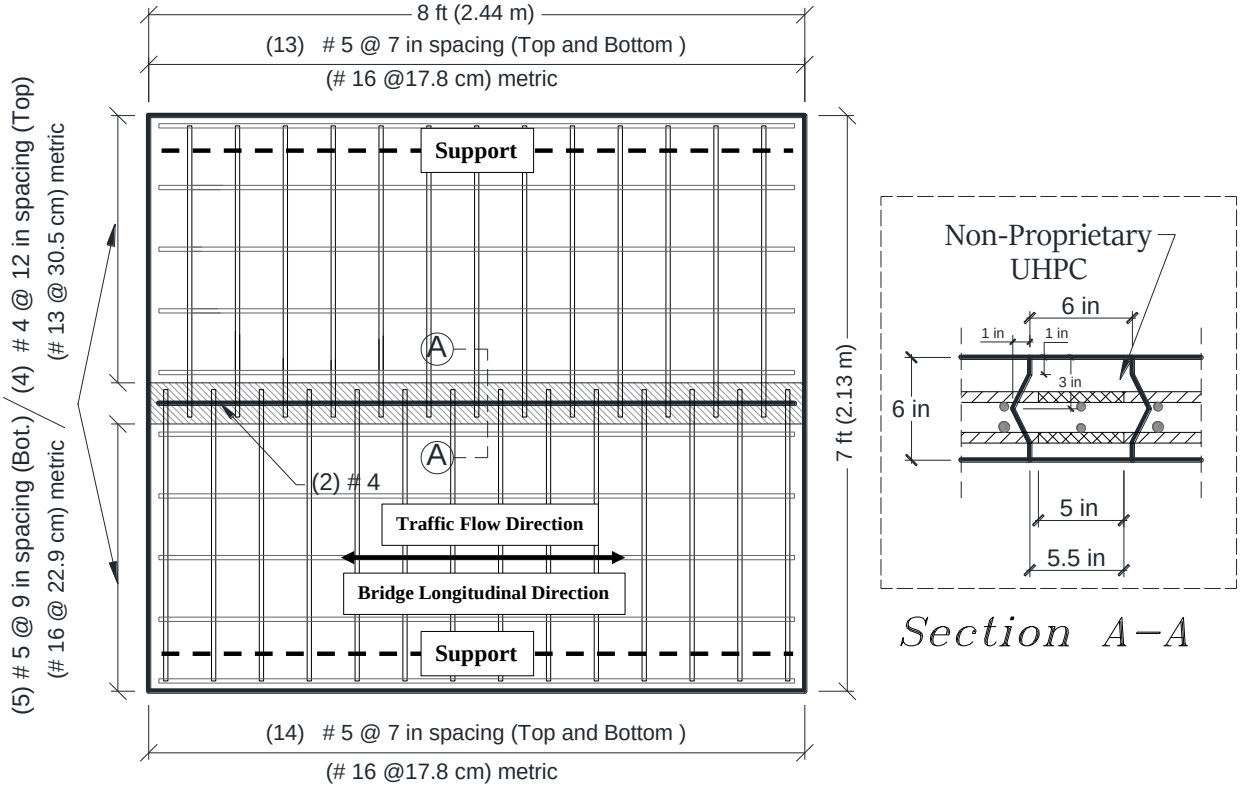

Figure 4-2: General Dimensions and structural details of the test specimens and a cross-sectional view of the longitudinal field joint (1 in = 2.54 cm, 1 ft = 30.48 cm).

Many practical considerations were taken into account during the choice of the longitudinal field joint details in order to enhance constructability and decrease the onsite activities. Hence, a non-contact lap splice was used to facilitate the assembly of the precast deck panels. Moreover, the use of advanced UHPC materials in such joints has eliminated the need for reinforcement post-tensioning (Graybeal, 2014; Graybeal, 2010 b; Graybeal, 2010 c), mechanical splicing (Mante et al., 2015), or splice confinement requirements (Badie et al., 1998) which were previously required

to connect the precast elements. A diamond-shaped shear key was used for the longitudinal joint interface to enhance durability and decrease the likelihood of having interface cracks between the joint and the precast elements. The 6 in (15.24 cm) width of the longitudinal field joint (see Figure 4-2) was determine based on the bond tests developed by OU on the baseline NP-UHPC mix in addition to recommendations of previous research studies (Graybeal, 2010 a, Abokifa et al., 2021; Abokifa and Moustafa, 2021). The transverse bars have a 5.5 in (14 cm) embedment length inside the field joints, which satisfied the minimum development length requirements of 8 times the diameter of the bar ($8d_b$) as recommended by the FHWA (Graybeal, 2014).

The top and bottom concrete covers of the test specimen were selected based on the AASHTO code provisions for bridge decks with normal condition exposure in a non-corrosive environment. Thus, the test specimens had a 2 in (5 cm) top cover and a 1 in (2.5 cm) bottom cover. The transverse reinforcement was considered as the main reinforcement of the top DBT flanges and hence they were placed as the outermost layers to increase the moment capacity of the specimen that will consequently subject the field joint to higher load demands. All reinforcement used in this study was of Grade 60 steel that conforms to the ASTM A706 specification. The precast panels, which represent parts of the DBT top flanges, were fabricated using a normal strength concrete with a minimum specified compressive strength of 5 ksi (34.5 MPa) after 28 days.

The fabrication process of the test specimens is divided into several phases that mimic the way the DBT girders and longitudinal field joints are typically constructed in real field applications. However, it is noted that both specimens were constructed separately at two different times since the proprietary UHPC specimen was previously constructed as part of another precedent research project as previously mentioned. The fabrication process was done at the fabrication yard of the EEL at UNR as shown in Figure 4-3 and summarized in the following section. The DBT girders are usually fabricated away from the bridge site location and then left on the fabrication facility to cure in a controlled environment before shipping them to the field and connecting them using longitudinal field joints. Hence, for each specimen, two precast deck panels which represent a portion of the top flanges of the DBT girders were constructed first. Then, they were left to cure on-site under the normal ambient air conditions for more than 28 Days to gain full strength. Then, both precast panels were reassembled next to each other to form the 6 in (15.24 cm) field joint. Finally, the closure pour material (e.g. NP-UHPC) was then mixed and poured inside the joints and left to cure on-site before moving the specimens to the laboratory for experimental testing.

Figure 4-3: Photographs from the fabrication process and illustration of the sequence of constructing test specimens.

4.2.2 Test Setup and Loading Protocol

The experimental testing of the test specimens was done at the EEL at UNR. The test setup was adopted to investigate the local flexural behavior of the representative DBT flange portions and field joint performance under the typical AASHTO truck wheel patch size. However, other minor load effects were not considered in the utilized experimental test setup such as the action between the flanges and DBT girder web parts and the resulting forces due to adjusting the differential cambers in DBT girder bridges. Moreover, the test setup did not account for the axial restraint at both specimen ends and the associated contribution to the load-bearing capacity of the specimen as the test specimen only represents the distance between two adjacent bending inflection points in the bridge transverse direction. Hence, rubber bearing pads were used at both ends of the test specimen to allow for rotation at support locations. Wheel loads or live loads are typically considered the main demands while designing bridge decks and deck field joints, and in turn, other load effects were eliminated to allow for the simplicity of the test setup. A photograph and a schematic drawing of the test setup showing the seat beams and applied load locations are shown in Figure 4-4.

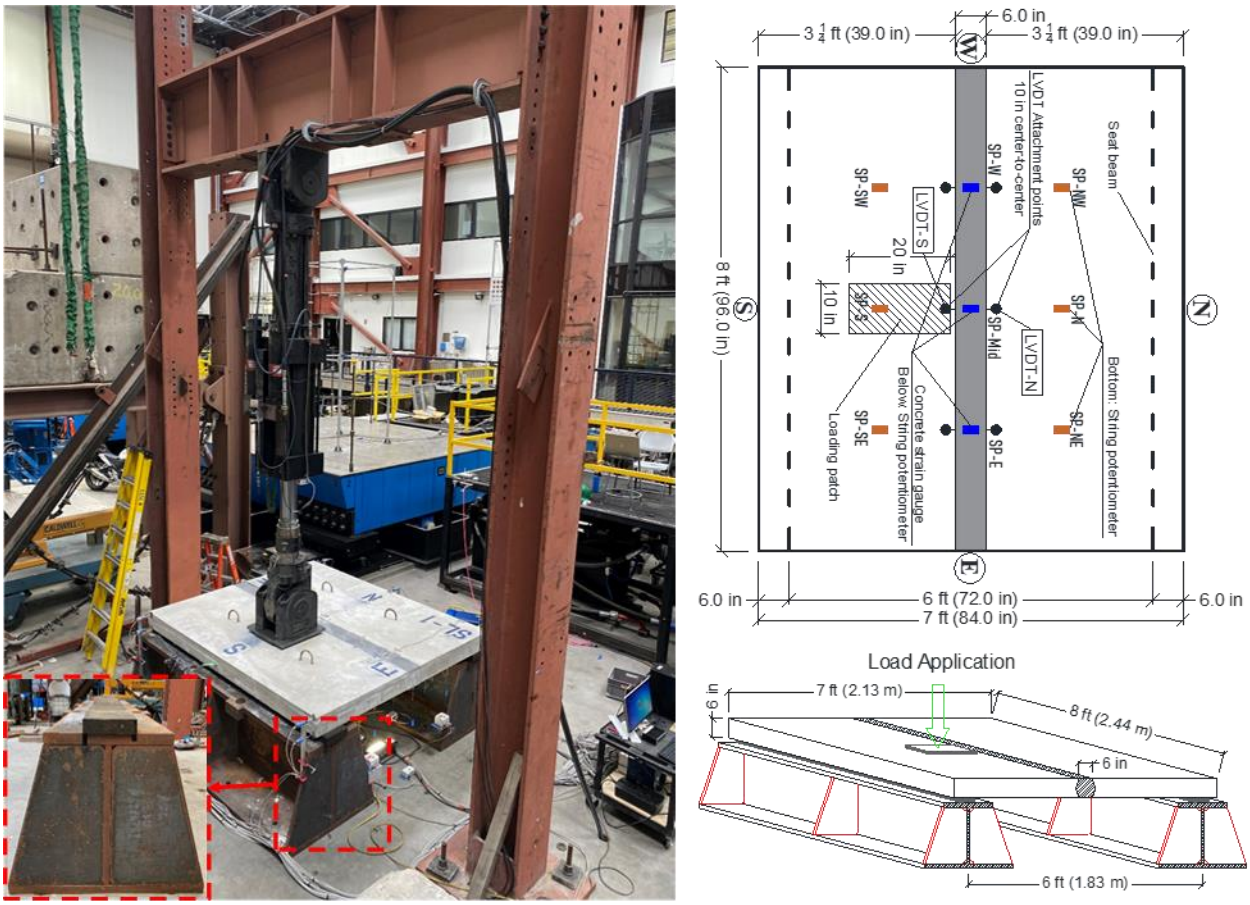

Figure 4-4: Photograph and schematic drawing of the test setup (1 in = 2.54 cm, 1 ft = 30.48 cm).

The test specimens were simply supported over two seat beams that were aligned parallel to the longitudinal field joint. The test specimens were loaded using a hydraulic actuator (with up to 220-kip (978.6 kN) capacity) through a rubber pad of 20 in × 10 in (50.8 cm × 25.4 cm) footprint dimensions. The load was applied at the mid-span of the longitudinal direction of the test specimen and adjacent to the field joint to impose shear forces at the interface surface between the field joint and the precast deck panel. The loading procedure used in this part of study consisted of four cycles of loading and unloading at small load levels to investigate the performances of the field joints at representative service load conditions and to estimate the average early flexural stiffness of the test specimens. The first two cycles included loading of the specimen up to 15 kips (66.72 kN) and then unloading. The second two cycles included loading of the specimen up to 30 kips (133.44 kN) and then unloading. The loading and unloading of the first four cycles were applied using a force control method with a rate of 5 kips/min (22.24 kN/min). Finally, displacement-control monotonic loading at a rate of 0.075 in/min (1.9 mm/min) was applied until failure to determine the peak load capacity in addition to assessing the post-peak response and determine the modes of failure of the test specimens.

4.2.3 Instrumentation Plan

The instrumentation plan for the test specimens, as shown in Figure 4-5, consisted of 35 reinforcement strain gauges that were installed to measure the strains of the transverse and longitudinal bars and monitor the load level at which the yielding occurs. Moreover, 15 string potentiometers were attached at the bottom of the specimen in a mesh configuration to measure the vertical deflection of the specimen. Finally, the instrumentation plan also included six linear variable displacement transducers (LVDTs) installed horizontally across the interface between the joint and the precast panels to measure the width of the interface crack that could happen through the test. Three cameras were also used below the specimen to monitor the progression of the crack through the test. A photograph of some of the instrumentation devices used in this study is shown in Figure 4-6.

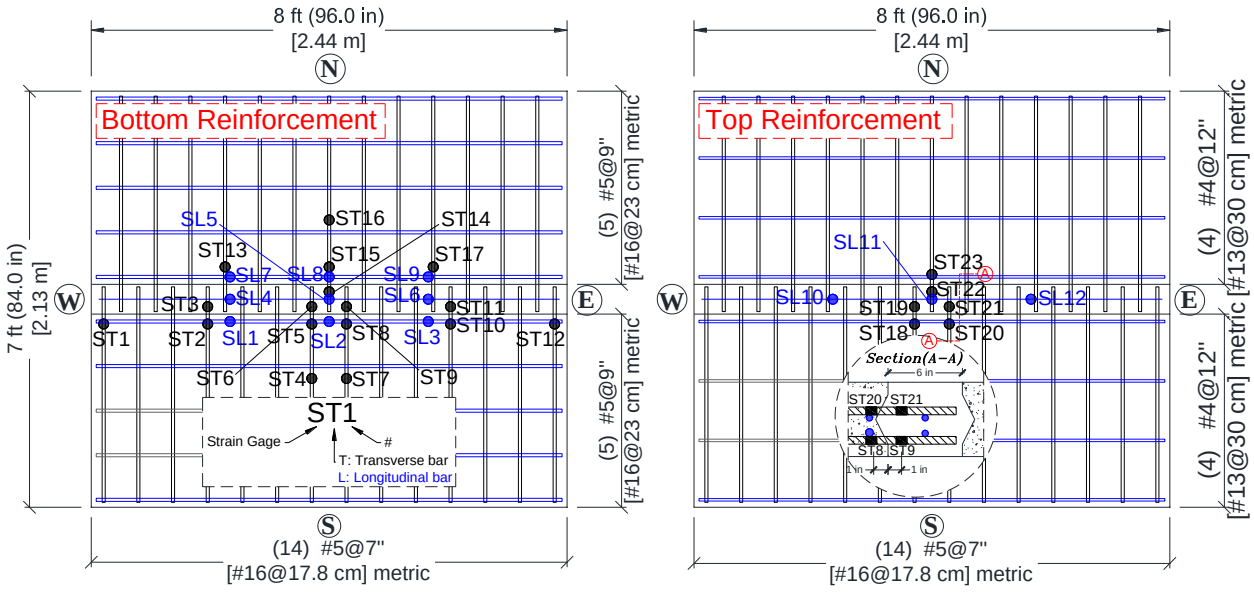

Figure 4-5: Reinforcement strain gages distribution for the bottom and top reinforcement of S1-NP-UHPC.

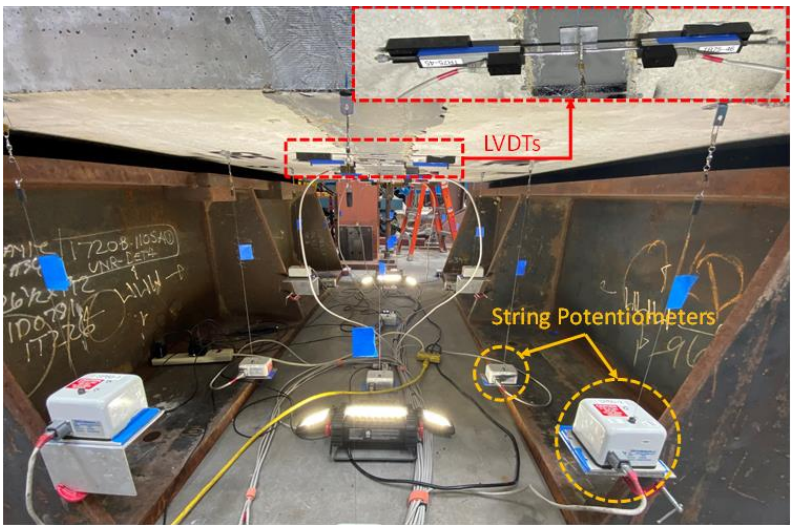

Figure 4-6: Photograph of some of the instrumentation devices used in this study.

4.3 Test Results and Comparative Behavior

The discussion of the global and local behaviors of both tested specimens is provided in this section and distributed among several subsections. As mentioned earlier, the experimental program included testing of two specimens. The first specimen used a NP-UHPC longitudinal field joint is denoted by "S1-NP-UHPC" throughout the rest of the discussion. The second specimen used a proprietary UHPC joint is denoted by "S2-P-UHPC". The proprietary UHPC product used in the joint of specimen S2-P-UHPC is the commercially available Ductal® JS1000 mix from LafargeHolcim. The research team has previous experience in mixing and testing this robust commercial Ductal UHPC product (Aboukifa et al., 2019; Aboukifa et al., 2020).

For completeness and consistency, the compressive strength of 3 in × 6 in cylinders of both proprietary and NP-UHPC used in this part of study were prepared and tested at different ages in accordance with the ASTM C1856 (ASTM C1856/C1856M-17, 2017) along with ASTM C39 (ASTM C39, 2012). The compressive strength results were 24.8 ksi (171 MPa) and 27.8 ksi (191.7 MPa) for the Ductal UHPC at 28 days and the day of the test, respectively. The compressive strength of the NP-UHPC used in the test specimen was 13.86 ksi (95.6 MPa) and 22.52 ksi (155.3 MPa) at 7 days and test day, respectively. The test results are mostly presented herein in the form of a detailed comparison between both specimens to validate the use of the developed NP-UHPC for longitudinal field joints. The structural performance of both tested specimens is presented and discussed in the following four subsections, which include the damage progression, load and deflection behavior, strains of the transverse and longitudinal reinforcing bars, and bonding at the joints interface.

4.3.1 Global Behavior of Specimens

The global behavior of the tested specimens is assessed by studying the flexural response of both specimens as represented by load-deflection relationships in addition to a detailed discussion of the damage progression, crack patterns, and modes of failure.

4.3.1.1 Damage Progression

A summary and overview of key experimental test results are provided first in Table 4-1 for both tested specimens. The table shows the peak load capacities in comparison to the calculated peak load values of both specimens in addition to the vertical deflections at the center of the specimens reported at the peak load and the AASHTO service and ultimate loads. It is worth noting that the theoretical or the calculated peak load values, as shown in Table 4-1, were calculated based on the moment-curvature analysis of the slab cross-section using the actual material properties. The table also shows the initial flexural stiffness of both specimens. The table provides an overall idea of the behavior of both specimens up to failure in a comparative way, before providing a detailed discussion of the global flexural behavior of the specimens later in this section. It is worth noting that the test continued until failure to investigate whether the whole precast system with field joint will remain intact with no significant interface cracking or slippage of reinforcement within the joint. This is mostly an academic point and not expected to represent a real-life scenario as bridge decks are usually designed to remain within the linear elastic range under code limits of service and ultimate loads. For the latter purpose, the reinforcement strains will be verified later in the

following sections to determine the loads at which the onset of yielding occurs and compare it with the service and ultimate loads.

Table 4-1: Summary of main experimental test results

Specimen	Peak Load, Kips (kN)	Calculated Peak Load, Kips (kN)	Middle Deflection at, in (cm)			Initial Stiffness, kip/in (kN/cm)
			Peak Load	Service Load	Ultimate Load	
S1-NP-UHPC	121.3 (539.6)	104 (462.6)	1.517 (3.85)	0.223 (0.57)	0.391 (0.99)	215 (376.5)
S2-P-UHPC	115.8 (515.1)	93 (413.7)	1.510 (3.83)	0.193 (0.49)	0.387 (0.98)	240 (420.3)

Several conclusions can be quickly deduced from the previous table as both specimens have very comparable behavior in terms of load-carrying capabilities and corresponding deflections. However, it can be seen that specimen S1-NP-UHPC has a higher flexural capacity than specimen S2-P-UHPC. This higher capacity is attributed to the higher compressive strength of the precast panels of specimen S1-NP-UHPC, i.e. 7.5 ksi at the test day, compared to 5.2 ksi for specimen S2-P-UHPC panels. It can be seen that the peak load values of both specimens exceeded the calculated load values assuming the continuity of the deck specimen or in other words monolithic deck systems. From the calculated and measured peak load values, the over the strength of specimen S1-NP-UHPC is less than that of specimen S2-P-UHPC, i.e. 16.6 % and 24.5 %, respectively, as a result of the higher mechanical properties of the proprietary UHPC compared to the NP-UHPC. Moreover, the initial stiffness of specimen S2-P-UHPC is first shown to be slightly higher than the other specimen because of the higher mechanical strength of the proprietary UHPC compared to the developed NP-UHPC. However, the flexural behavior of both tested specimens was almost similar, as such flexural members are commonly designed to be tension-controlled, i.e. under reinforced sections, which allows the main steel to yield before the crushing of concrete happens. Hence, the observed mode of failure for both specimens was yielding in the bottom transverse reinforcement followed by crushing of the normal strength concrete around the loading position in the south precast panel. When the applied load exceeded the code service and ultimate loads, the flexural cracks at the bottom of the specimens become more obvious and aggressively propagated until reaching the peak load capacity of the specimen where extremely wide cracks were observed in the precast panels. One of the benefits of using UHPC as field joint material is that it has significantly higher tensile strength compared to the precast NSC panels. Consequently, no flexural cracks were observed at the early stages of loading for both specimens as the first observed crack in the proprietary and NP-UHPC were at approximately 100 kips (444.8 kN) and 65 kips (289.1 kN), respectively. The reason for this difference is that the NP-UHPC has a relatively lower tensile strength compared to the proprietary UHPC.

The flexural cracks in both field joints (shown in Figure 4-7) were relatively limited to three or four main localized cracks with relatively narrow widths compared to cracks in the precast panels. Most of the flexural cracks at the bottom of the specimen were localized under the loading position in the middle of the specimen at the south precast panel as shown in Figures 4-7 a and 4-7 b for specimens S1-NP-UHPC and S2-P-UHPC, respectively. Crushing of concrete happened slightly

before reaching the peak load capacity for both specimens as shown in Figures 4-7 c and 4-7 d for specimens S1-NP-UHPC and S2-P-UHPC, respectively. As mentioned earlier, concrete crushing happened only in the south precast panel as it started at the load pad location at mid-span and propagated to the west and east ends. It is worth noting that no interface cracks were observed between the joint and the precast panels up to the AASHTO ultimate load. However, a short-length interface crack was observed at the bottom of specimen S1-NP-UHPC between the south concrete panel and the joint at approximately 70 kips (311.4 kN). On the other hand, specimen S2-P-UHPC had only experienced interface cracking at the end of the test. One more key observation for both tested specimens is that there is no bar slip happened to the lap splices within the field joints throughout the test, this can be a good conclusion that the 5.5 in (13.97 cm) satisfied the lap length requirements and was adequate to transfer forces between both precast panels up to failure load. Moreover, no bar rupture was observed through the entire testing regime for both specimens. The test was stopped upon reaching a certain criterion when a specimen lose at least 20% of the observed peak load capacity.

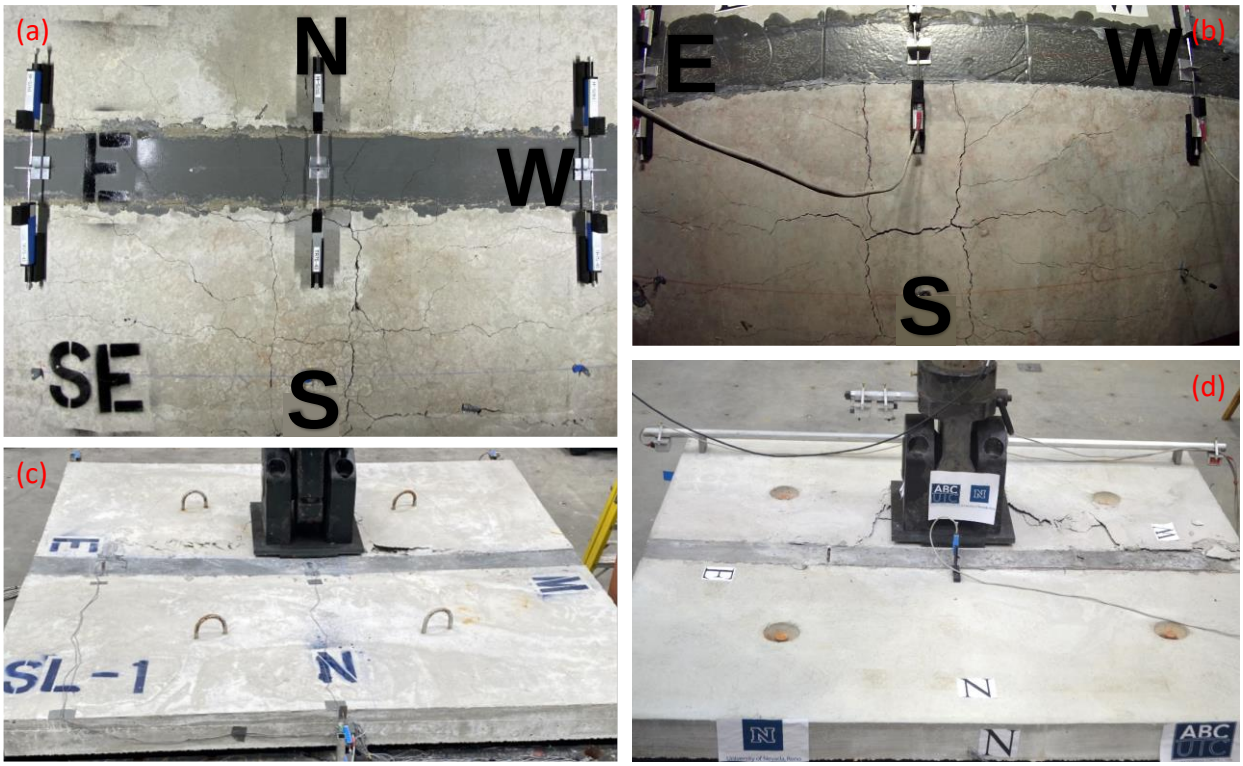

Figure 4-7: Flexural crack pattern and concrete crushing at (a) bottom of S1-NP-UHPC; (b) bottom of S2-P-UHPC; (c) top of S1-NP-UHPC; and (d) top of S2-P-UHPC.

4.3.1.2 Load-deflection relationship

The second aspect of assessing the global behavior of both tested specimens is investigating the load versus the vertical displacement behavior. The main aim of this section is to establish a comparison and detailed discussion of the flexural behavior of both specimens as evaluated at different load levels and highlight the key observations from the tests. Figure 4-8 shows the load-

deflection relationships for both tested specimens as it shows deflection readings at three different locations, i.e. two quarter-span locations and at mid-span.

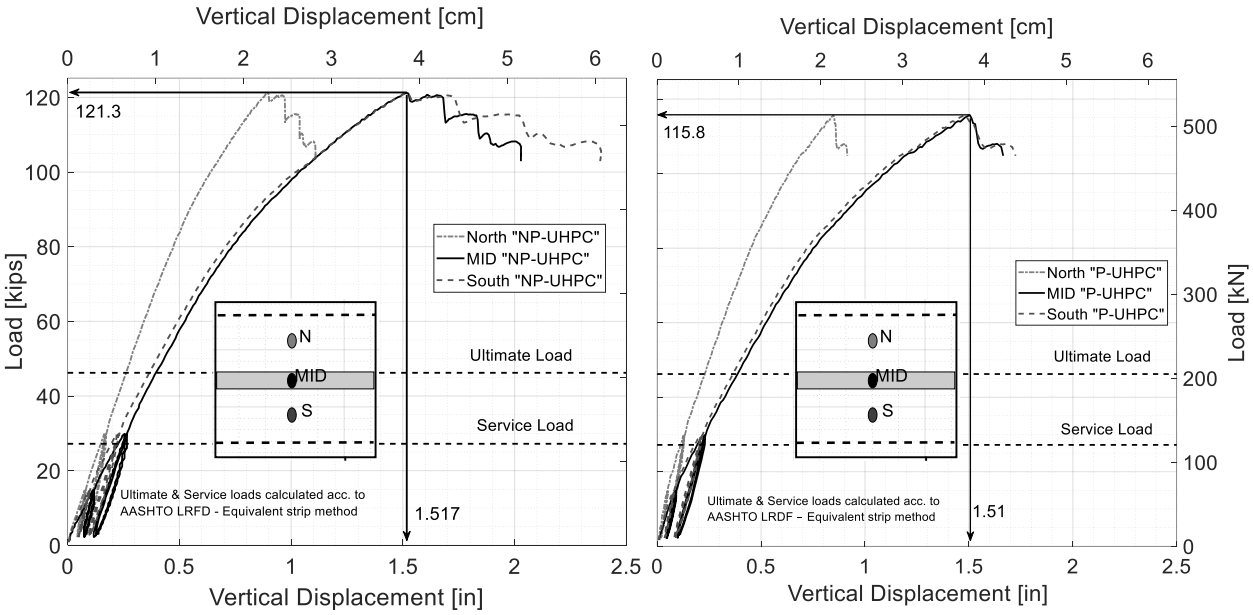

Figure 4-8: Load versus vertical displacements at quarter- and mid-span locations of the non-proprietary S1-NP-UHPC specimen (left) and proprietary S2-P-UHPC specimen (right).

In general, it can be seen from Figure 4-8 that both specimens have a very comparable flexural behavior. As mentioned earlier, specimen S1-NP-UHPC has a slightly higher peak load capacity compared to specimen S2-P-UHPC because of the higher compressive strength of the precast panels of this specimen. On the other hand, specimen S2-P-UHPC has a slightly higher initial stiffness because of two main reasons. First, the stress distribution over the specimen cross-section was still within the linear elastic range when looking at the initial stiffness. Hence, the difference in the compressive strength of the NSC did not have any significant contribution to the stiffness and global initial flexural behavior of the specimens. Second, the integrated system (precast panels plus UHPC joint) at the beginning of the test was still fully-engaged and the mechanical properties and stiffness of the proprietary UHPC in the joint were comparably higher than the NP-UHPC. In such a case, the proprietary UHPC acted as a rigid beam in the middle of the specimen that helped more in uniformly distributing the load over the specimen. Consequently, the initial deflections of specimen S2-P-UHPC were smaller than S1-NP-UHPC and the initial stiffness was higher. Another key observation from Figure 4-8 is that the flexural capacity of both specimens significantly exceeded the AASHTO LRFD ultimate limit state. From the above key observations, both proprietary and NP-UHPC were capable of providing viable solutions for use in the precast deck field joints in which the deck systems can satisfy the target behavior of conventional cast-in-place monolithic decks in terms of strength and load distribution requirements.

The load-deflection responses for both tested specimens change with increasing the applied loads. Initially, the flexural behavior of both specimens started as linear elastic up to the service load limit, i.e. up to 15 kips (66.7 kN). During this linear behavior, no cracks were observed in the precast panels or the field joints as both specimens did not yet reach the cracking moment.

Moreover, no interface debonding or bar slippage was observed up to this service limit loading. Then, as loading increased, the flexural response started to be a nonlinear behavior where the precast panels in both specimens started to have cracks and lost stiffness but the main steel was not yet yielded. During this stage, the load-deflection relationship behaved slightly non-linear in which both specimens had only small value deflections corresponding to the largely applied load increments. Moreover, and more importantly, no interface cracks or flexural cracks were observed in both joints due to the high tensile strength of both closure joint materials compared to the NSC in the precast panels. This initial part of non-linearity continued as the load increased to the onset of yielding of the main bars for both tested specimens. Upon reaching the yielding limit, the flexural stiffness of both specimens was significantly decreased because of the extensive flexural cracking in the precast panels associated with the yielding of the transverse bottom bars.

The flexural behavior of both specimens then showed global softening in which large deflection values were associated with small applied load increments. During this severe non-linear response, flexural cracks were observed in the NP-UHPC joint and a small length interface crack was also observed in that specimen S1-NP-UHPC. However, specimen S2-P-UHPC had only severe cracks in the precast panels without any cracking in the joint or at the joint interface. It is worth noting that no bar slip or bar rupture happened through the test. At the end of this non-linear response and just before reaching the peak load capacity, concrete crushing started to take place in the NSC of the south precast panel at the loading location and propagated to the east and west sides. After then, a degradation in the load capacity of the specimens was observed. For specimen S2-P-UHPC, sudden loss of the load capacity of the specimen was observed with increasing the applied displacements due to the crack localization in the UHPC and propagation of concrete crushing. However, for specimen S1-NP-UHPC, the failure was more ductile. Again, the main goal of loading the specimens beyond the code loading limits was to determine the modes of failure and to make sure that the weakest link in the integrated system is not expected to be the field joint, and instead, the failure should be governed by the precast panels.

It can be seen from Figure 4-8 above that the measured deflections at the middle and under the loading pad are almost identical. However, the measured deflections at the north side panels were comparably smaller. There are two main reasons for this difference in deflections. First, the asymmetry of loading in the north-south direction as the load was applied on the south precast panel and adjacent to the connection. Second, the capability of the field joint to provide the continuity of load transfer between both precast panels. This difference in deflections can be used as a useful tool in assessing the performance of the field joints in terms of load transfer capabilities. The less this difference indicates the better field joint performance. It can also be seen that this difference in deflections is increasing with the increase of the applied loads due to the increase of the flexural cracking that leads to a significant reduction in the stiffness of the specimens. The reason for this behavior complies with the research findings from a previous analytical study as a part of the NCHRP 10-71 project (French et al., 2011) which proves that the demands on the field joint decreases with the stiffness reduction associated with the extensive flexural cracking of the precast panel. It can be seen that the difference in deflections between the middle and north panel deflections for specimen S2-P-UHPC is slightly bigger than that of specimen S1-NP-UHPC. The difference between the middle and north side deflections at the measured peak loads were 0.62 in

(1.57 cm) and 0.66 in (1.67 cm) for specimens S1-NP-UHPC and S2-P-UHPC, respectively. To further illustrate the aforementioned deformed shape observations, a three-dimensional graph of the deflected shape is shown for one of the specimens at peak load. Figure 4-9 provides the deflection shape and deflection values (reported in inches) for S1-NP-UHPC at peak load.

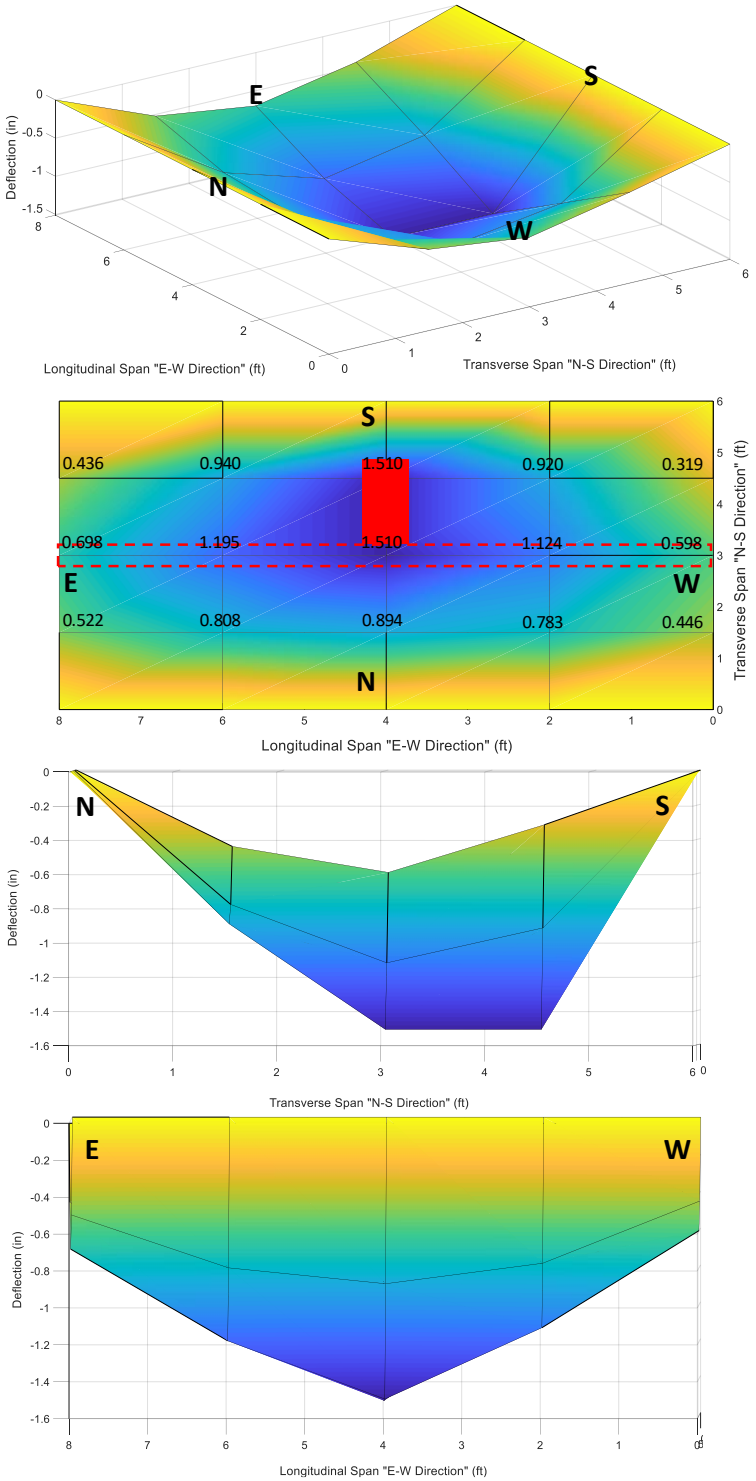

Figure 4-9: Deflected shape of specimen S1-NP-UHPC at peak load.

4.3.2 Local Behavior of Specimens

This section provides selected results from the measured strains of the transverse and longitudinal reinforcement in addition to measurements of the interface crack opening between the field joints and the adjacent precast panels.

4.3.2.1 Transverse reinforcement strains

The load versus the measured strain readings from selected bottom transverse reinforcement strain gages that were located near the mid-span location are shown in Figure 4-10 and discussed in this subsection. It is worth noting that some of the strain gages were eventually damaged during the tests at higher load levels. Figure 4-10 indicates which strain gages used for the presented results were damaged and at which load level.

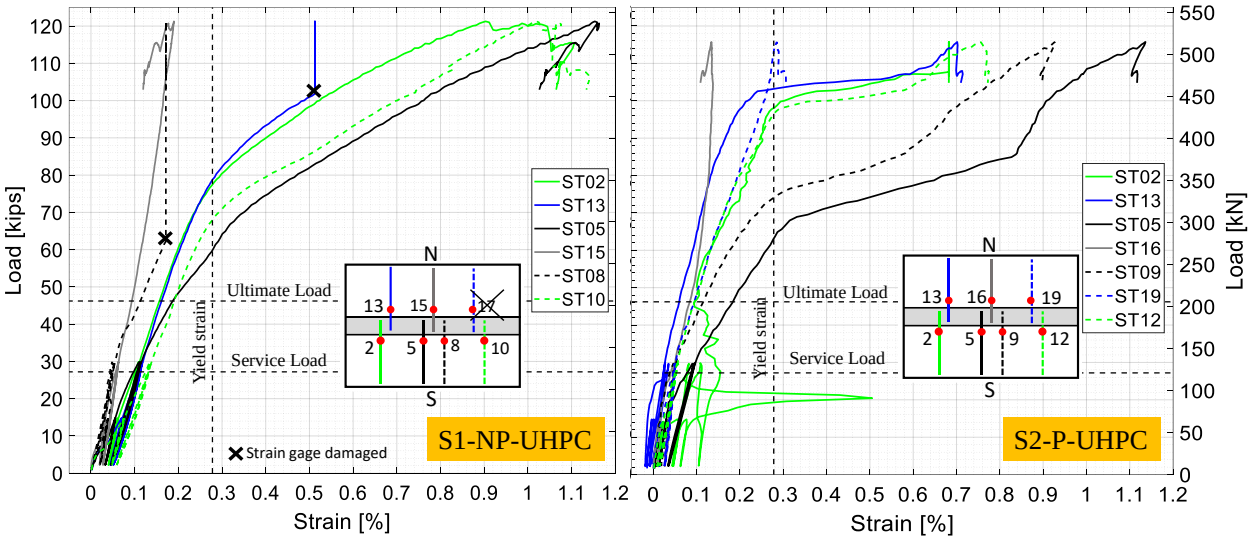

Figure 4-10: Load versus strain of selected bottom transverse reinforcement.

It can be seen from Figure 4-10 that the strains of the bottom reinforcement for both specimens were very comparable. However, the strain distribution of specimen S1-NP-UHPC was more uniform than specimen S2-P-UHPC as the middle bars in the south precast panel were more strained than the other adjacent bars. As shown in Figure 4-10, the bars in the south precast panel, on which the load, was applied had the highest recorded strains, especially at the middle two bars. The onset of yielding for both tested specimens was observed in one of the middle bars of the south precast panel at 60 kips (266.9 kN) and 64 kips (284.7 kN) for specimen S1-NP-UHPC and S2-P-UHPC, respectively. The calculated yielding load values based on the curvature analysis of the precast slab cross-section are 57 kips (253.6 kN) and 55.2 kips (245.5 kN) for specimens S1-NP-UHPC and S2-P-UHPC, respectively. Based on the transformed section method, the yielding load values were 68.4 kips (304.3 kN) and 67.2 kips (298.9 kN) for specimens S1-NP-UHPC and S2-P-UHPC, respectively. It can be seen that the main steel for both specimens yielded after satisfying the AASHTO ultimate load level. This was expected because of many reasons such as the use of the nominal values for steel yielding strength and concrete compressive strength when calculating the AASHTO ultimate load and the use of a reduction factor (Φ-factor) of 0.9 that magnifies the

ultimate moment and consequently increase the required steel area. However, it can be concluded that the proposed deck systems with proprietary and NP-UHPC field joints remained elastic up to the code limit.

As mentioned earlier, the load-deflection response of both specimens (see Figure 4-8 above) completely changed to severe non-linear after many bars of the transverse bottom reinforcement were yielded. It can be seen that most of the transverse bottom bars were yielded at approximately 80 kips (355.9 kN) and 100 kips (444.8 kN) for specimens S1-NP-UHPC and S2-P-UHPC, respectively. This non-linearity in behavior associated with yielding of the main reinforcement and severe cracking has resulted in global softening of specimens with large deflection increments with the application of small load intervals. After yielding all the main transverse reinforcement, crushing of concrete was observed at the south precast panel as shown previously in Figure 4-7. It is worth mentioning that the bottom transverse reinforcement of both specimens has yielded inside both proposed field joints as shown in Figure 4-11. This can provide a good idea that both the proposed proprietary and NP-UHPC field joints with 6 in width can sufficiently provide a proper development length for the bars inside the joint. This in turn will ensure adequate load transfer between both precast panels.

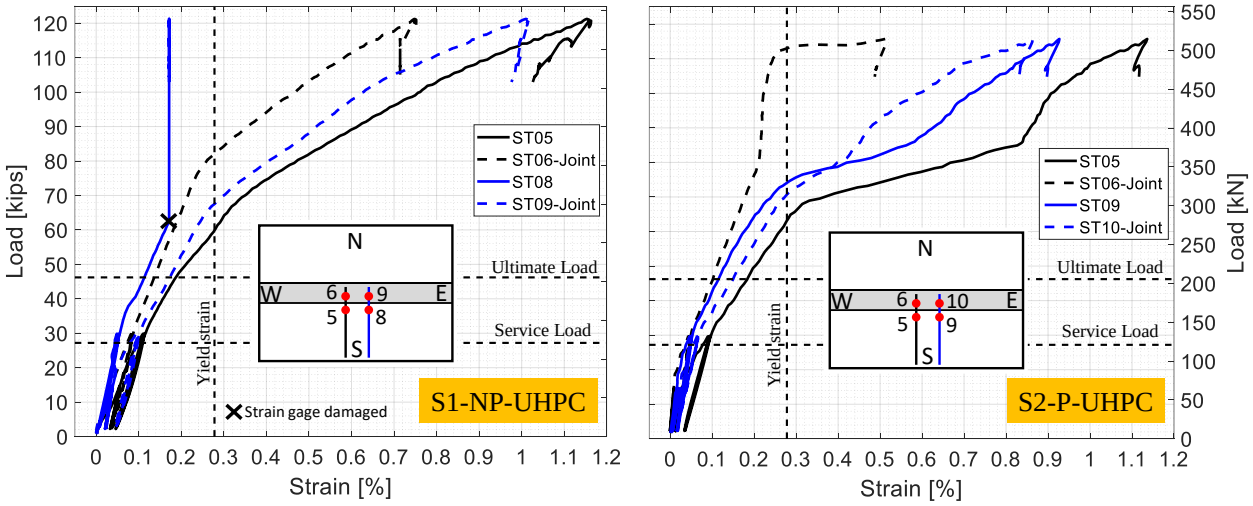

Figure 4-11: Load versus strain of selected transverse reinforcement inside and outside the joint.

4.3.2.2 Longitudinal reinforcement strains

While the previous section was focused on strains of the transverse bottom bars (main steel), the load versus strain readings of the longitudinal bars (secondary steel) at the middle of both tested specimens is presented in Figure 4-12 for completeness. The figure shows that the strains of the middle longitudinal bars for both specimens were again very comparable, like the other aspects of behavior. Specimen S2-P-UHPC seemed to have slightly higher strain values after yielding than specimen S1-NP-UHPC. This can be attributed to the fact that specimen S2-P-UHPC suffered from more bending in the longitudinal direction than the other specimen. The difference in compressive strength of NSC of the precast panels can be one of the possible reasons for having a more rigid behavior of specimen S2-NP-UHPC in the longitudinal direction and consequently less bending in this direction. It can also be seen that the longitudinal bars inside the field joints and

the precast panels were yielded after reaching the AASHTO ultimate load limit. Hence, the proposed deck systems were confirmed to have remained elastic up to the specified code limits. As can be seen from Figure 4-12, the strains of the bottom longitudinal bars inside the field joint and the south precast panels were comparably higher than the strains of the longitudinal bar in the north precast panel because of the position of the loading pad at the middle of the south precast panel and adjacent to the joint.

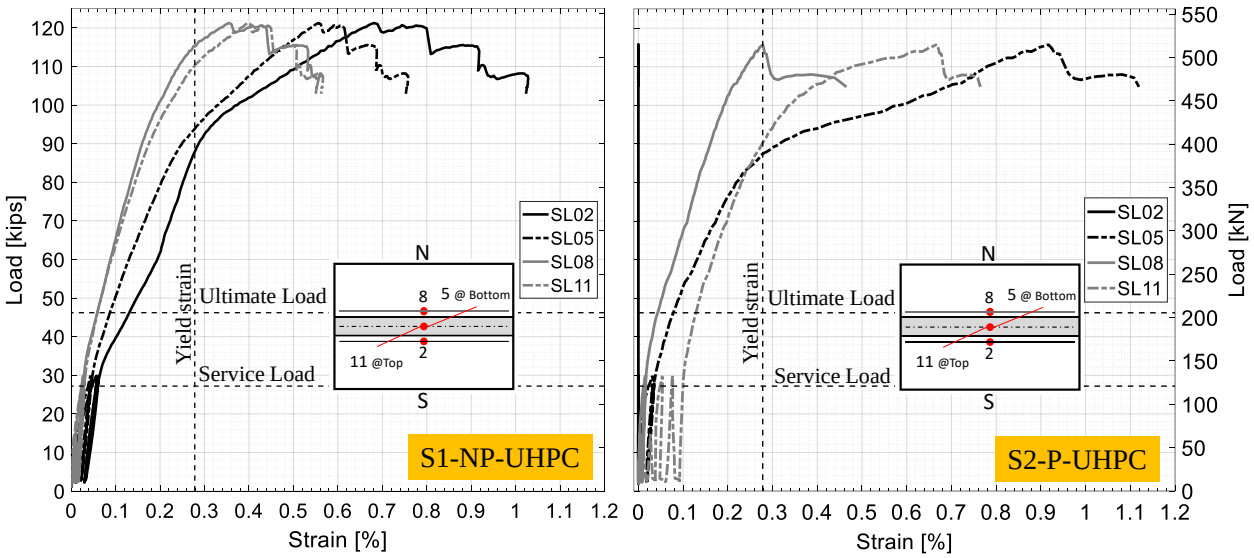

Figure 4-12: Load versus strain at the middle of the top and bottom longitudinal bars.

4.3.2.3 Field joint interface

As mentioned earlier, six horizontal LVDTs were used to monitor the interface crack opening between the joint and the adjacent panels at the bottom of both tested specimens. Table 4-2 reports the measured values for the interface opening of both specimens at the AASHTO service and ultimate loads. The table is arranged in a comparative way to verify if the bond properties of the NP-UHPC joint are adequate and are comparable to that of the proprietary UHPC joint. The AASHTO LRFD does not specify any limitations for the maximum allowable values for the interface crack opening. However, the AASHTO LRFD Article 5.6.7 (AASHTO, 2014) specifies a maximum spacing between the reinforcing bars to limit the width of the flexural cracks. These maximum spacing limitations were set based on the maximum allowable flexural crack width of 0.017 in (0.43 mm) for “class 1” exposure and 0.013 in (0.33 mm) for “class 2” exposure. The “class 2” exposure is typically used for situations in which the concrete is subjected to severe corrosion conditions.

It can be seen from the table that the interface crack width of specimen S1-NP-UHPC is slightly higher than that of specimen S2-P-UHPC. This is an indication that the bond strength of the proprietary UHPC is relatively better than the NP-UHPC. However, the interface crack width of both specimens at the AASHTO service load satisfied the crack width limitations for class 1 and class 2 exposures. This can confirm that the interface bond between the proprietary or NP-UHPC joints and the adjacent precast panels satisfied the design requirements and the code service load limits.

Table 4-2: Interface crack opening at the AASHTO LRFD service and ultimate loads.

LVDT Name (See Figure 4-5)	S1-NP-UHPC				S2-P-UHPC			
	Service load		Ultimate load		Service load		Ultimate load	
	in ($\times 10^{-3}$)	mm	in ($\times 10^{-3}$)	mm	in ($\times 10^{-3}$)	mm	in ($\times 10^{-3}$)	mm
LVDT-NW	12.6	0.32	19.9	0.51	8.8	0.22	17.6	0.45
LVDT-SW	11.7	0.3	21.3	0.54	6.8	0.17	11.6	0.29
LVDT-N	11.6	0.29	20.5	0.52	8.6	0.22	18.5	0.47
LVDT-S	13.7	0.35	25.5	0.65	7.6	0.19	17.9	0.45
LVDT-NE	11.8	0.3	18.1	0.46	N/A	N/A	N/A	N/A
LVDT-SE	10.9	0.28	16.8	0.43	7.4	0.19	12.2	0.31

4.4 Summary

This chapter presented results from comprehensive large-scale testing of representative DBT girder panels with both non-proprietary and commercial proprietary UHPC-filled longitudinal joint as alternative closure pour materials. The presented experimental results is part of a bigger collaborative project among the ABC-UTC consortium that aims at providing and demonstrating the viability of a NP-UHPC mix for ABC applications. The chapter discussed the structural performance of the proposed NP-UHPC longitudinal field joint in comparison to a readily implemented commercial proprietary UHPC product. Both global and local experimental behavior of two identical full-scale specimens with proprietary and NP-UHPC field joints were compared to verify the adequacy of using the newly developed UHPC as a closure material. The specimens considered representative DBT top flange parts and a 6-in (15.2-cm) wide diamond-shaped shear key joint and were tested under static vertical loading.

5. Summary and Conclusions

This research study presented the implementation of an emerging class of NP-UHPC for ABC field joints. The ABC-UTC NP-UHPC mixes has been designed at OU and this study investigated the repeatability and reproducibility of a baseline mix using local materials from Western US. This report was divided into three main sections in which each section had its own approach and objectives and was considered as a standalone sub-study. This study initially provided the mechanical characterization and behavior relationships of the NP-UHPC mixes that can be used for future modeling and larger applications. A total of five NP-UHPC mixes have been considered to investigate the effect of varying material sources as well as aggregate types and nominal sizes on the main mechanical properties. The flow properties of the developed mixes were investigated in addition to different sets of testing were conducted to test the compressive, flexural, and direct tensile strength and full behavior of the different NP-UHPC mixes. Then, this report presented the static structural performance of the transversely and longitudinally connected precast bridge deck panels using NP-UHPC field joints. The results of the NP-UHPC test specimens were compared to the results of similar reference specimens with P-UHPC joints to verify their structural performance. A total number of five full-scale test specimens have been tested in this study under vertical static loading. The experimental program included testing of three full scale bridge deck specimens with transverse NP-UHPC joints. The test parameters included different joint splice details, joint widths, closure joint materials, and longitudinal reinforcement configurations. The experimental program also included a single full-scale specimen with NP-UHPC longitudinal field joint which represented the typical connection in a DBT girders bridge. The study provided a detailed discussion of the structural behavior of the test specimens and the damage schemes. Moreover, this study provided assessment of the performance of the field joints at different load levels such as the AASHTO ultimate and service loads. The following observations and concluding remarks can be drawn from this experimental study:

- The basic characteristics of the ABC-UTC NP-UHPC mix originally designed at OU based on materials from the Midwest and South US regions can be successfully replicated using full independent set of materials and different aggregate types from Western US.
- Overall, the flow properties of all different NP-UHPC mixes is acceptable according to the flow requirements specified by ASTM C1856 or emerging FHWA reports. However, the fresh mixes with non-sieved sand (i.e. B1 and B3 in this study) are shown to have less uniform steel fiber dispersion because of the accumulation of the steel fibers around bigger sand particles.
- The developed NP-UHPC mixes with sieved and non-sieved sand both meet the minimum compressive strength requirements specified by ASTM C1856 (117 MPa). The equations for predicting UHPC compressive strength gain over time are validated for use for NP-UHPC mixes up to 56 days, but underestimate the strength at higher ages. Moreover, other equations for predicting compressive stress-strain behavior of UHPC are also validated for NP-UHPC.
- The compressive strength of NP-UHPC with 2% steel fibers is less sensitive than the ones with 1% steel fibers to the variability in aggregate types or material sources. Meanwhile, NP-UHPC mixes with local materials from Western US and non-sieved sand (i.e. B1 and B3) have higher compressive strength and more rapid early strength gain compared to other mixes.

- The various equations proposed in the literature for estimating UHPC modulus of elasticity seem to be inaccurate and overestimate that property for NP-UHPC mixes. Thus, based on the conducted test results, the following preliminary equation is proposed to use for estimating the ABC-UTC NP-UHPC modulus of elasticity: $E_c = 2{,}860\sqrt{f'c}$ (for f'_c in MPa), but more future testing is needed to further verify and update this equation.
- The flexural behavior and tensile behavior of the different NP-UHPC mixes are very comparable and they all have sustained strain hardening without brittle or sudden failure. Moreover, using 1% steel fibers by volume instead of the more common 2% is shown to reduce both flexural and direct tensile strengths only by about 15% and 30% for NP-UHPC mixes with sieved sand and non-sieved sand, respectively.
- Based on all the material characterization tests, comparisons, and assessment conducted in this study, the ABC-UTC NP-UHPC mix with 1% steel fiber and non-sieved sand (i.e. B3) strikes the best balance between acceptable mechanical properties and cost (less fibers, less work for sieving, etc.). Therefore, this mix provides a reasonable NP-UHPC candidate and hence, is recommended for future implementation and large-scale ABC applications.
- Based on the conducted material characterization of the proposed NP-UHPC mixes, the local sources in Nevada and California that have been identified for the various material components used in the mix are confirmed to be adequate. The main mechanical properties of the mixes sourced from different regions of the country at UNR and OU were very comparable. Hence, the Np-UHPC mixes are deemed acceptable and insensitive to local resourcing as suggested by repeatable mechanical properties and they can be further extended to field implementation.
- This study enriches the literature by providing full tensile and compressive stress-strain relationships for NP-UHPC which can be readily used for defining constitutive laws and future modeling to further explore more applications of NP-UHPC.
- In general, the structural behavior and joint performance of the precast bridge decks with full-depth transverse NP-UHPC field joints are demonstrated to be acceptable and viable for ABC. The global and local behaviors of the test specimens with transverse NP-UHPC were very comparable to that of the currently implemented and acceptable practice of the specimens using the commercial or P-UHPC.
- Similarly, the structural behavior and joint performance of the representative DBT girder's top flange parts with full-depth longitudinal non-proprietary UHPC field joints are demonstrated to be a viable alternative for ABC. The performance of the longitudinal NP-UHPC joint was very comparable to that of the currently acceptable and adopted practice using robust proprietary/commercial UHPC mixes.
- Flexural load capacities of the test specimens were found to be much higher than the AASHTO LRFD service and ultimate load limits. Moreover, the peak load capacity of the NP-UHPC specimen was slightly higher than that of the proprietary UHPC, which was attributed to the higher compressive strength of the NSC used in the precast panels of the non-proprietary UHPC specimen.

- All the test specimens have flexure dominated failure in which yielding of reinforcement was observed before the concrete crushing and failure. While the NP-UHPC joints were confirmed not to be the weakest links in the integrated deck system.
- The proposed deck systems with NP-UHPC field joints were able to fulfill the AASHTO LRFD service and ultimate load requirements without any major damage, splice slippage or interface cracking. While some interface cracks were observed at later loading stages which did not affect the failure of the specimens.
- The test specimens remained essentially elastic up to the AASHTO LRFD ultimate load in which no yielding of reinforcement was observed. The tensile strains of the reinforcement splices inside the joint indicated that the proposed overlap lengths were sufficient to yield the reinforcement inside the joint.
- The initial stiffness and load capacities of the deck systems with NP-UHPC transverse joints, which have a 2% steel fibers amount, were slightly greater than that of the deck systems with NP-UHPC joints with only 1% steel fibers.
- For the transverse specimens, the compressive strength of the conventional concrete and NP-UHPC showed that concrete crushing took place just before the failure of the specimens and after yielding of reinforcement (tension-controlled). The measured concrete strains indicated that the loop splices enhanced the load distribution across the specimen's cross section while the use of NP-UHPC mix with 1% steel fibers has resulted in a slightly less favorable load distribution.
- For the longitudinal specimens, the interface crack width of the NP-UHPC specimen appeared to be slightly higher than that of the other specimen. This suggests that the bond strength of the proprietary UHPC is better than the non-proprietary UHPC, but with no further implications as the interface crack width of both specimens was well below the AASHTO LRFD specified crack width limitations for class 1 and class 2 exposures.
- In summary, non-proprietary UHPC mixes sourced from Nevada and California local materials can be effectively used for closure joint materials for full-depth bridge deck field joints without requiring any post-tensioning or mechanical splicing. This study demonstrated that the 15.2-20.3 cm field joint width, typically used for proprietary UHPC, is also sufficient for non-proprietary UHPC to provide monolithic-equivalent deck systems in terms of load distribution.

6. References

AASHTO (American Association of State Highway and Transportation Officials). AAHSTO LRFD Bridge Design Specifications, 7th ed.; American Association of State Highway and Transportation Officials: Washington, DC, USA, 2014.

Abokifa, M., Moustafa, M. A., & Itani, A. M. (2020). More Choices for Connecting Prefabricated Bridge Deck Elements (No. ABC-UTC-2016-C1-UNR03-Final). Accelerated Bridge Construction University Transportation Center (ABC-UTC).

Abokifa, M., & Moustafa, M. A. (2021). Experimental behavior of poly methyl methacrylate polymer concrete for bridge deck bulb tee girders longitudinal field joints. Construction and Building Materials, 270, 121840.

Abokifa, M., & Moustafa, M. A. (2021). Full-scale testing of non-proprietary ultra-high performance concrete for deck bulb tee longitudinal field joints. Engineering Structures, 243, 112696.

13. Abokifa, M., M.A. Moustafa, A. Itani, (2021). Comparative Behavior of Precast Bridge Deck Panels with UHPC and Polymer Concrete Transverse Field Joints, Engineering Structures, 247, 113195

Abokifa, M., & Moustafa, M. A. (2021). Development of Non-Proprietary UHPC Mix: Application to Deck Panel Joints. Quarterly Progress Report.

Abokifa, M., M.A. Moustafa, (2021). Experimental Behavior of Precast Bridge Deck Systems with Non-Proprietary UHPC Transverse Field Joints, Materials, 14 (22), 6964

Abokifa, M., M.A. Moustafa, (2021). Mechanical Characterization and Material Variability Effects of Emerging Non-Proprietary UHPC Mixes for Accelerated Bridge Construction Field Joints, Construction and Building Materials, 308, 125064

Aboukifa, M., Moustafa, M. A., Itani, A. M., & Naeimi, N. (2019). Durable UHPC Columns with High-Strength Steel (No. ABC-UTC-2013-C3-UNR02-Final). Accelerated Bridge Construction University Transportation Center (ABC-UTC).

Aboukifa, M., M. A. Moustafa, M. S. Saiidi, (2020). "Seismic Response of Precast Columns with Non-Proprietary UHPC-Filled Ducts ABC Connections," Report No. CCEER-20-08, October 2020.

Aboukifa, M., Moustafa, M. A., & Itani, A. M. (2020). Comparative Structural Response of UHPC and Normal Strength Concrete Columns under Combined Axial and Lateral Cyclic Loading. ACI SP 341. 71-96.

Aboukifa, M., Moustafa, M. A., & Saiidi, M. S. (2021). Seismic Response of Precast Bridge Columns with Composite Non-Proprietary UHPC Filled Ducts ABC Connections. Composite Structures, 114376.

ACI Committee. (2008). Building code requirements for structural concrete (ACI 318-08) and commentary. American Concrete Institute.

ACI (American Concrete Institute). Guide for the Use of Polymers in Concrete; ACI 548.1R-09; ACI: Farmington Hills, MI, USA, 2009.

ACI Committee 233. (2011). Slag Cement in Concrete and Mortar. American Concrete Institute (233R–03). American Concrete Institute.

Alkaysi, M., El-Tawil, S., Liu, Z., & Hansen, W. (2016). Effects of silica powder and cement type on durability of ultra-high performance concrete (UHPC). Cement and Concrete Composites, 66, 47-56.

Allena, S., & Newtson, C. M. (2011). Ultra-high strength concrete mixtures using local materials. Journal of Civil Engineering and Architecture, 5(4), 322-330.

Alsalman, A., Dang, C. N., & Hale, W. M. (2017). Development of ultra-high performance concrete with locally available materials. Construction and Building Materials, 133, 135-145.

American Road and Transportation Builders Association (ARTBA) 2020 bridge report.

Arora, A., Almujaddidi, A., Kianmofrad, F., Mobasher, B., & Neithalath, N. (2019). Material design of economical ultra-high performance concrete (UHPC) and evaluation of their properties. Cement and Concrete Composites, 104, 103346.

ASTM A706/A706M-16 Standard Specification for Deformed and Plain Low-Alloy Steel Bars for Concrete Reinforcement. West Conshohocken, PA; ASTM International, 2016.

ASTM, A. (2014). Standard specification for flow table for use in tests of hydraulic cement. ASTM Int., 1-6.

ASTM C109, American Society for Testing and Materials, 1992. Standard test method for compressive strength of hydraulic cement. Annual Book of ASTM Standards.

ASTM C136/C136M-14 (2014) “Standard Test Method for Sieve Analysis of Fine and Coarse Aggregates, ASTM International”, West Conshohocken, PA.

ASTM C1437. (2006). Standard Test Method for Flow of Hydraulic Cement Mortar, Annual Book of ASTM Standards, vol. 04-01. West Conshohocken, PA, USA.

ASTM C1609/C1609M-07. Standard test method for flexural performance of fiber-reinforced concrete (using beam with third-point loading). American Society of Testing and Materials (2007).

ASTM, C1611. (2009). Standard test method for slump flow of self-consolidating concrete.

ASTM C1856/C1856M-17. (2017). Standard practice for fabricating and testing specimens of ultra-high performance concrete. ASTM International”, West Conshohocken, PA.

ASTM C230/C230M. (1998). Standard specification for flow table for use in tests of hydraulic cement.

ASTM C39. Standard Test Method for Compressive Strength of Cylindrical Concrete Specimens. American Society for Testing and Materials Standard Practice C39, Philadelphia, PA, 2001.

ASTM C469/C469M-14. Standard Test Method for Static Modulus of Elasticity and Poisson's Ratio of Concrete in Compression. American Society of Testing and Materials (2014).

ASTM C579-18. Standard Test Methods for Compressive Strength of Chemical-Resistant Mortars, Grouts, Monolithic Surfacings, and Polymer Concretes. West Conshohocken, PA; ASTM International, 2018.

Badie, S. S., Baishya, M. C., & Tadros, M. K. (1998). NUDECK-An efficient and economical precast prestressed bridge deck system. PCI journal, 43(5).

Banthia, N., & Islam, S. T. (2013). Loading rate concerns in ASTM C1609. Journal of Testing and Evaluation, 41(6), 1032-1036.

Berry, M., Snidarich, R., & Wood, C. (2017). Development of non-proprietary ultra-high performance concrete (No. FHWA/MT-17-010/8237-001). Montana. Dept. of Transportation. Research Programs.

California Department of Transportation, Notice to Bidders and Special Provision. Contract No. 06-0K4604, Project ID 0612000105, 2015.

Collepardi, S., Coppola, L., Troli, R., & Collepardi, M. (1997). Mechanical properties of modified reactive powder concrete. ACI SPECIAL PUBLICATIONS, 173, 1-22.

Coufal, R., Vitek, J. L., Rehacek, S., Kolisko, J., & Citek, D. (2016, July). UHPC Connection of Precast Bridge Deck. In International Interactive Symposium on Ultra-High Performance Concrete (Vol. 1, No. 1). Iowa State University Digital Press.

De Larrard, F., & Sedran, T. (1994). Optimization of ultra-high-performance concrete by the use of a packing model. Cement and concrete research, 24(6), 997-1009.

Dhakal, S., & Moustafa, M. A. (2019). MC-BAM: Moment–curvature analysis for beams with advanced materials. SoftwareX, 9, 175-182.

Dinitz A. M., Ferri R. “Polymer Concrete (MMA) for Bridge Rehabilitation Applications” (1985). ACI SP-89-8, Polymer Concrete: Uses, Materials, and Properties, pp. 141-159.

El-Tawil, S., Alkaysi, M., Naaman, A. E., Hansen, W., & Liu, Z. (2016). Development, characterization and applications of a non proprietary ultra high performance concrete for highway bridges (No. RC-1637). Michigan. Dept. of Transportation.

Fontana J. J., Webster R., Kukacka L. E. “Rapid patching of deteriorated concrete using polymer concrete” (1978). Proceedings, 2nd International Congress on Polymers in Concrete, University of Texas, Austin, pp. 105-119.

Fowler D. W., Paul D. R. “Polymer concrete for repair of bridge decks” (1978). Proceedings, 2nd International Congress on Polymers in Concrete, University of Texas, Austin, pp. 337-350.

Fowler D. W., Meyer A. H., Paul D. R. “Implementation manual for polymer concrete repair” (1983). Research Report No. 246-4F, Center for Transportation Research, University of Texas, Arlington.

French CE, Shield CK, Klaseus D, Smith M, Eriksson W, Ma ZJ, et al. Cast-in-place concrete connections for precast deck systems (No. NCHRP Project 10-71); 2011.

Funk, J. E., & Dinger, D. R. (2013). Predictive process control of crowded particulate suspensions: applied to ceramic manufacturing. Springer Science & Business Media.

Graybeal, B. A. (2006). Material property characterization of ultra-high performance concrete (No. FHWA-HRT-06-103). United States. Federal Highway Administration. Office of Infrastructure Research and Development.

Graybeal, B. A. (2007). Compressive behavior of ultra-high-performance fiber-reinforced 990 concrete. ACI materials journal, 104(2), 146.

Graybeal, B. (2010) a. Behavior of Field-Cast Ultra-High Performance Concrete Bridge Deck Connections Under Cyclic and Static Structural Loading; Report No. FHWA-HRT-11-023; Federal Highway Administration, McLean, VA, 2010.

Graybeal, B. A. (2010, February) b. Behavior of Ultra-High Performance Concrete connections between precast bridge deck elements. In Proceedings of the 2010 Concrete Bridge Conference: Achieving Safe, Smart & Sustainable Bridges, Phoenix, AZ, USA (Vol. 24).

Graybeal, B. (2010) c. Field-cast UHPC connections for modular bridge deck elements (No. FHWA-HRT-11-022).

Graybeal, B. (2011). Ultra-high performance concrete (No. FHWA-HRT-11-038).

Graybeal, B. A., & Stone, B. (2012). Compression response of a rapid-strengthening ultra-high performance concrete formulation (No. FHWA-HRT-12-065). United States. Federal Highway Administration. Office of Infrastructure Research and Development.

Graybeal, B. A. (2013). Development of Non-Proprietary Ultra-High Performance Concrete for Use in the Highway Bridge Sector: TechBrief (No. FHWA-HRT-13-100). United States. Federal Highway Administration.

Graybeal, B. (2014). Design and construction of field-cast UHPC connections (No. FHWA-HRT-14-084; HRDI-40/10-14 (750) E). United States. Federal Highway Administration.

Graybeal, B. A. (2015). Compression testing of ultra-high-performance concrete. Advances in Civil Engineering Materials, 4(2), 102-112.

Graybeal, B. A., & Baby, F. (2019). Tension testing of ultra-high performance concrete (No. FHWA-HRT-17-053). United States. Federal Highway Administration. Office of Infrastructure Research and Development.

Haber, Z. B., De la Varga, I., Graybeal, B. A., Nakashoji, B., & El-Helou, R. (2018). Properties 887 and behavior of UHPC-class materials (No. FHWA-HRT-18-036). United States. Federal 888 Highway Administration. Office of Infrastructure Research and Development.

Haber, Z. B., & Graybeal, B. A. (2018). Performance of Grouted Connections for Prefabricated Bridge Deck Elements (No. FHWA-HIF-19-003). United States. Federal Highway Administration. Office of Infrastructure Research and Development.

Hartwell, D. R. "Laboratory testing of Ultra High Performance Concrete deck joints for use in accelerated bridge construction" (2011). Graduate Theses and Dissertations. 10420.

Hernandez, J. A. A. (2016). Development and laboratory testing of Ultra High Performance Concrete (Doctoral dissertation).

Holschemacher, K., & Weiße, D. (2005). Economic mix design ultra high-strength concrete. Special Publication, 228, 1133-1144.

Hsu M., Fowler D. W. "Creep and fatigue of polymer concrete" (1985). ACI, SP 89-17, pp. 323-343.

Hwang H., Park S. Y. "A study on the flexural behavior of lap-spliced cast-in-place joints under static loading in ultra-high performance concrete bridge deck slabs" (2014). Canadian Journal of Civil Engineering, 41:615-623.

Joe CD, Moustafa MA. Cost and ecological feasibility of using UHPC in bridge piers. In first international interactive symposium on UHPC; 2016. p. 18-20.

Kim, H., Koh, T., & Pyo, S. (2016). Enhancing flowability and sustainability of ultra high performance concrete incorporating high replacement levels of industrial slags. Construction and Building Materials, 123, 153-160.

Kosmatka, S. H., Kerkhoff, B., & Panarese, W. C. (2002). Design and control of concrete mixtures (Vol. 5420, pp. 60077-1083). Skokie, IL: Portland Cement Association.

Kukacka L. E., Fontana J. "Polymer concrete patching materials" (1977). Implementation Package No. 77-11, Volume 1 and 3, Federal Highway Administration, Washington, DC.

Kusumawardaningsih, Y., Fehling, E., & Ismail, M. (2015). UHPC compressive strength test specimens: Cylinder or cube?. Procedia Engineering, 125, 1076-1080.

Leboeuf S. V., Charron J. P., Massicotte B. "Design and behavior of UHPFRC field-cast transverse connections between precast bridge deck elements" (2017). Journal of Bridge Engineering.

Li L., Jiang Z. “Flexural behavior and strut-and-tie model of joints with headed bar details connecting precast members” (2016). Perspectives in Science. Volume 7, pp. 253-260, ISSN 2213-0209.

Looney, T., McDaniel, A., Volz, J., & Floyd, R. (2019). Development and characterization of ultra-high performance concrete with slag cement for use as bridge joint material. Development, 1(02).

Looney, T., Coleman, R., Funderburg, C., Volz, J., & Floyd, R. (2021). Concrete Bond and Behavior of Nonproprietary Ultrahigh-Performance Concrete Bridge Slab Joints. Journal of Bridge Engineering, 26(2), 04020128.

Lowke, D., Stengel, T., Schießl, P., & Gehlen, C. (2012). Control of rheology, strength and fibre bond of UHPC with additions-effect of packing density and addition type. In Proc., 3rd Int. Symp. on UHPC and Nanotechnology for High Performance Construction Materials (pp. 215-224).

Mantawy, I.; Chennareddy, R.; Genedy, M.; Taha, M.R. Polymer Concrete for Bridge Deck Closure Joints in Accelerated Bridge Construction. Infrastructures 2019, 4, 31.

Mante, D. M., Abbas, H. H., Ramey, G. E., & Barnes, R. W. (2015). Full-Scale Implementation and Testing of Full-Depth Precast Bridge Deck Panels. Transportation Research Record, 2522(1), 3-17.

Mendonca, F., El-Khier, M. A., Morcous, G., & Hu, J. (2020). Feasibility Study of Development of Ultra-High Performance Concrete (UHPC) for Highway Bridge Applications in Nebraska (No. SPR-P1 (18) M072). Nebraska Department of Transportation.

Meng, W., Valipour, M., & Khayat, K. H. (2017). Optimization and performance of cost-effective ultra-high performance concrete. Materials and structures, 50(1), 1-16.

Naeimi, N., & Moustafa, M. A. (2020). Numerical modeling and design sensitivity of structural and seismic behavior of UHPC bridge piers. Engineering Structures, 219, 110792.

Naeimi, N., & Moustafa, M. A. (2021). Compressive behavior and stress–strain relationships of confined and unconfined UHPC. Construction and Building Materials, 272, 121844.

National Cooperative Highway Research Program. Cast-in-Place Concrete Connections for Precast Deck Systems. NCHRP Report 10-71. Transportation Research Board, Washington DC, 2011.

Park, J. J., Kang, S. T., Koh, K. T., & Kim, S. W. (2008). Influence of the ingredients on the compressive strength of UHPC as a fundamental study to optimize the mixing proportion. In Proceedings of the second international symposium on ultra high performance concrete (pp. 105-112). Kassel Germany.

PCI (Precast/Prestressed Concrete Institute) PCI Bridge Design Manual, 3rd ed.; First Release, 2011.

Perry, V., Krisciunas, R., and Stofko, B. (2012). “Mackenzie River Twin Bridges—The largest field-cast UHPC connections project in North America.” Proc., PCI—National Bridge Conf., Precast/Prestressed Concrete Institute, Chicago.

Perry, V., Krisciunas, R., & Stofko, B. (2014). Mackenzie River Twin Bridges: North America’s Largest Field-Cast Ultra-High-Performance Concrete Connections Project. PCI Journal, 59(2).

Peruchini, T. J. (2017). Investigation of Ultra-High Performance Concrete for Longitudinal Joints in Deck Bulb Tee Bridge Girders (Doctoral dissertation).

Qiao, P., Zhou, Z., & Allena, S. (2016). Developing Connections for Longitudinal Joints between Deck Bulb Tees-Development of UHPC Mixes with Local Materials (No. WA-RD 869.1). Washington (State). Department of Transportation.

Reis J.M.L., Ferreira A.J.M. “Fracture behavior of glass fiber reinforced polymer concrete” (2003). Polymer Testing, Volume 22, Issue 2, pp. 149-153, ISSN 0142-9418.

Resplendino, J. (2011). Introduction: What is a UHPFRC? Designing and Building with UHPFRC, 3-14.

Ribeiro M., Tavares C., Ferreira A. “Chemical resistance of epoxy and polyester polymer concrete to acids and salts” (2011). Journal of Polymer Engineering, Volume 22, Issue 1, pp. 27-44.

Russell, H. G., Graybeal, B. A., & Russell, H. G. (2013). Ultra-high performance concrete: A state-of-the-art report for the bridge community (No. FHWA-HRT-13-060). United States. Federal Highway Administration. Office of Infrastructure Research and Development.

Schröfl, C., Gruber, M., & Plank, J. (2008). Structure performance relationship of polycarboxylate superplasticizers based on methacrylic acid esters in ultra high performance concrete. In Second International Symposium on Ultra High Performance Concrete (pp. 383-390).

Shahrokhinasab, E., & Garber, D. (2021). Development of “ABC-UTC Non-Proprietary UHPC” Mix, Final Report # ABC-UTC-2016-C2-FIU01-Final, ABC-UTC, Miami, FL.

Shi, C., Wu, Z., Xiao, J., Wang, D., Huang, Z., & Fang, Z. (2015). A review on ultra high performance concrete: Part I. Raw materials and mixture design. Construction and Building Materials, 101, 741-751.

Sritharan S., Aaleti S., Garder J., Bierwagen D., Abu-Hawash A. “Use of ultra-high performance concrete in bridge design” (2012).

Subedi, D., M. A. Moustafa, M. S. Saiidi, (2019). “Non-Proprietary UHPC for Anchorage of Large Diameter Column Bars in Grouted Ducts,” Report No. CCEER-19-03, May 2019.

Teichmann, T., & Schmidt, M. (2002). Mix Design and Durability of Ultra High Performance Concrete (UHPC). In Proceedings of the 4th International Ph. D. Symposium in Civil Engineering (pp. 19-21).

Verger-Leboeuf, S., Charron, J. P., & Massicotte, B. (2017). Design and behavior of UHPFRC field-cast transverse connections between precast bridge deck elements. Journal of Bridge Engineering, 22(7), 04017031.

Vitek, J.L., Kolisko, J., Citek, D., Rehacek S., Coufal R. “UHPC connection of precast bridge deck” (2016). First International Interactive Symposium on UHPC.

Wang, D., Shi, C., Wu, Z., Xiao, J., Huang, Z., & Fang, Z. (2015). A review on ultra high performance concrete: Part II. Hydration, microstructure and properties. Construction and Building Materials, 96, 368-377.

Whitney, D.P.; Fowler, D.W. New applications for polymer overlays. Adv. Mater. Res. 2015, 1129, 277–282.

Wille, K., Naaman, A. E., & Parra-Montesinos, G. J. (2011). Ultra-High Performance Concrete with Compressive Strength Exceeding 150 MPa (22 ksi): A Simpler Way. ACI materials journal, 108(1).

Wille, K., Naaman, A. E., El-Tawil, S., & Parra-Montesinos, G. J. (2012). Ultra-high performance concrete and fiber reinforced concrete: achieving strength and ductility without heat curing. Materials and structures, 45(3), 309-324.

Xie, T., Fang, C., Ali, M. M., & Visintin, P. (2018). Characterizations of autogenous and drying shrinkage of ultra-high performance concrete (UHPC): An experimental study. Cement and Concrete Composites, 91, 156-173.

Yazıcı, H., Yardımcı, M. Y., Yiğiter, H., Aydın, S., & Türkel, S. (2010). Mechanical properties of reactive powder concrete containing high volumes of ground granulated blast furnace slag. Cement and Concrete Composites, 32(8), 639-648.

Yu, R., Spiesz, P. H. J. H., & Brouwers, H. J. H. (2015). Development of an eco-friendly Ultra-High Performance Concrete (UHPC) with efficient cement and mineral admixtures uses. Cement and Concrete Composites, 55, 383-394.

Yuan, J., & Graybeal, B. (2015). Bond of reinforcement in ultra-high-performance concrete. ACI Structural Journal, 112(6), 851.

Zhu P., Ma Z. J., Cao Q., French C. E. “Fatigue evaluation of transverse U-bar joint details for accelerated bridge construction” (2012). Journal of Bridge Engineering. Volume 17, No. 2, pp. 191-200.